



Three dimensional finite element analysis of matrix cracks in multidirectional composite laminates
by Modayur Shrinivas

A thesis submitted in partial fulfillment of the requirements for the degree of Master of Science in
Mechanical Engineering
Montana State University
© Copyright by Modayur Shrinivas (1993)

Abstract:

This thesis presents the results of three dimensional finite element analyses of cross-plyed ([0/90/0]) and angle-plyed ([0/±45]s) laminates with cracks in the off-axis plies. The materials are modelled with homogenous orthotropic layers or regions. The effects of actual microstructures are considered in two stages, first by including matrix interlayers between plies, and then by including discrete strands of fibers within the layers. The discrete strands model the structure of the reinforcement in typical wind turbine blades and other common composites. This work does not model interply delamination regions, which will be introduced in subsequent studies.

The [0/90/0] laminates were analyzed for two different sets of material properties representing glass fiber/epoxy and carbon fiber/epoxy composites. These two classes of laminates were analyzed for three different models: a) no epoxy layer between plies, b) uncracked epoxy layer between plies, and c) cracked epoxy layer between plies. Stress concentrations were lower in general in carbon/epoxy laminates than in glass/epoxy laminates. The three-dimensional analysis appears necessary to predict the effects of off-axis ply cracking on axial-ply failure for the glass/epoxy case. The presence of an epoxy interlayer reduces the stress concentrations considerably. While most of the stress components increase moderately if the interlayer is cracked (relative to an uncracked layer), some interlaminar stresses were reduced by cracking the layer. The interlayer results are consistent with experimental observations of O0 ply failure resulting from off-axis ply cracking in fatigue if the layers were stitched tightly together, preventing the formation of an interlayer.

The [0/90/0] laminate was also analyzed with a discrete band of high fiber material surrounded by pure matrix in the O0 ply, instead of homogenous ply properties. The crack then penetrated through the 90° ply, the epoxy interlayer, and the epoxy region in the O0 ply. This geometry corresponds to many composites composed of strands which are woven or stitched together. The shape of the strand cross-section was also found to be important. In general, the axial stresses in the high fiber region were increased relative to homogenous layers, but the other stress components were not strongly affected.

Similar results were obtained for a [0/±45]s laminate with both homogenous plies and a O0 ply with a strand structure. The laminates contained crossing matrix cracks in the (+) and (-) 45° plies. Stress concentrations at the intersection were higher than for the [0/90/0] case due to the off-axis ply orientation and the greater proportion of off-axis plies. Stress concentrations appear high enough to cause O0 ply failure when the ±45 plies crack, even at low applied stresses. The interlaminar stresses are also very high, and should lead to interply delamination. Both of these findings are consistent with experimental observations.

**THREE DIMENSIONAL FINITE ELEMENT ANALYSIS OF MATRIX CRACKS
IN MULTIDIRECTIONAL COMPOSITE LAMINATES**

by

Modayur Shrinivas

a thesis submitted in partial fulfillment
of the requirements for the degree

of

Master of Science

in

Mechanical Engineering

**MONTANA STATE UNIVERSITY
Bozeman, Montana**

May 1993

71378
Sh 866

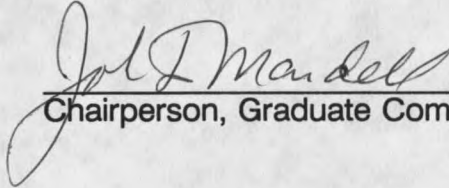
APPROVAL

of a thesis submitted by

Modayur Shrinivas

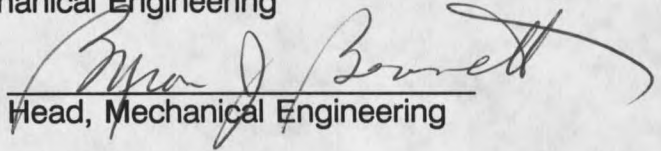
This thesis has been read by each member of the thesis committee and has been found to be satisfactory regarding content, English usage, format, citations, bibliographic style, and consistency, and is ready for submission to the College of Graduate Studies.

4/22/93
Date


Chairperson, Graduate Committee

4/22/93
Date

Approved for Mechanical Engineering


Head, Mechanical Engineering

4/30/93
Date

Approved for the College of Graduate Studies


Graduate Dean

STATEMENT OF PERMISSION TO USE

In presenting this thesis in partial fulfillment of the requirements for a master's degree at Montana State University, I agree that the library shall make it available to borrowers under rules of the library.

If I have indicated my intention to copyright this thesis by including a copyright notice page, copying is allowable only for scholarly purposes, consistent with "fair use" as prescribed in the U.S. Copyright Law. Requests for permission for extended quotation from or reproduction of this thesis in whole or in parts may be granted only by the copyright holder.

Signature *M. Shumway*

Date 04/22/93

ACKNOWLEDGEMENTS

There are a few people to whom credit should be extended for making this research and thesis possible. First and foremost, I would like to extend my thanks to Dr. John Mandell, who provided the inspiration and guidance that gave shape and substance to this thesis. I wish to thank Dr. Jerry Dwyer for his proofreading and constructive criticism. I am grateful to my fellow graduate students and friends who helped me during this research in one way or the other. I wish to acknowledge Dr. VanLuchene of the Civil Engineering Department and the staff of the Chemical Engineering Department for providing the computing resources. Special mention must be made of the National Center for Super Computing Applications, for the use of their super computer. Financial support for this research was provided by Sandia National Laboratories, for which I am grateful. I thank my family who stood behind me all through my pursuit of a graduate degree.

TABLE OF CONTENTS

	Page
1. INTRODUCTION	1
Damage	1
Damage in Cross-ply Laminates	1
Fatigue of Wind Turbine Blade Materials	4
Thesis Objective and Approach	6
Thesis Organization	7
2. TEST PROBLEM	8
Introduction	8
Problem Formulation	8
Results and Discussion	12
Summary	18
3. ANALYSIS OF [0/90/0] COMPOSITE LAMINATES WITH A CRACKED 90 ⁰ ply	20
Introduction	20
Model Geometry	20
Models Analyzed	22
Problem Formulation	22
Results and Discussion	28
Summary	64
4. ANALYSIS OF [0/90/0] LAMINATES WITH A DISCRETE HIGH FIBER STRAND	66
Introduction	66
Model Analyzed	66
Results and Discussion	75
Summary	86
5. ANALYSIS OF [0/±45] _s LAMINATE WITH CRACKED ANGLE PLIES	88
Introduction	88
Model	88
Results and Discussion	94
Summary	106

TABLE OF CONTENTS-Continued

6. ANALYSIS OF A $[0/\pm 45]_s$ LAMINATE WITH A DISCRETE HIGH FIBER STRAND	108
Introduction	108
Model Analyzed	108
Results and Discussion	112
Summary	123
7. CONCLUSIONS AND RECOMMENDATIONS	124
Conclusions	124
Recommendations	126
REFERENCES	128
APPENDICES	132
Appendix A - Static Analysis Using ANSYS 4.4a	133
Appendix B - Three Dimensional Anisotropic Solid Element - STIF64	135
Appendix C - Wavefront Solver in ANSYS	138

LIST OF TABLES

Table	Page
1. Material Properties	28
2. STIF64 Element Description	135

LIST OF FIGURES

Figure		Page
1.	Radiograph showing transverse crack, longitudinal cracks and delaminations in a cross-ply laminate. The schematic shows details around a delamination. From [1].	3
2.	Test Problem - Model Geometry	11
3.	Test Problem - Present Study.	14
4.	Test Problem - Comparison. Stresses in the $[\pm 45]_s$ Laminate . . .	15
5.	Interlaminar Stress in the $[0,90]_s$ Laminate. Normal Stress S_z along $z=h$ for $b/h=8$	16
6.	Interlaminar Stress in the $[0,90]_s$ Laminate (near free edge). Normal Stress S_z along $z=h$ for $b/h=8$	17
7.	$[0/90/0]$ Composite Laminate with a Cracked 90° ply (without epoxy interlayer)	21
8.	$[0/90/0]$ Composite Laminate with a Cracked 90° Ply (with epoxy interlayer)	23
9.	$[0/90/0]$ Composite Laminate with a Cracked 90° Ply (Quadrant modelled)	24
10.	Finite Element Mesh of the $[0/90/0]$ Laminate	26
11.	Finite Element Mesh of the $[0/90/0]$ Laminate (Close-up View) . .	27
12.	Through-thickness Stresses. $[0/90/0]$ Glass/Epoxy Laminate . . .	30
13.	Through-thickness Stresses - Comparison (glass/epoxy laminate)	33
14.	Stress in the Y direction in the 90° Ply (glass/epoxy laminate) . . .	34
15.	Stresses in the Y Direction at the $0/90$ Interface (glass/epoxy laminate)	35
16.	Stress in the Y direction in the 0° Ply	36

LIST OF FIGURES-Continued

Figure	Page
17. Through-thickness Stresses at the crack (carbon/epoxy laminate)	37
18. Through-thickness Stresses - Comparison (carbon/epoxy laminate)	38
19. Stress in the Y direction in the 90 ⁰ Ply (carbon/epoxy laminate) .	40
20. Stresses in the Y Direction at the 0/90 Interface (carbon/epoxy laminate)	41
21. Stress in the Y direction in the 0 ⁰ Ply (carbon/epoxy laminate) . .	42
22. Through-thickness Stresses. [0/90/0] Glass/Epoxy Laminate . . .	43
23. Through-thickness Stresses - Comparison (glass/epoxy laminate)	44
24. Stress in the Y direction in the 90 ⁰ Ply (glass/epoxy laminate) . . .	45
25. Stresses in the Y Direction at the 0/90 Interface (glass/epoxy laminate)	46
26. Stress in the Y direction in the 0 ⁰ Ply (glass/epoxy laminate)	47
27. Through-thickness Stresses at the crack (carbon/epoxy laminate)	48
28. Through-thickness Stresses - Comparison (carbon/epoxy laminate)	49
29. Stress in the Y direction in the 90 ⁰ Ply (carbon/epoxy laminate) .	50
30. Stresses in the Y Direction at the 0/90 Interface (carbon/epoxy laminate)	51
31. Stress in the Y direction in the 0 ⁰ Ply (carbon/epoxy laminate) . .	52
32. Through-thickness Stresses. [0/90/0] Glass/Epoxy Laminate . . .	54
33. Through-thickness Stresses - Comparison (glass/epoxy laminate)	55
34. Stress in the Y direction in the 90 ⁰ Ply (glass/epoxy laminate) . . .	56

LIST OF FIGURES-Continued

Figure	Page
35. Stresses in the Y Direction at the 0/90 Interface (glass/epoxy laminate)	57
36. Stress in the Y direction in the 0° Ply (glass/epoxy laminate)	58
37. Through-thickness Stresses at the crack (carbon/epoxy laminate)	59
38. Through-thickness Stresses - Comparison (carbon/epoxy laminate)	60
39. Stress in the Y direction in the 90° Ply (carbon/epoxy laminate) .	61
40. Stresses in the Y Direction at the 0/90 Interface (carbon/epoxy laminate)	62
41. Stress in the Y direction in the 0° Ply (carbon/epoxy laminate) . .	63
42. Cracking in 0° Ply of [0/±45] _s Triax glass/polyester Wind Turbine Blade Material, Showing High Fiber Content Strands with Matrix in between [25]	67
43. Model Geometry of the [0/90/0] Laminate	71
44. Cross-section of the [0/90/0] Laminate at the Crack Rectangular High Fiber Region	72
45. Cross-section of the [0/90/0] Laminate at the Crack Rounded High Fiber Region	73
46. Finite Element Mesh at the Crack - Rounded High Fiber Region .	74
47. Stresses around the High Fiber Region - Effect of Corner Angle .	76
48. Through Thickness Stresses in the High Fiber Region	78
49. Through Thickness Stresses in the Average Fiber Region	79
50. Stresses in the 0° Ply Parallel to the X axis	81
51. Stresses in the Y direction at the High Fiber/Epoxy Interface . . .	83

LIST OF FIGURES-Continued

Figure	Page
52. Stresses in the Y direction at the High Fiber/Epoxy Interface . . .	84
53. Deformation in the Laminate (deformation exaggerated)	85
54. $[0/\pm 45]_s$ Laminate Model Geometry	89
55. Cross-section of the $[0/\pm 45]_s$ Laminate	91
56. Finite Element Mesh of the $[0/\pm 45]_s$ Laminate	92
57. Finite Element Mesh of the $[0/\pm 45]_s$ Laminate (Close-up View). .	93
58. Through Thickness Stresses at the Intersection of +45 and -45 Cracks	95
59. Through Thickness Stresses at the Intersection of +45 and -45 Cracks (Comparison)	98
60. Along -45 Crack/Epoxy Layer Interface from point (1) to point (2)	99
61. Along +45 Crack/Epoxy Layer Interface from point (1) to point (2)	100
62. Through Thickness Stresses near the Crack Intersection passing through +45 Crack Only	101
63. Through Thickness Stresses near the Crack Intersection Passing Through -45 Crack Only	102
64. Through Thickness Stresses Passing Through +45 Crack Only	104
65. Through Thickness Stresses Passing Through -45 Crack Only	105
66. $[0/\pm 45]_s$ Laminate with Discrete High Fiber Strand - Model Geometry	109
67. $[0/\pm 45]_s$ Laminate with Discrete High Fiber Strand - Cross Section	110
68. Through Thickness Stresses at the Intersection of +45 and -45 Cracks	113

LIST OF FIGURES-Continued

Figure		Page
69.	Through Thickness Stresses at the Intersection of +45 and -45 Cracks (Comparison)	115
70.	Along +45 Crack/Epoxy Layer Interface. (along 1-2-3)	116
71.	Along -45 Crack/Epoxy Layer Interface. (along 1-2-3)	117
72.	Stresses Around the High Fiber Region at the +45 Crack Plane .	119
73.	Through Thickness Stresses, passing through +45 Crack Only . .	120
74.	Through Thickness Stresses, passing Through -45 Crack Only . .	121
75.	* STIF 64 3-D Solid Element	137

ABSTRACT

This thesis presents the results of three dimensional finite element analyses of cross-plyed ($[0/90/0]$) and angle-plyed ($[0/\pm 45]_s$) laminates with cracks in the off-axis plies. The materials are modelled with homogenous orthotropic layers or regions. The effects of actual microstructures are considered in two stages, first by including matrix interlayers between plies, and then by including discrete strands of fibers within the layers. The discrete strands model the structure of the reinforcement in typical wind turbine blades and other common composites. This work does not model interply delamination regions, which will be introduced in subsequent studies.

The $[0/90/0]$ laminates were analyzed for two different sets of material properties representing glass fiber/epoxy and carbon fiber/epoxy composites. These two classes of laminates were analyzed for three different models: a) no epoxy layer between plies, b) uncracked epoxy layer between plies, and c) cracked epoxy layer between plies. Stress concentrations were lower in general in carbon/epoxy laminates than in glass/epoxy laminates. The three-dimensional analysis appears necessary to predict the effects of off-axis ply cracking on axial-ply failure for the glass/epoxy case. The presence of an epoxy interlayer reduces the stress concentrations considerably. While most of the stress components increase moderately if the interlayer is cracked (relative to an uncracked layer), some interlaminar stresses were reduced by cracking the layer. The interlayer results are consistent with experimental observations of 0° ply failure resulting from off-axis ply cracking in fatigue if the layers were stitched tightly together, preventing the formation of an interlayer.

The $[0/90/0]$ laminate was also analyzed with a discrete band of high fiber material surrounded by pure matrix in the 0° ply, instead of homogenous ply properties. The crack then penetrated through the 90° ply, the epoxy interlayer, and the epoxy region in the 0° ply. This geometry corresponds to many composites composed of strands which are woven or stitched together. The shape of the strand cross-section was also found to be important. In general, the axial stresses in the high fiber region were increased relative to homogenous layers, but the other stress components were not strongly affected.

Similar results were obtained for a $[0/\pm 45]_s$ laminate with both homogenous plies and a 0° ply with a strand structure. The laminates contained crossing matrix cracks in the (+) and (-) 45° plies. Stress concentrations at the intersection were higher than for the $[0/90/0]$ case due to the off-axis ply orientation and the greater proportion of off-axis plies. Stress concentrations appear high enough to cause 0° ply failure when the ± 45 plies crack, even at low applied stresses. The interlaminar stresses are also very high, and should lead to interply delamination. Both of these findings are consistent with experimental observations.

CHAPTER 1

INTRODUCTION

Damage

One of the first mechanisms of failure to occur in many composite laminates under static or fatigue loading is the development of cracks in the cross plies and angle plies [1]. These cracks are often the cause of the development of other types of damage like delamination which finally lead to catastrophic failure of the whole laminate. The word "damage" is often used loosely to describe some undesirable change which is thought to have occurred to a material or structure [2]. The damage and its effect on the structure are separate entities. A particular way to define damage is to identify it with the changes in the constitution (microstructure or macrostructure, depending on the scale) of the material. The changes in the material (or structural) response (i.e. properties) can then be related to the appropriate measures of the underlying changes of the material constitution. Thus, damage and its consequences are separate entities.

Damage in Cross-ply Laminates

Cross-ply laminates are composed of unidirectional layers (with parallel aligned fibers). The direction of the layers (plies) alternate in mutually perpendicular directions, such as 0/90/0/90..., where the angle given is relative to the load direction. This class of laminates has been studied extensively and the data

concerning damage and its effect have been richly documented. In the following, a brief description of damage in cross-ply laminates of carbon/epoxy is given. Further details are described in Jamison et al. [3].

When a cross-ply laminate of carbon/epoxy is loaded in tension along the longitudinal direction, a number of cracks appear in the transverse plies at a certain value of the applied stress. The cracks span the thickness of the transverse plies and almost immediately grow in the transverse direction (Stage I). As the stress is increased, more cracks appear in the transverse direction between previously formed cracks. The planes of the cracks are roughly normal to the direction of stress and the spacing is fairly uniform. Under fatigue loading, the crack spacing is found to decrease further and a minimum spacing may eventually result irrespective of the loading path. Beyond this saturation spacing, further loading appears to change the nature of the cracking process. Figure 1, taken from [3] shows the crack pattern in Stage II. The horizontal lines are 90° ply cracks (cracks parallel to the fibers of the 90° plies) and the vertical lines are axial cracks parallel to the fibers in the 0° plies, which are symmetrically placed on both sides of the transverse plies. The dark zones in the radiograph seen at intersections of transverse and longitudinal lines were shown by Jamison et al. [3] to be delaminations (cracks in the plane of the sheet between the 0° and 90° plies). The final stage, Stage III of the damage development in cross-ply laminates was shown by Jamison et al. [3] to consist of coalescence of delaminations in regions between two longitudinal cracks, and fiber failures in the axial (0°) plies.

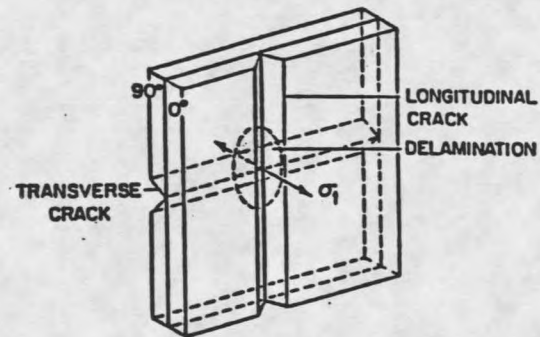
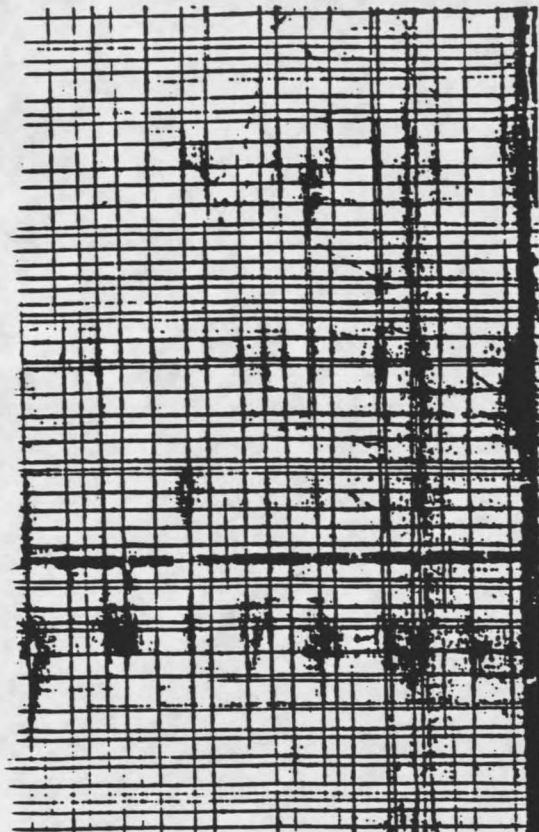


Figure 1. X-ray radiograph showing transverse crack, longitudinal cracks and delaminations in a cross ply laminate. The schematic shows details around a delamination. From [1].

The high mechanical performance of fiber reinforced plastics is generally governed by the fiber properties. However, the matrix properties can be important under certain loading conditions and fiber configurations [4]. Matrix micro-damage occurs in cross-ply fiber reinforced plastics even when the matrix has a higher failure strain than the fibers [5-12]. Generally, the onset of matrix micro-failure in glass-reinforced polyester specimens occurs between 0.2 and 0.5% strain and is associated with the characteristic "knee" found in the stress-strain curves of cross-ply laminates [4].

Fatigue of Wind Turbine Blade Materials

The high cycle fatigue resistance (lifetime in the 10^6 to 10^9 cycle range) of composite materials used in wind turbine rotor blades has been recognized as a major uncertainty in predicting the reliability of wind turbines over their design lifetime [13,14]. These blades typically experience 10^8 to 10^9 significant fatigue cycles over their lifetime of 20 to 30 years. This is well beyond the cycle range of most aerospace structures.

As with other laminates, the fatigue behavior of these materials is distinguished by several important general features [14-17] :

1. Failure is usually progressive, resulting from the gradual accumulation and interaction of dispersed damage, rather than by the nucleation and growth of a dominant crack.

2. As damage accumulates, the constitutive relations of the material may change significantly.
3. A number of distinct damage modes can be identified, including fiber dominated tension and compression, matrix dominated cracking parallel to fibers and interlaminar cracking between plies. While some of these may cause failures directly, certain modes like matrix cracking may have an indirect effect on failure by causing load transfer to fibers.
4. Under tensile loading, the strains to produce matrix cracking are generally well below those to produce fiber failure. As a consequence, in multidirectional composites, cracking tends to initiate first in domains where fibers are at the greatest orientation relative to maximum tensile stress (like 90° plies). Cracking accumulates in these domains and then in domains of lesser orientation (like the 45° plies). Delamination between plies may occur at cut edges, ply terminations or at the intersection of matrix cracks in adjoining plies. Finally, gross failure occurs by fiber breakage in any domains which have plies with the least orientation to maximum stress (like the 0° plies).
5. Large-scale delamination between plies has been a significant failure mode for composite structures, particularly with out-of-plane loads.
6. Theoretical models for damage progression and failure are under development, but no general approach to lifetime prediction for

composites is widely accepted. Only delamination failures have a well developed theoretical context in classical fracture mechanics.

Cracks in composite laminates affect the stiffness and strength of the laminate on the macro scale. The stress distributions around the cracks can be quite complex even under relatively simple static loading. Analytical approaches are often not adequate for completely describing the stress distributions around cracks. A numerical approach is much more feasible under these circumstances. The cracks are sites of high stress gradients and the problem is completely three dimensional. The nature of the problem is amenable to finite element analysis.

Thesis Objective and Approach

Point 3 cited above is the particular focus of this thesis. The stress redistribution due to matrix cracking is especially important as it may lead to laminate failure. The thesis explores the load transfer to the plies which have fibers oriented parallel to maximum applied stress. This knowledge is important as it addresses stress distribution on a micro scale and the possible course of future delamination as well as fiber failures.

The nature of the stress gradients near the crack are examined using three dimensional finite element analysis. Particular attention is paid to interlaminar shear stresses as these stresses are responsible for delamination at a later stage. The type of laminates that have been studied are the $[0/90/0]$ and $[0/\pm 45]_s$; in each case, crack symmetries representative of experimental observation are considered.

Three levels of representation of the material structure are included : uniform orthotropic plies, uniform orthotropic plies with a pure matrix layer between each ply and plies with discrete strands of high fiber content. The latter is the closest representation of the actual materials used in wind turbine blades.

Thesis Organization

Chapter 2 gives the results of a test case for comparison with literature results. This establishes the validity of the finite element model and mesh refinement chosen for the actual case. Chapter 3 presents the results and discussion of the effects of 90^0 ply matrix cracking on the stress field, including the effects of ply elastic constants and a matrix interlayer between plies (both cracked and uncracked layers). Chapter 4 extends these results to discrete fiber strands rather than uniform plies. Chapter 5 analyzes the $[0/\pm 45]_s$ laminates, considering similar structural parameters. Chapter 6 explores the stress distributions in a $[0/\pm 45]_s$ laminate with a discrete fiber strand in the 0^0 ply. Chapter 7 discusses conclusions and recommendations.

CHAPTER 2

A TEST PROBLEM - INTERLAMINAR STRESSES IN COMPOSITE LAMINATES

Introduction

The response of a finite-width composite laminate under uniform axial extension is analyzed using finite element techniques. These techniques are employed to obtain solutions for stresses throughout the region of interest with special emphasis on the laminate free edges. Results for material properties typical of a high modulus graphite epoxy system are presented and are compared with several literature solutions to the same problem. The purpose of this exercise is to establish the accuracy of the method employed in this study and to establish the finite element mesh refinement needed to obtain accurate results for stress gradients of this general type.

Problem Formulation

Symmetric laminates are laminates in which plies are stacked symmetrically about the mid-thickness, such as $[+45,-45,-45,+45]$. The analytical technique for determining the in-plane, elastic response of a laminated composite called the lamination theory (see Ref.[18] for a detailed discussion of this theory), is based upon the assumption that a state of plane stress exists for symmetric laminates under in plane tractions. When the laminate is composed of layers of different orientations, lamination theory implies certain impossible boundary tractions on a

free edge [19-21,28]. This problem is modelled without such assumptions using finite element techniques and the results are compared with published results.

Consider a laminate loaded by tractions applied only on its ends $x = \text{constant}$ (Figure 2), such that the stress components are independent of x . Now, assuming Saint Venant's principle holds for a laminate, this stress distribution will exist in regions sufficiently removed from areas of load introduction.

The strain-displacement relations are as follows

$$\begin{aligned} \epsilon_x &= u_{,x} & \epsilon_y &= v_{,y} & \epsilon_z &= w_{,z} \\ \gamma_{yz} &= w_{,y} + v_{,z} & \gamma_{xz} &= w_{,x} + u_{,z} & \gamma_{xy} &= v_{,x} + u_{,y} \end{aligned}$$

where a comma denotes partial differentiation. The u, v and w are displacements along x, y and z directions respectively and ϵ and γ denote normal and shear strains respectively. By Saint Venant's principle, the equilibrium conditions take the reduced form,

$$\tau_{xy,y} + \tau_{xz,z} = 0$$

$$\sigma_{y,y} + \tau_{yz,z} = 0$$

$$\tau_{yz,y} + \sigma_{z,z} = 0$$

Since we are concerned only with symmetric angle-ply laminates under extensional loading, we can enforce symmetric boundary conditions for the displacements with respect to the x - y and x - z planes.

(1) x - y plane

$$u(x,y,z) = u(x,y,-z)$$

$$v(x,y,z) = v(x,y,-z)$$

$$w(x,y,z) = -w(x,y,-z)$$

(2) x-z plane

$$v(x,y,z) = -v(x,-y,z)$$

$$w(x,y,z) = w(x,-y,z)$$

These symmetry conditions are for the whole laminate. When half a quadrant of the model is built to exploit these symmetry conditions, appropriate boundary conditions (B.C.'s) are imposed as will be explained later.

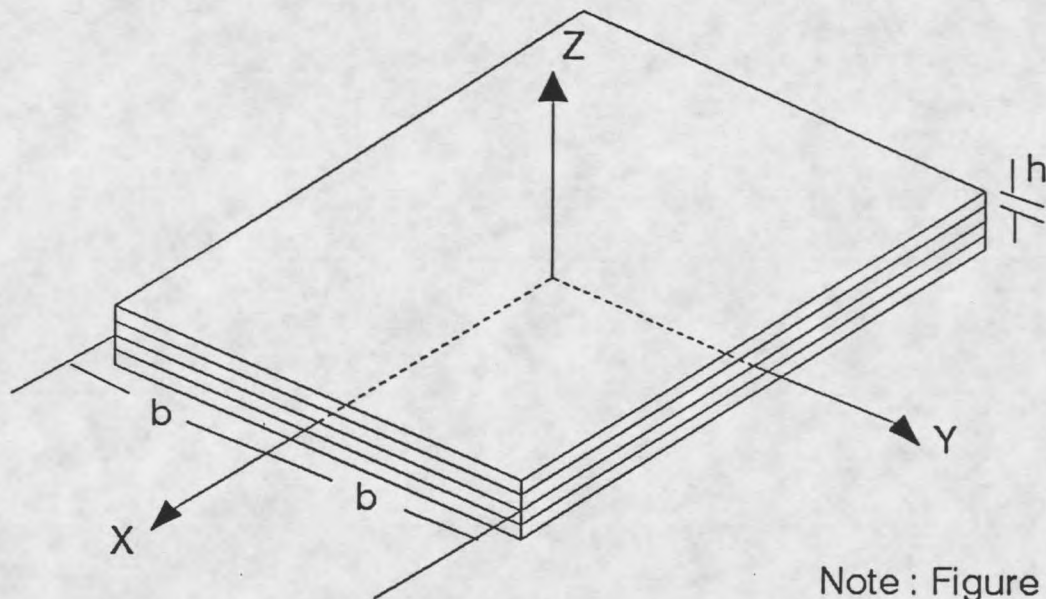
The problem was solved using the finite element method. By this method, the continuous material region was replaced by discrete elements. Discrete values of the dependent variables (like stresses) are determined at discrete points (nodes) on the elements. A large number of elements are required at the material free edges to capture the high stress gradients in these areas. So, in building the model, a fine mesh is used near the free edges to capture the high stress gradients in these regions. The finite element method software ANSYS 4.4a was used and STIF64 anisotropic brick elements (refer Appendix B for details on this element type) were used to build the F.E. model. This element is a complete 3-D anisotropic element which is required by the nature of our problem.

The boundary conditions imposed were

$$u(0,y,z) = 0 \quad v(x,0,z) = 0 \quad w(x,y,0) = 0$$

and the extension condition

$$u(X_0,y,z) = U$$



Note : Figure not to scale.

Figure 2. Test Problem - Model Geometry.

U is a displacement boundary condition value from which the uniform axial strain can be calculated as,

$$U/X_0 = \epsilon_x$$

The F.E. mesh is graded so that smaller elements are used near the laminate free edges. The smallest element size used near the free edge was $h/25$. Different element sizes were used near the laminate free edge and the results compared. For an element size less than $h/25$, stress values near the free edge were not significantly different from the values for $h/25$. Since lowering the element size increases the number of degrees of freedom, the smallest element size was kept at $h/25$ ($0.04 h$). The problem was modelled and solved on an IBM RS/6000 workstation.

Results and Discussion

The laminate under consideration is a $\pm 45^\circ$ laminate under a uniform axial strain, ϵ_x . Laminate theory predicts a uniform, planar state of stress in each layer with the axial stress component σ_x , and a non-zero in-plane shear stress component τ_{xy} , which arises from the shear coupling term of the layer stiffness matrices. These results are accurate for laminates of theoretically infinite width. However, they are inaccurate for a finite width laminate since the in-plane shear stress is required to vanish along the free edge (see Figure 2).

A high modulus carbon/epoxy system was modelled with the geometric relationship $b=8h$, and material properties,

$$E_{11} = 20.0 \times 10^6 \text{ psi}; \quad E_{22} = E_{33} = 2.1 \times 10^6 \text{ psi}; \quad G_{12} = G_{13} = G_{23} = 0.85 \times 10^6 \text{ psi};$$

$$\nu_{12} = \nu_{13} = \nu_{23} = 0.21$$

where the subscript '1' refers to the fiber direction and '2' refers to the direction perpendicular to the fiber direction in the plane of the laminate and '3' refers to the direction normal to the plane of the laminate. This geometry and properties were chosen to follow the literature case for comparison in References [22] and [23] as well as for comparison with a solution for $[0,90]_s$ laminates by Wang and Dickson [24].

Figure 3 shows the stress distribution at the interface of $\pm 45^\circ$ plies. Actually, the results are plotted at $z = .992 h$ instead of $z = h$ to avoid stress averaging that takes place at the interface which is a region of two dissimilar layers. The interlaminar stresses decay rapidly away from the free edge.

The results are compared with the works of Pipes and Pagano [22], Puppo and Evensen [21], Wang and Crossman [23] and Wang and Dickson [24]. It is seen quite clearly that the work of Puppo and Evensen, being an approximate formulation, has failed to capture the high stress gradients near the free surfaces. In particular, the interlaminar shear stress τ_{xz} in the Puppo and Evensen work does not appear singular, but rather takes on finite magnitude at the free edge. Comparing the results with those of Pipes and Pagano, it is seen that the stresses σ_x and τ_{xy} peak at a distance of $.05 b$ away from the free edge, and the stress τ_{xz} rises rapidly near the free edge. The results of Pipes and Pagano show no such sharp peak and there is only a very gradual and barely noticeable rise and dip in

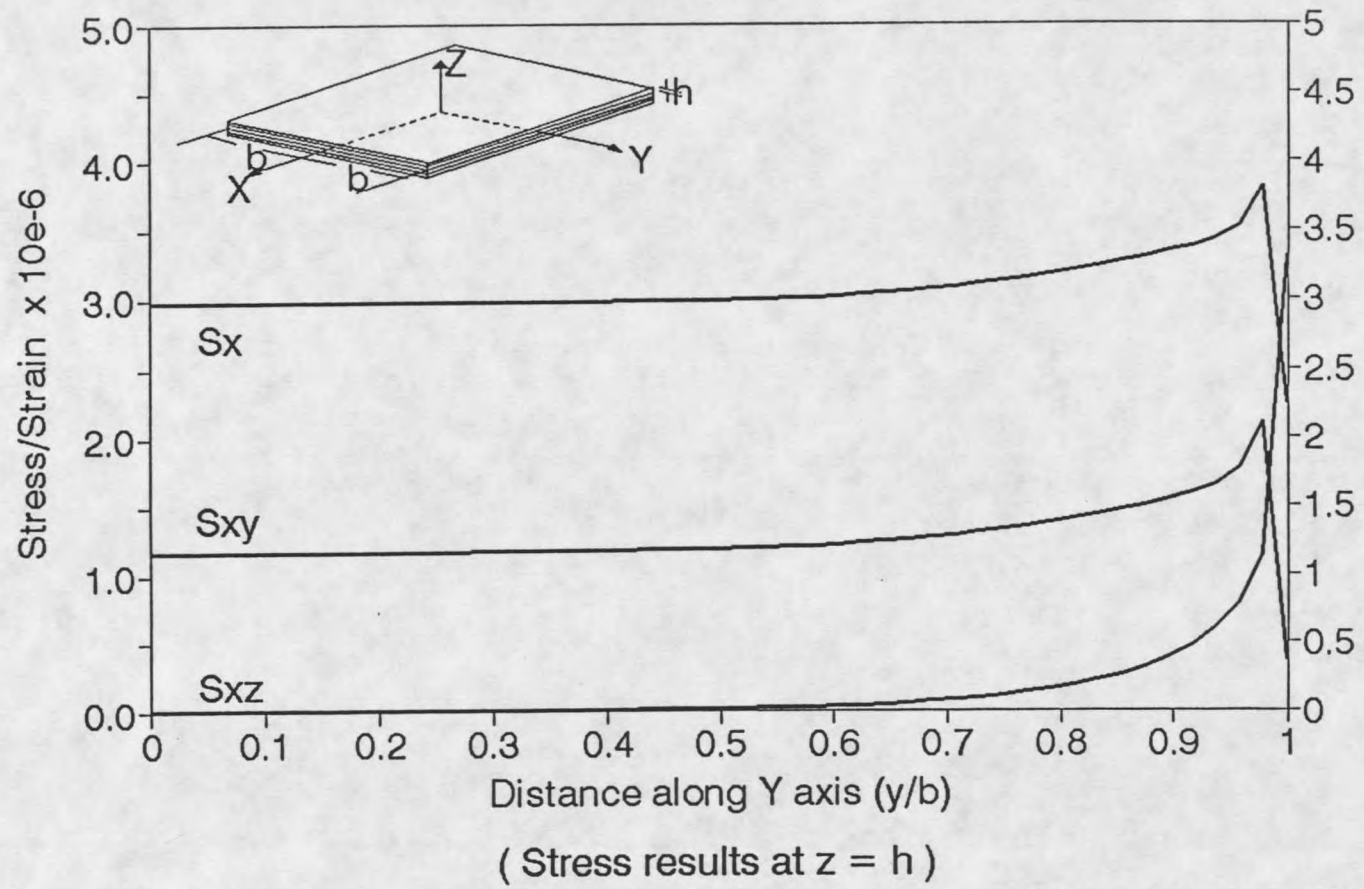


Figure 3. Test Problem - Present Study.

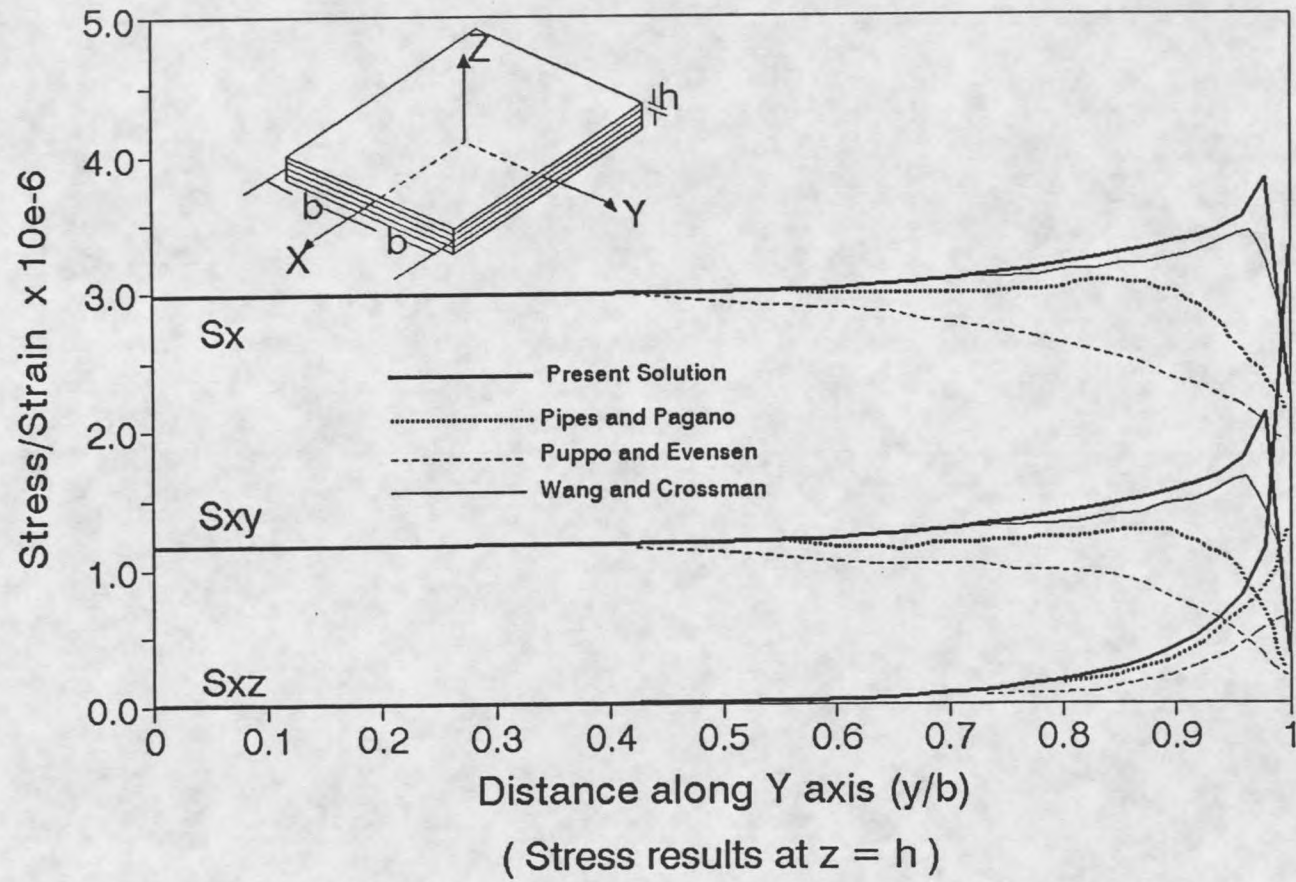


Figure 4. Test Problem - Comparison. Stresses in the $[\pm 45]_s$ Laminate.

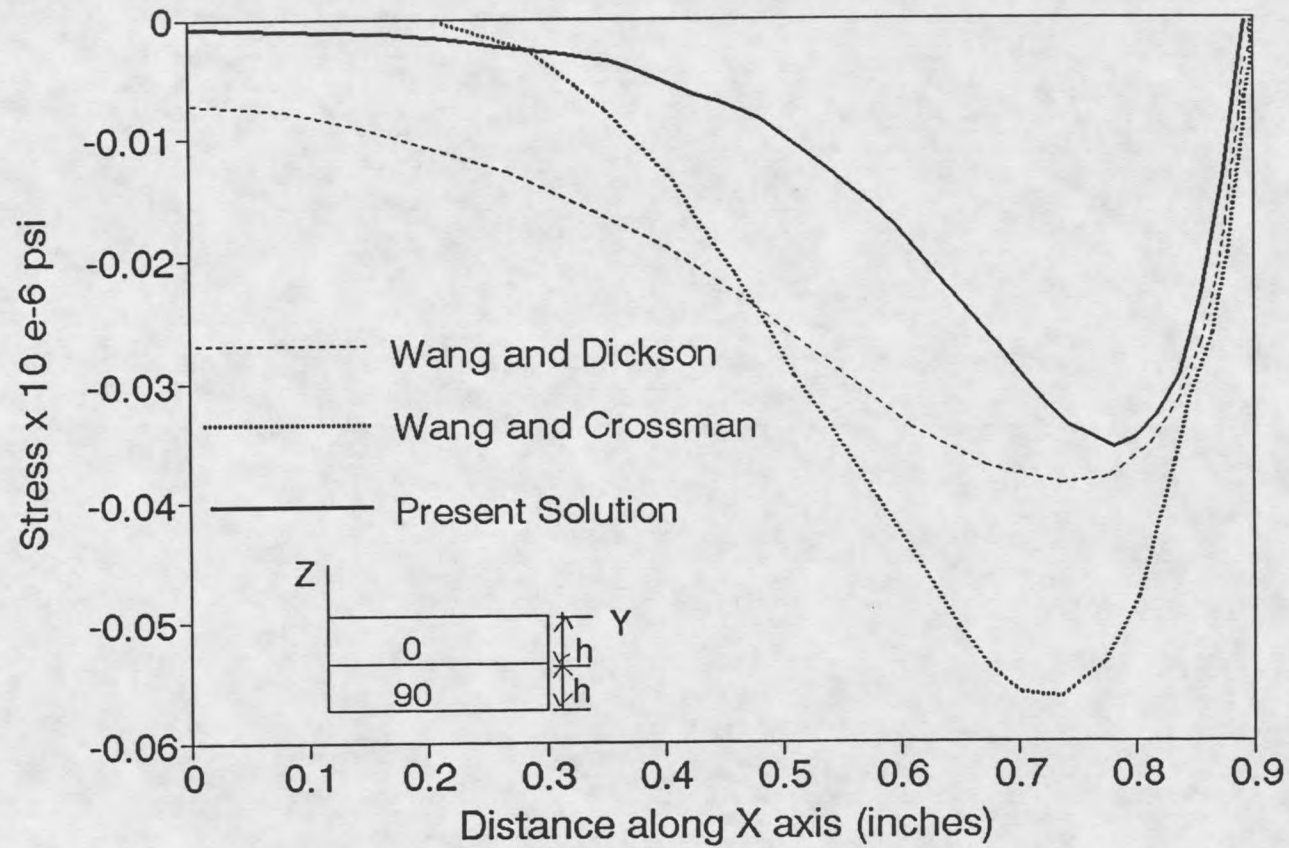


Figure 5. Interlaminar Stresses in the $[0/90]$, Laminate. Normal Stress S_z along $Z=h$ for $b/h=8$.

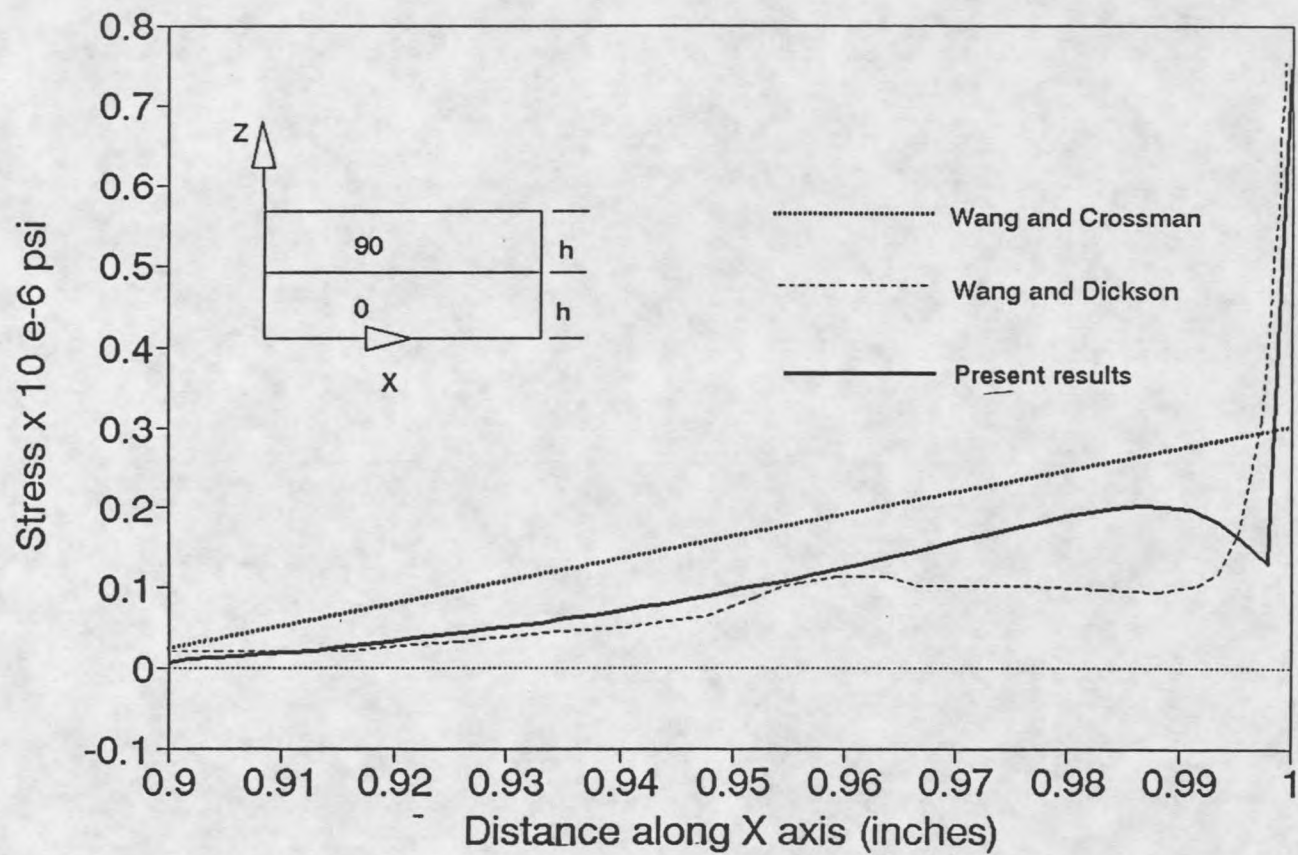


Figure 6. Interlaminar Stress in [0/90], Laminate (near free edge). Normal Stress S_z along $Z=h$ for $b/h=8$.

the σ_x and τ_{xy} stresses. Comparing the present results with the work of Wang and Crossman who employed a finite element approach to the problem, it is seen that the results compare very favorably with all the stress values, the only deviation is that the σ_x and τ_{xy} peak values differ by a small amount. Also, by looking at the τ_{xz} stress, it is clearly apparent that the values obtained by Wang and Crossman indicate a slightly more gradual rise than the present work.

The interlaminar stress σ_z , in the [0,90]_s laminates is plotted in Figures 4 and 5. The result compares very favorably with that of Wang and Dickson [24]. Comparing it with the results of Wang and Crossman [23], it is seen that the results compare approximately for values away from the free edge ($Y/b < 0.9$). For values near the free edge, the results of Wang and Crossman indicates a rather gradual rise while the present results show a sharper rise (Figure 6).

Summary

A finite element approach was undertaken for the study of the stress distributions in angle-ply and cross-ply laminates under uniaxial extension. The results show that significant interlaminar shear stresses are required to allow shear transfer between layers of laminates. This widely accepted observation will be relevant in subsequent solutions of cracked cross-ply and angle-ply laminates. Also these edge effects are restricted to regions approximately the extent of ply thickness [22]. These local high stresses may cause delamination of the laminate.

The work of Puppo and Evensen is approximate and is not capturing the true nature of the high stress gradients near the free edge. The results obtained by Pipes and Pagano [22] also do not reflect the true singular nature of the free edge. A probable reason is that the early results used a coarse mesh (The minimum element size they used was $0.29 h$). The finite element approach used by Wang and Dickson [24] and Wang and Crossman [23] has yielded much better results. Their results show the peaking of stresses near the free edge which is consistent with the singular nature of stresses near the region. Our results with a fine mesh closely compare with those of Wang and Crossman [23] and Wang and Dickson [24]. These results, which were tested to be mesh independent for the smallest element dimension less than $h/25$, reflect the nature of stresses near the free edge in a very reasonable manner. This general scale of mesh refinement has been used in the solutions which follow.

CHAPTER 3

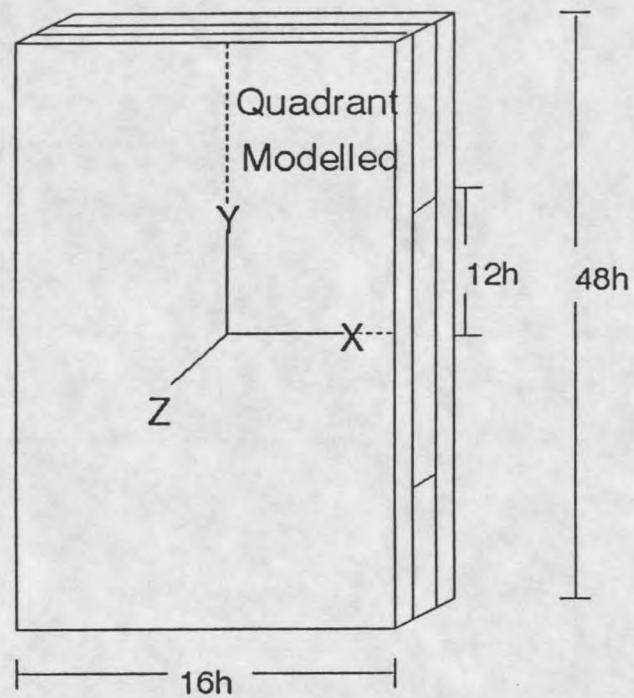
ANALYSIS OF [0/90/0] COMPOSITE LAMINATES WITH A CRACKED 90° ply

Introduction

This chapter presents the results of [0/90/0] laminates with a cracked 90° ply. The 0/90 laminates have been extensively studied. Much research has been done in the area of matrix cracking in the 90° ply of these laminates. This chapter explores the nature of stress fields around such matrix cracks. Three dimensional finite element analysis is employed to determine the stress distribution around the matrix crack in the 90° ply and to examine the stresses carried by the 0° ply as a result of such a crack in the 90° ply. Particular attention is paid to the interlaminar stresses in the laminate, especially near the crack, as these stresses are the key contributors to delamination in the laminate.

Model Geometry

The actual model is a 48 h x 16 h [0/90/0] composite laminate with a ply thickness of h (Figure 7). Taking advantage of the symmetry of the problem, only one quadrant of the model is analyzed. Symmetry boundary conditions are imposed on the XY, XZ and YZ planes. Only the 90° ply is cracked. The crack is modelled as a gap 1/125 h deep measured perpendicular to the plane of the crack.



[0,90,0] Composite Laminate with Cracked 90 deg Ply
(without epoxy interlayers between plies)

Figure 7. [0/90/0] Composite Laminate with a Cracked 90° ply (without epoxy interlayer between plies).

Models Analyzed

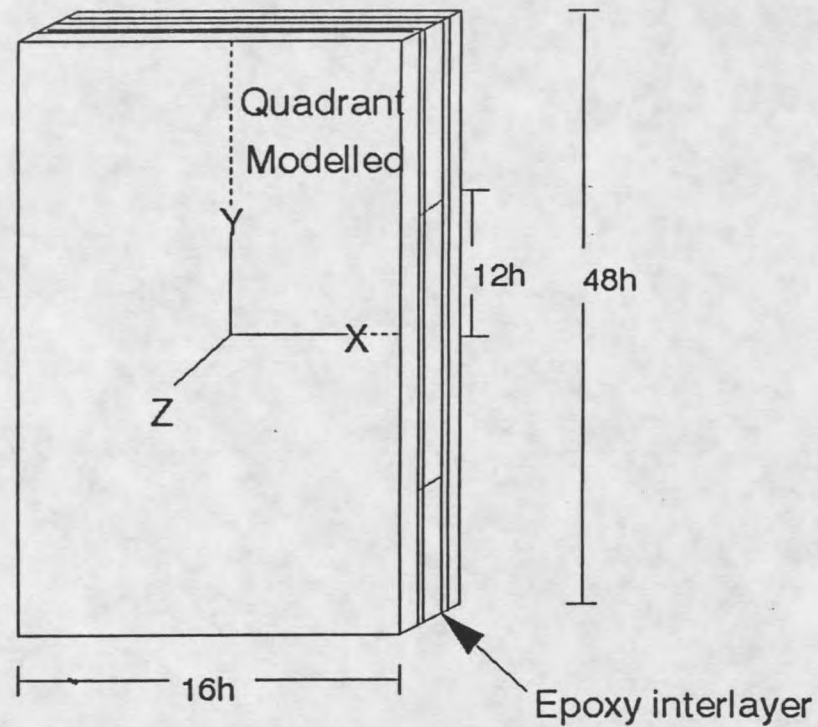
The first case analyzed is for uniform orthotropic plies which are assumed to be bonded together. The effect of an epoxy layer (0.08 h thick) between plies on the stress distribution around the crack is then analyzed. Also, a comparison is then made of the effect of such a layer being cracked on the plane of the 90° ply crack. These three different cases,

- 1) no epoxy layer between plies,
- 2) epoxy layer between plies, not cracked, and
- 3) epoxy layer between plies, cracked,

are analyzed for both the glass/epoxy laminates and carbon/epoxy laminates. Thus, six different models in all were constructed and analyzed. The three main cases were run for the two different materials by changing just the material properties. However, certain interesting differences were observed for different material properties as will be discussed later.

Problem Formulation

A uniform extension is applied to the laminate so that the average stress on the cross section is 50,000 psi (S_A). All dimensions are normalized in terms of the ply thickness h. Two cracks are present in the laminate 24 h apart. Of these two cracks, only one appears in the finite element model due to symmetry. The crack extends completely across the 90° ply width, parallel to the fibers. The crack is situated 12 h from the XZ plane as shown in Figure 7. The following symmetry



[0,90,0] Composite Laminate with Cracked 90 deg Ply
 (with epoxy interlayer between plies)

Figure 8. [0/90/0] Composite Laminate with a Cracked 90° ply (with epoxy interlayer between plies).

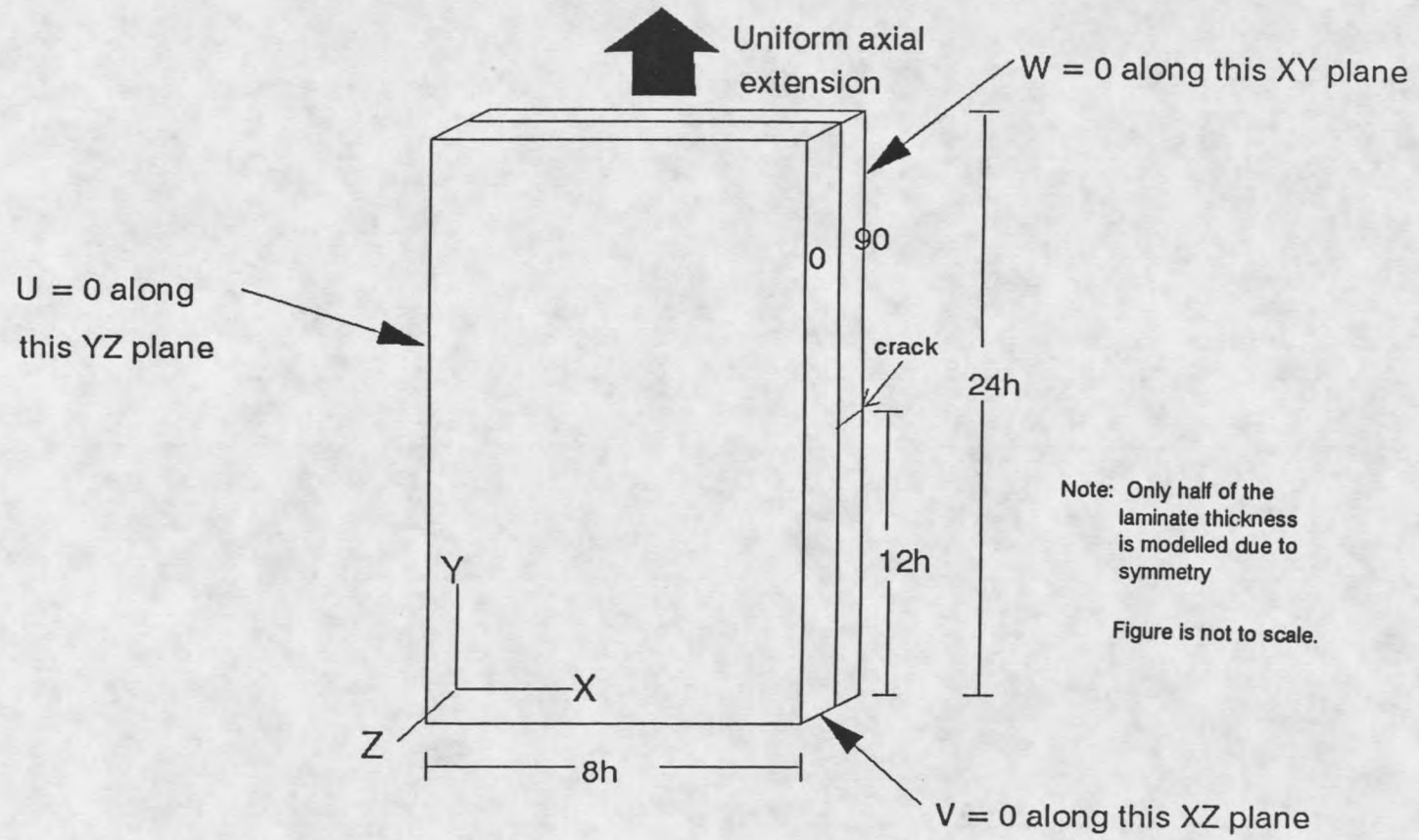


Figure 9. [0/90/0] Composite Laminate with a Cracked 90° ply (Quadrant Modelled).

boundary conditions are imposed on the model

$$U(0,y,z) = 0$$

$$V(x,0,z) = 0$$

$$W(x,y,0) = 0$$

In addition, a displacement boundary condition is imposed at $y = 24 h$, to effect a uniaxial extension to the model. This displacement is calculated such that the averaged stress (S_A) on the cross section of the model is 50,000 psi. The results are normalized by S_A .

The laminate is orthotropic with material property orientation depending on the direction of the lamina. For this problem, the STIF 64 element in ANSYS was chosen. This element is an anisotropic brick element with 8 nodes and three translational degrees of freedom. Further details about this element are found in Appendix B. Figures 7 and 8 depict a laminate without and with an epoxy interlayer respectively.

After the model was built, it was meshed. Figure 10 depicts the finite element mesh and Figure 11 shows a close up view of the mesh. Meshing was accomplished so that smaller elements were used in the regions of high stress gradients. Using the test problem as a guide, the smallest element dimension was selected to be $h/25$. Elements are smoothly graded, with larger elements in regions far removed from areas of high stress concentration. This is done to keep the number of degrees of freedom and hence the wavefront (refer to Appendix C for details on wavefront solver) to a minimum. At least two elements were used

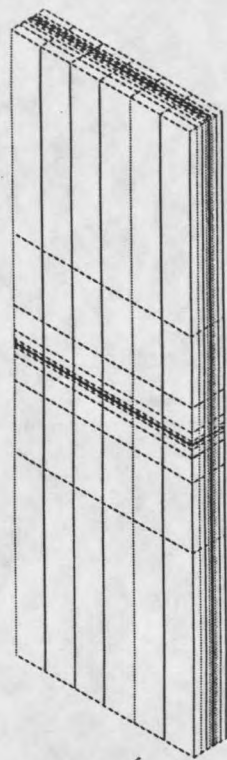


Figure 10. Finite Element Mesh of the [0/90/0] Laminate.

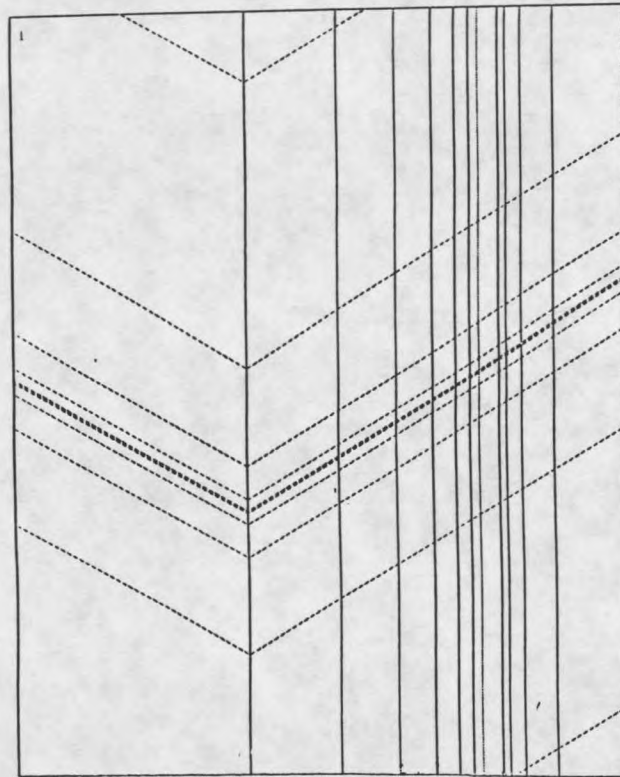


Figure 11. Finite Element Mesh of the [0/90/0] Laminate (Close-up View).

across the thickness of the epoxy layer between plies (in models with this layer) to avoid the effect of stress averaging across different materials. After meshing, element reordering was done to reduce the wavefront at the solution phase. This reordering was done on the basis of element connectivity. These problems were modelled and solved on an IBM RS/6000 workstation.

Table 1. Material Properties

Material	$E_L \times 10^6$ Psi	$E_T \times 10^6$ Psi	$G_{LT} \times 10^6$ Psi	ν_{LT}
Carbon / Epoxy	21	1.3	0.7	0.20
Glass / Epoxy	5	1.3	0.7	0.25
Epoxy Layer*	0.5	0.5	0.185	0.35

* Epoxy layer thickness was 0.08 h. Note that polyester, vinylester, and other polymers have properties similar to those assigned to the epoxy.

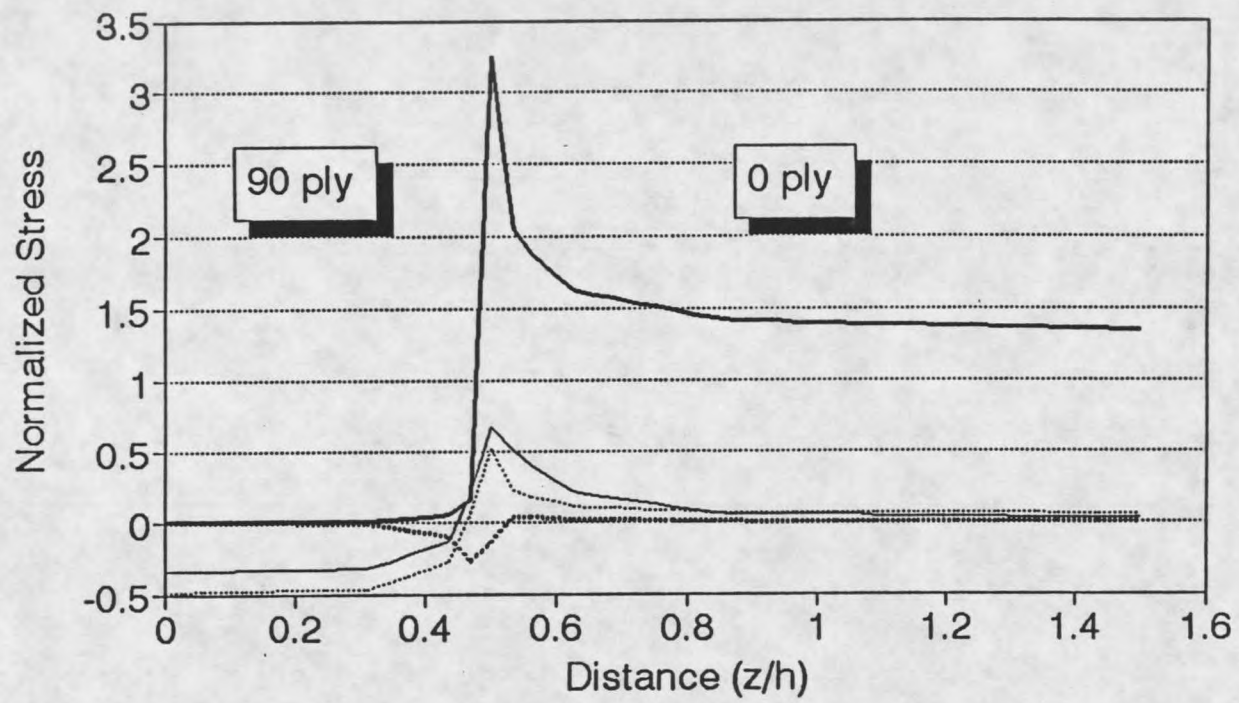
Results and Discussion

Figures 12-16 show the stresses in a glass/epoxy laminate with no epoxy layer between the plies. Figures 17-21 show the stresses in a carbon/epoxy laminate with no epoxy layer between the plies. Figures 22-26 refer to a glass/epoxy material with an uncracked epoxy layer between the plies. Figures 27-31 show the stresses in a carbon/epoxy laminate with an uncracked epoxy layer between the plies. Figures 32-36 refer to a glass/epoxy model with a cracked

epoxy layer between the plies. The layer is cracked on the plane of the 90° ply crack. Figures 37-41 refer to a carbon/epoxy model with a cracked epoxy layer between the plies.

First we consider the case of models with no epoxy layer between the plies. The two models analyzed for this type were the glass fiber / epoxy matrix (glass/epoxy) and carbon fiber / epoxy matrix (carbon/epoxy). As there is no 'softening' effect of an epoxy layer in these models, stresses at the ply interface are expected to be high. The results show this to be the case. All the stress values were normalized by the applied stress, S_A . Future models analyzed in this thesis also have the stresses normalized for comparison between solutions. The plots of stresses in the thickness direction (z - direction) near the crack show peaking of certain stresses near the $0/90$ interface. This is because, just above and below the crack, the 90° ply is not carrying any S_y at all. Load transfer to the 0° ply occurs here. As can be seen from Figure 12, the stress S_y reaches a peak value near the interface. The normalized stress values (which are dimensionless), show a rather sharp rise near the interface. S_y returns to the far-field value at points removed from the interface. As can be seen, no load is carried by the 90° ply in this region.

Looking at the interlaminar stresses S_{yz} and S_z in Figure 12, we see a marked rise near the $0/90$ interface. S_{yz} has a high negative value near the interface, which changes to a small positive value some distance away from the crack. S_{yz} is practically zero in both the 0 and 90 plies away from the interface. Examining S_z , it is seen that it rises quite sharply in the positive direction near the



(No epoxy layer between plies)

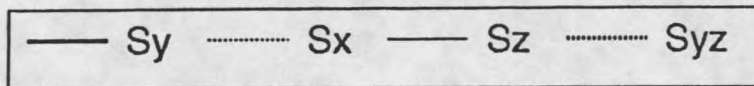


Figure 12. Through-thickness Stresses. [0/90/0] Glass/Epoxy Laminate.

interface, indicating a significant tensile (peeling) stress in the z direction. S_z also flattens to zero away from the crack, though the 90° ply is under compressive stress in the z direction near the crack. This may be due to the Poisson's effect, as Poisson's ratios differ strongly in the two plies. The expansion and contraction of material in the vicinity of the crack might be contributing to the compressive stress on the 90° ply near the crack. The interlaminar stresses are of particular importance because they may lead to catastrophic failure of the laminate by delamination. These stresses give an insight into the nature of the stress distribution around a crack and how it leads to delamination. From these plots we can see clearly how significant these stresses are around the crack. The fact that these stresses go to near zero values away from the crack shows the very localized nature of the crack stress field near the ply interface.

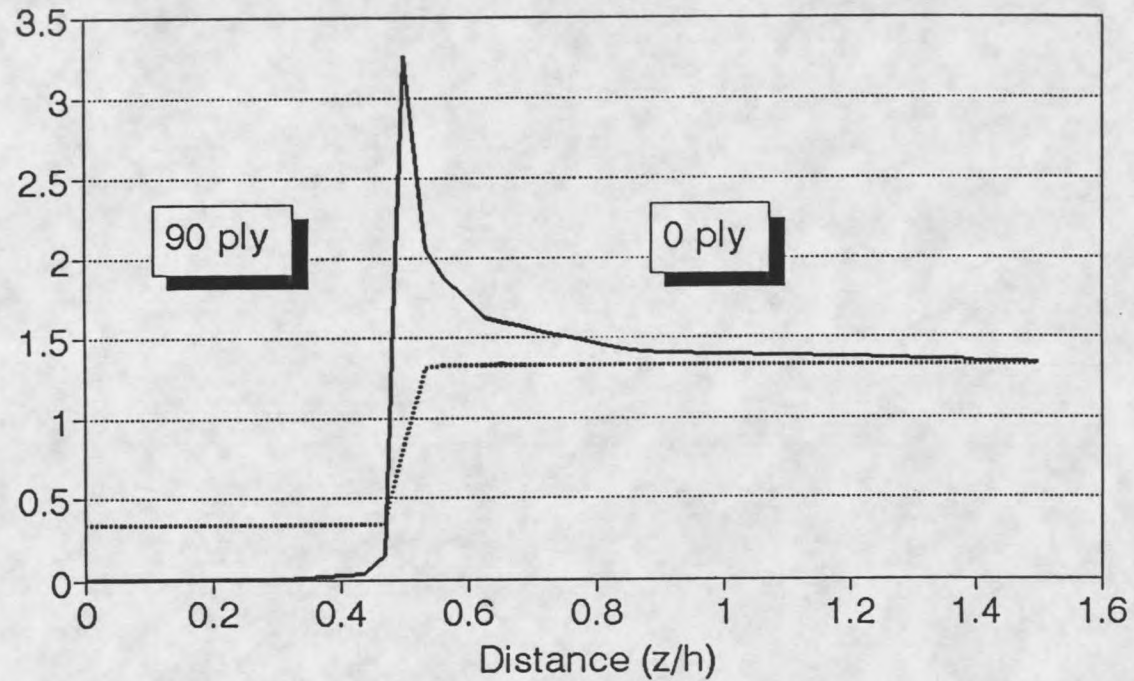
Comparing the S_y values near the crack and at the top (far-field), as shown in Figure 13, we can see how the load from the 90° ply is shifted to the 0° ply. We can examine the S_y values along the length of the laminate (Y direction) in the 0 and 90 plies. Referring to Figures 14 and 16, we find that as the load drops in 90° ply, it is carried by 0° ply. The load redistribution occurs within a distance of about h from the crack. We will compare this later with the carbon/epoxy case.

Examining the interlaminar shear S_{yz} and normal S_z stresses at the $0/90$ interface along the length of the laminate in Figure 15, we find that the interlaminar shear stress S_{yz} is negative and not as high as the normal stress S_z . The normal

stress rises very sharply in a distance less than $h/3$ away from the crack. The region of high stress gradient is very small.

Let us compare the results for the glass/epoxy laminate with those of carbon/epoxy laminate, Figures 12 vs. 17. These models are identical but for the difference in the material properties. Certain interesting differences emerge. First, the far-field stress values, S_y , for the carbon/epoxy are higher in the 0° ply as expected from the greater modulus difference in the 0° and 90° plies for the carbon/epoxy. The local stress S_y in the 0° ply near the crack in the glass/epoxy case reaches a far greater value than for the carbon/epoxy case and covers a larger region. This is mainly due to the fact that the (uncracked) 90° ply in the glass/epoxy laminate is carrying a load about four times higher than the load carried by the 90° ply in the carbon/epoxy laminate. This is explained by the ratio of the moduli E_y to E_x for the two laminates (Table 1). Load redistribution results in higher load transferred to the 0° ply in the glass/epoxy laminate. Another fact that is not so obvious is the difference in the S_y gradient in the z -direction. In the glass/epoxy laminate, the gradient is higher than in the carbon/epoxy laminate, (Figure 12 vs. 17).

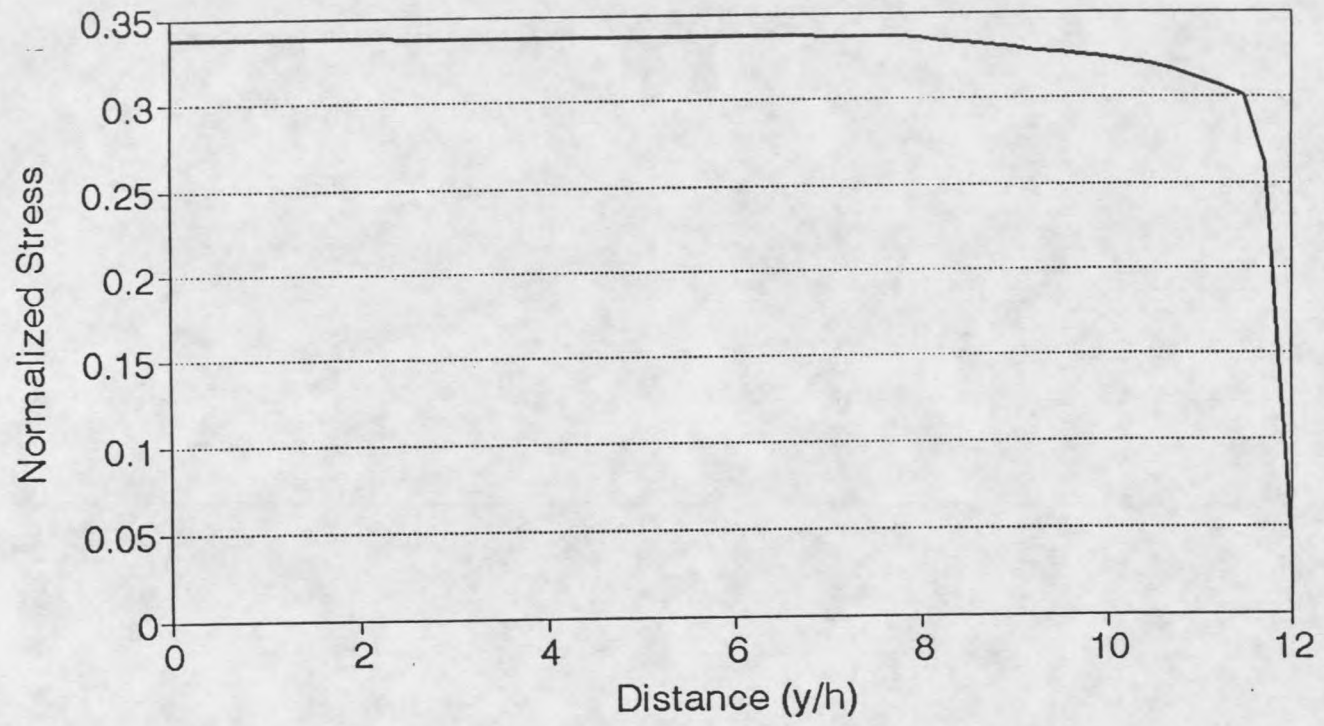
In these models there is no epoxy layer between plies. In an actual laminate, there is usually a thin layer of epoxy (or some matrix material with low modulus) present between plies, as well as discrete fibers and matrix within the plies. The effect of such an interlayer is to soften (spread out) the region of high stress gradient and to lower stress concentrations. We will examine the effect of such a



(No epoxy layer between plies)

— S_y at Crack S_y Far-field

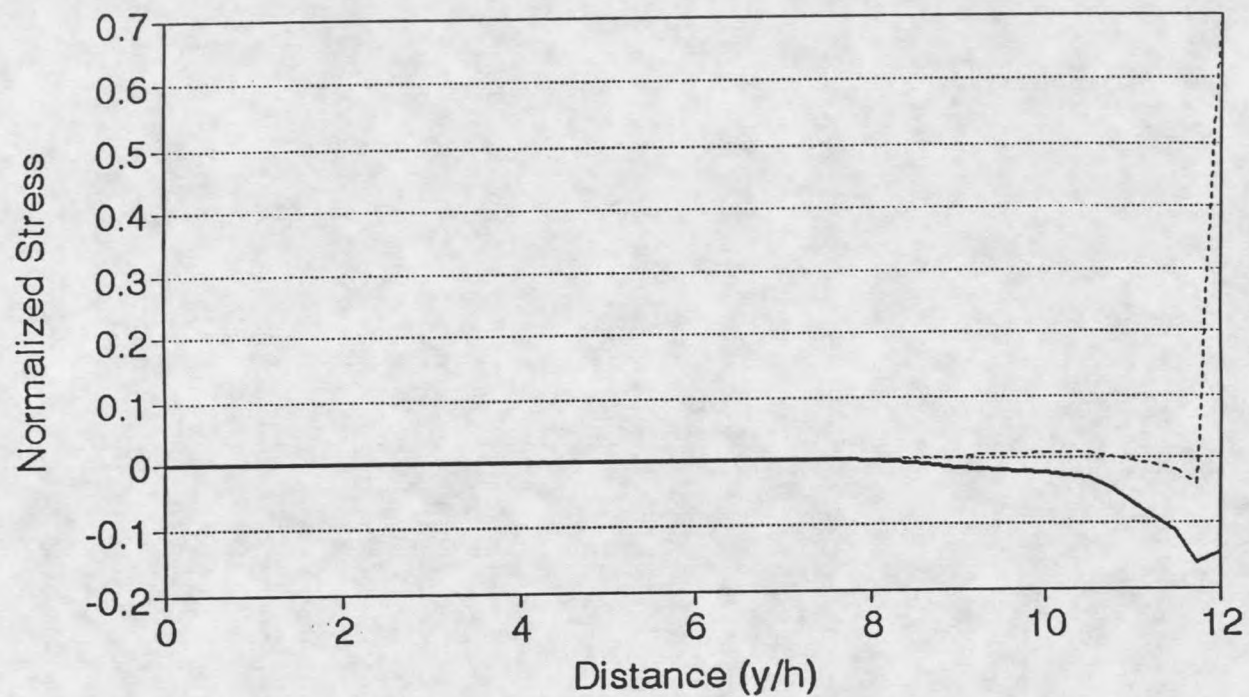
Figure 13. Through-thickness Stresses - Comparison (glass/epoxy laminate).



(No epoxy layer between plies)

— Sy

Figure 14. Stress in the Y direction in the 90° Ply (glass/epoxy laminate).



(No epoxy layer between plies)

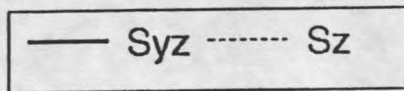
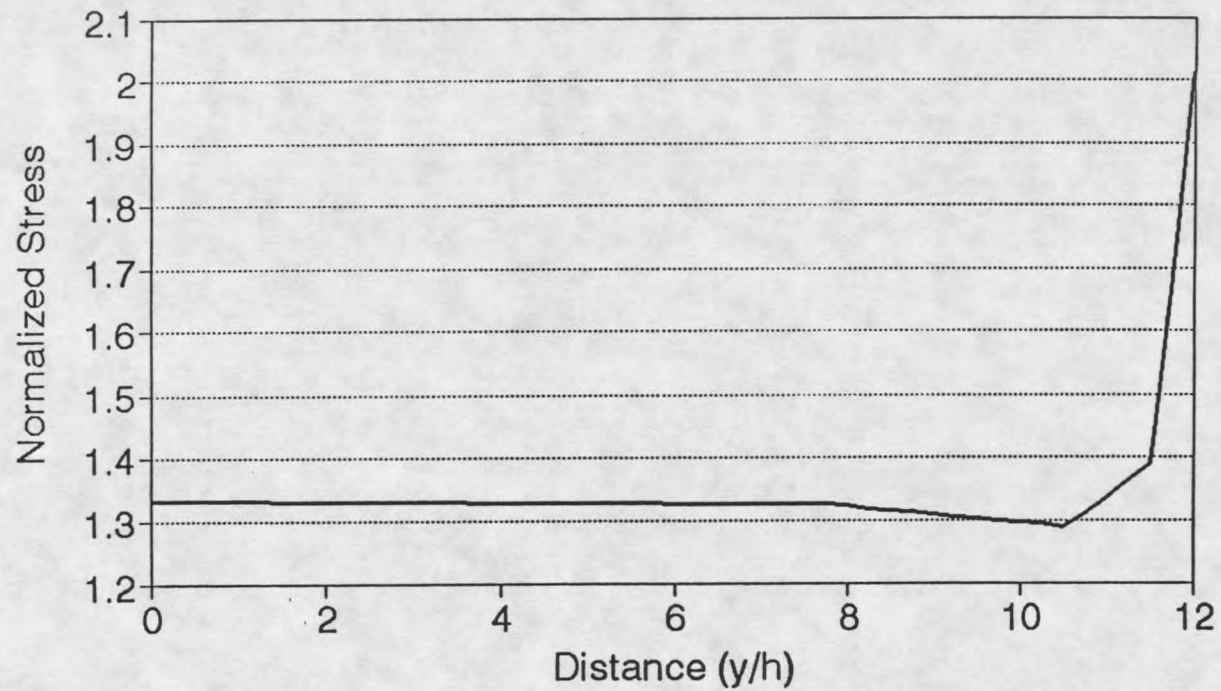


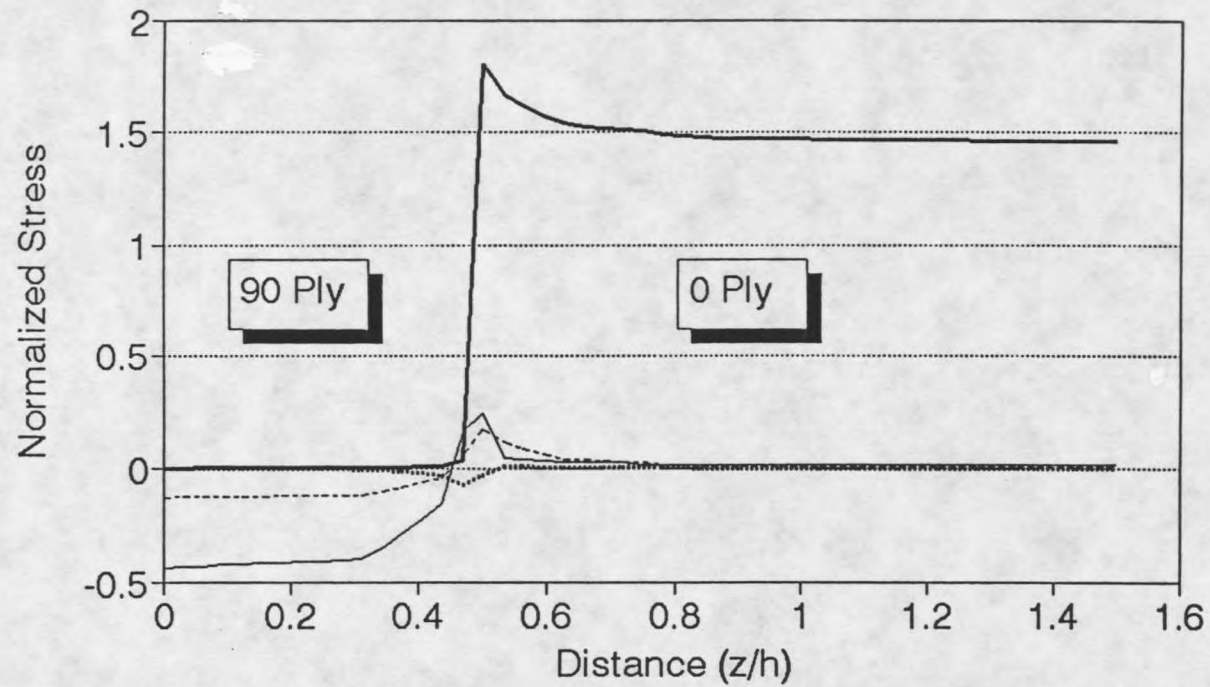
Figure 15. Stresses in the Y direction at the 0/90 Interface (glass/epoxy laminate).



(No epoxy layer between plies)

— Sy

Figure 16. Stress in the Y direction in the 0^0 Ply (glass/epoxy laminate).



(No epoxy layer between plies)

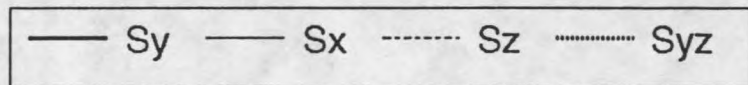
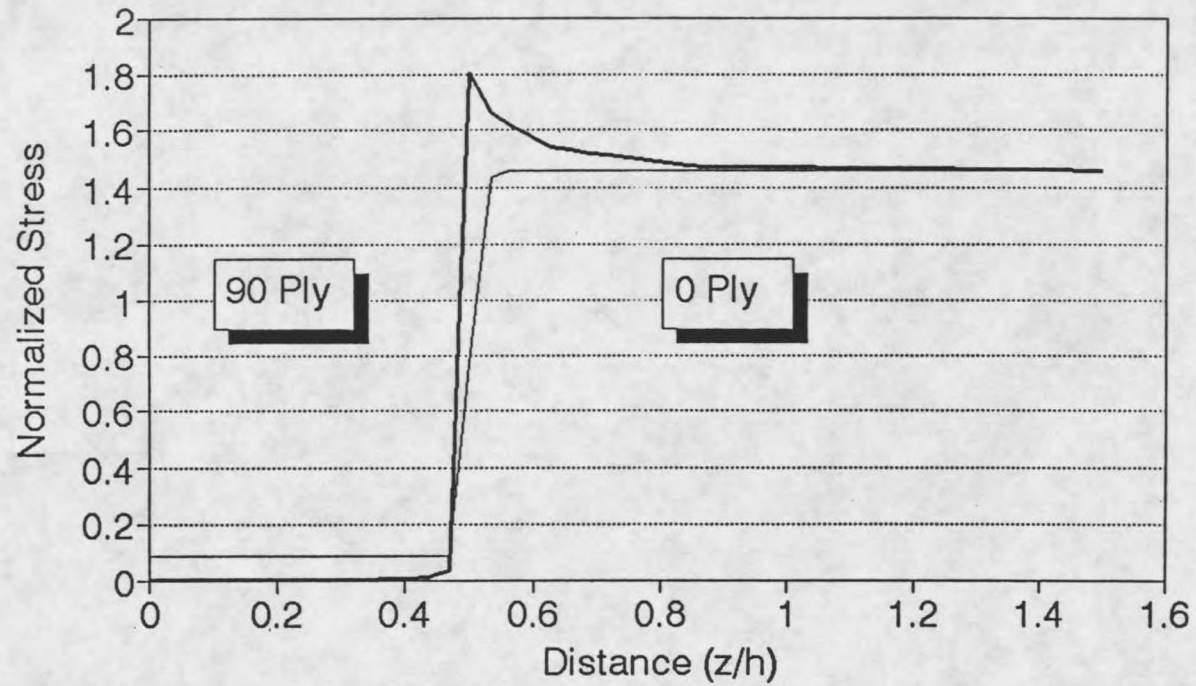


Figure 17. Through-thickness Stresses at the Crack (carbon/epoxy laminate).



(No epoxy layer between plies)

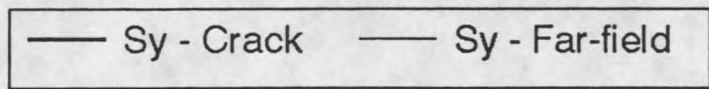
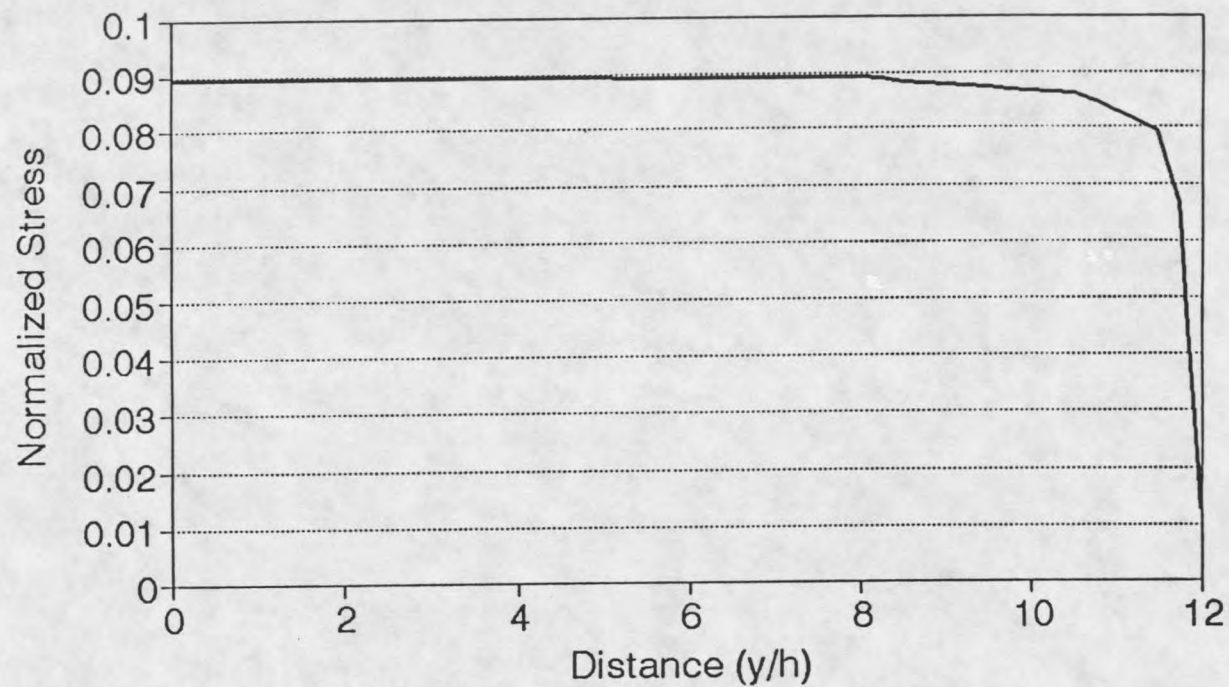


Figure 18. Through-thickness Stresses - Comparison (carbon/epoxy laminate).

layer between plies in the following models. These models present a more realistic picture of what is happening near cracks and ply interfaces. The interlayer may either crack along with the 90^0 ply, or else may remain uncracked.

The through-thickness stresses near the crack for a glass/epoxy laminate with an epoxy interlayer that is not cracked are shown in Figure 22. The corresponding stresses for a carbon/epoxy laminate is shown in Figure 27. Looking at S_y stress values, some differences can be observed. First, in the glass/epoxy case, due to the presence of a low modulus epoxy layer between the plies, the stress takes a sharp downward spike and then rises again before going down to zero in the 90^0 ply. It should be considered that stress averaging is done for the nodes common to two different materials. However, the downward spike is inside the epoxy layer and there is no stress averaging at that node. The very same model with different material properties, the carbon/epoxy laminate, does not show this sharp downward spike of S_y in the epoxy layer. Once again, in the carbon/epoxy laminate, very little load is carried by the 90^0 ply (or the epoxy layer) and hence less load is transferred onto to the 0^0 ply. This could explain the absence of such spikes in the soft epoxy layer. It is believed that the load transfer is not sufficient to precipitate such a response in the epoxy layer.

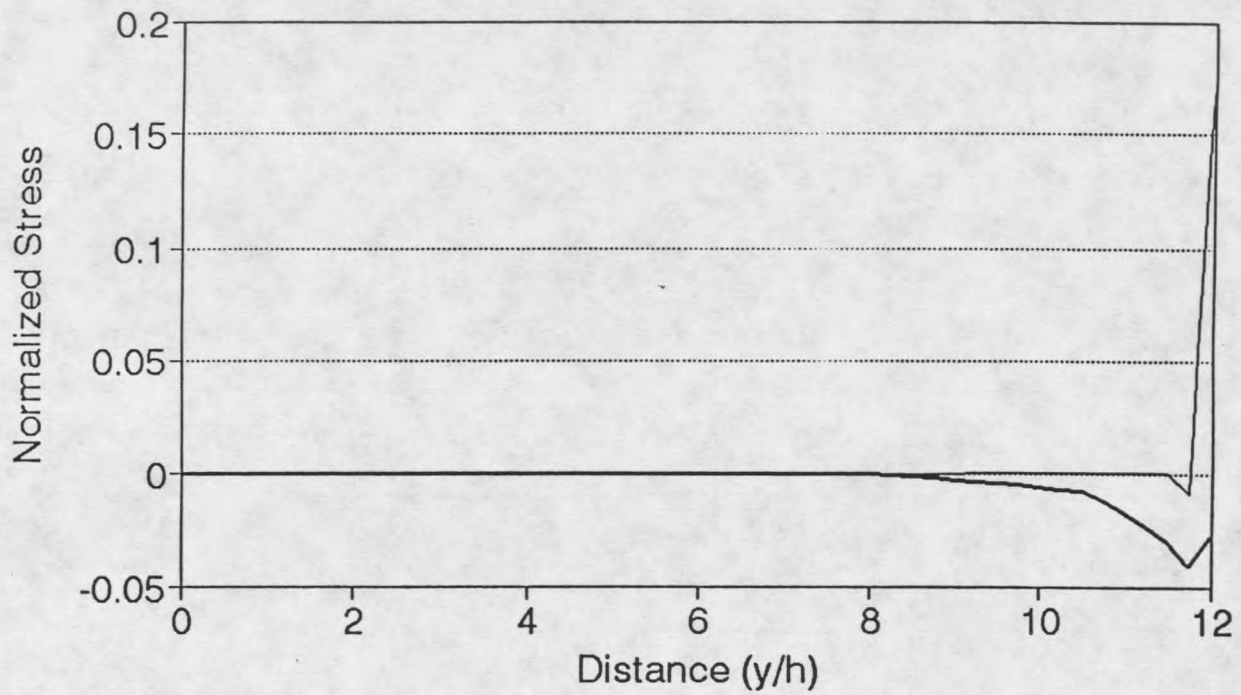
One important observation is the significant lowering of the S_y stress near the 0 /epoxy layer interface relative to the cases with no interlayer, Figures 23 vs. 12. This clearly shows the powerful effect that the thin layer of low modulus epoxy has in lowering the stress concentration in stress concentration regions. This



(No epoxy layer between plies)

— Sy

Figure 19. Stress in the Y direction in the 90° Ply (carbon/epoxy laminate).



(No epoxy layer between plies)

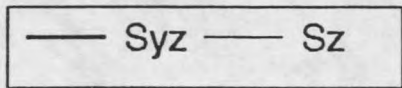
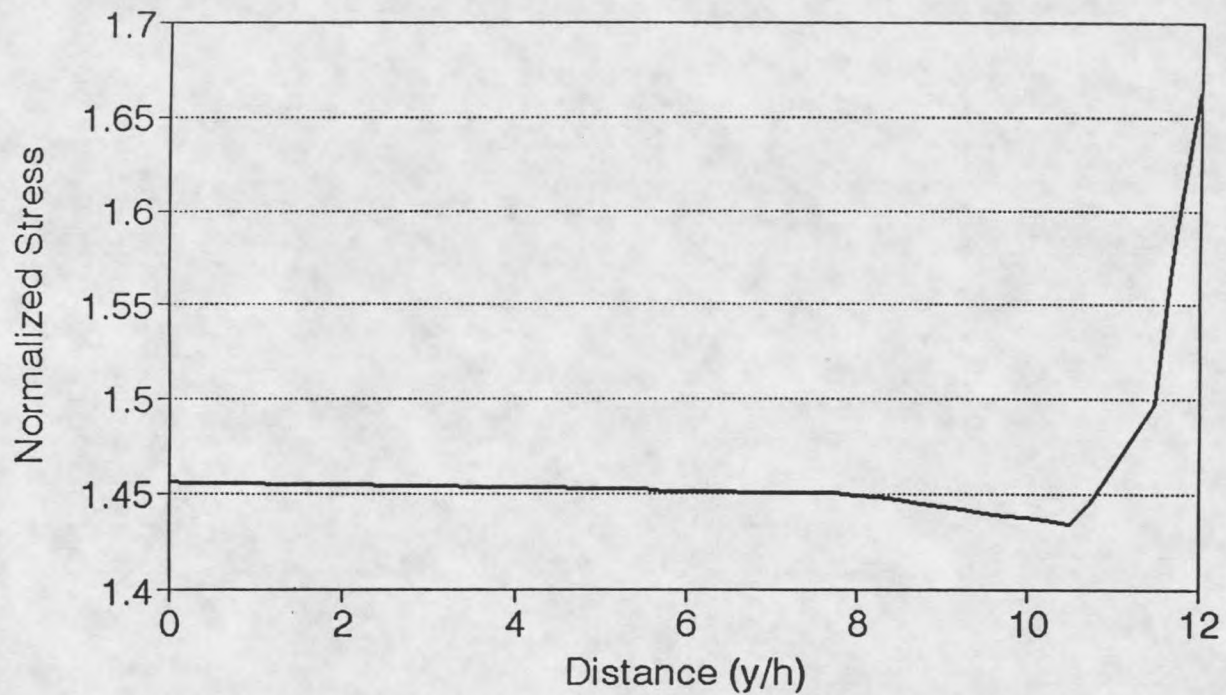


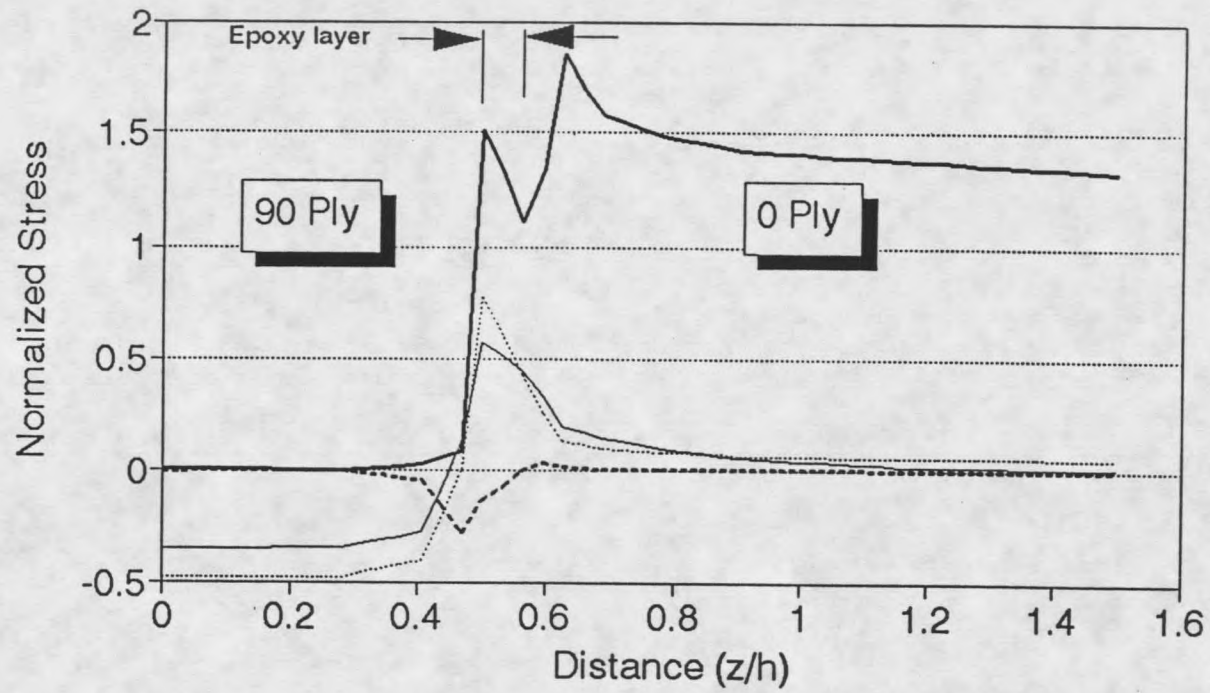
Figure 20. Stresses in the Y direction at the 0/90 Interface (carbon/epoxy laminate)



(No epoxy layer between plies)

— Sy

Figure 21. Stress in the Y direction in the 0° Ply (carbon/epoxy laminate).



(Epoxy layer between plies is not cracked)

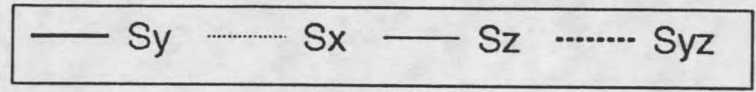
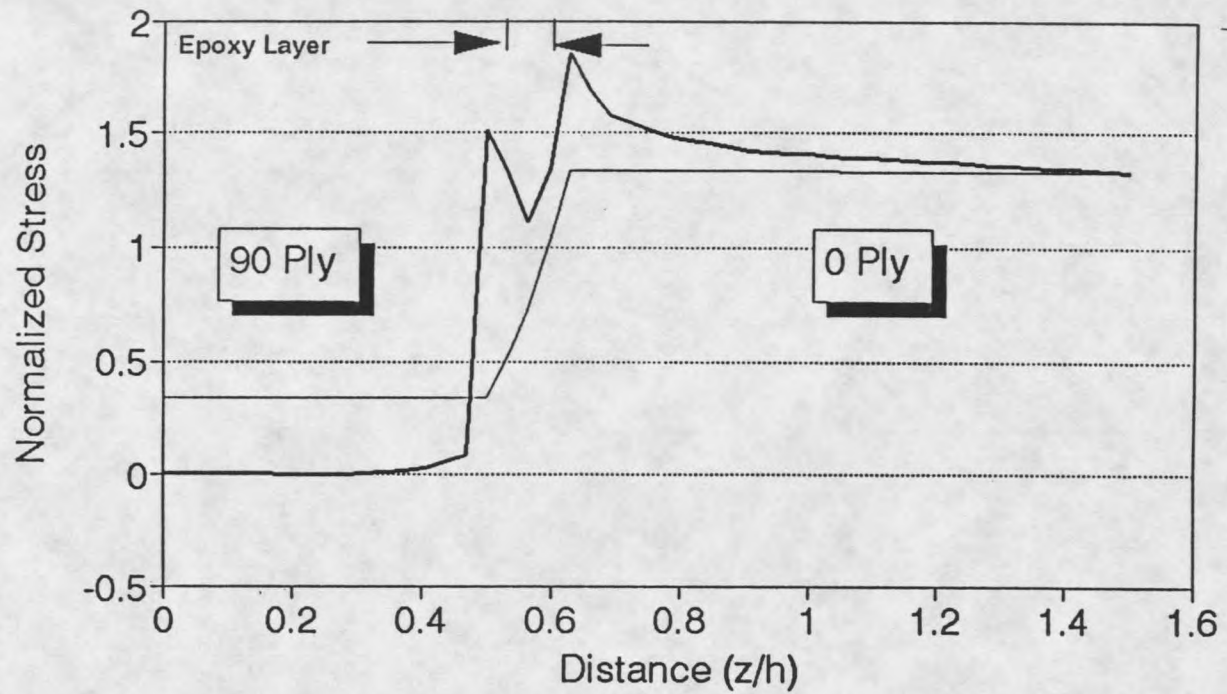


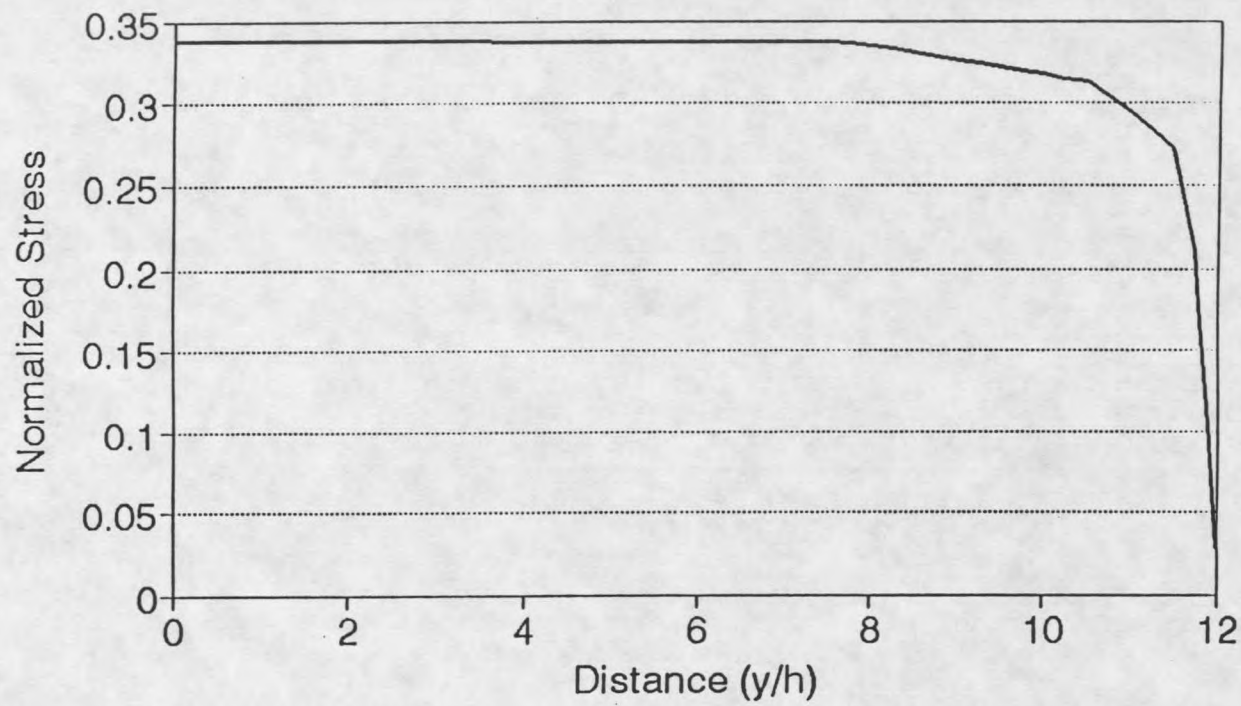
Figure 22. Through-thickness Stresses. [0/90/0] Glass/Epoxy Laminate.



(Epoxy layer between plies is not cracked)

— Sy Far-field — Sy at crack

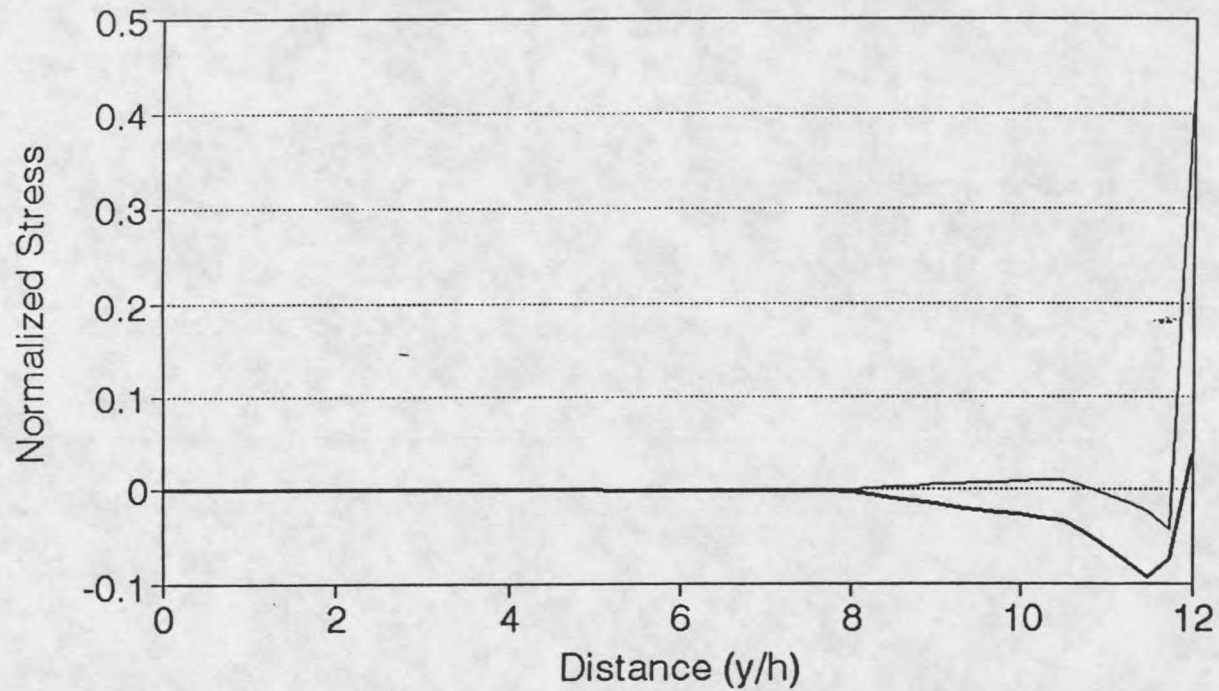
Figure 23. Through-thickness Stresses - Comparison (glass/epoxy laminate).



(Epoxy layer between plies is not cracked)

— Sy

Figure 24. Stress in the Y direction in the 90⁰ Ply (glass/epoxy laminate).



(Epoxy layer between plies is not cracked)

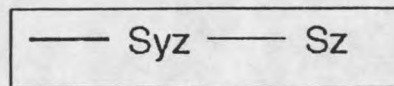
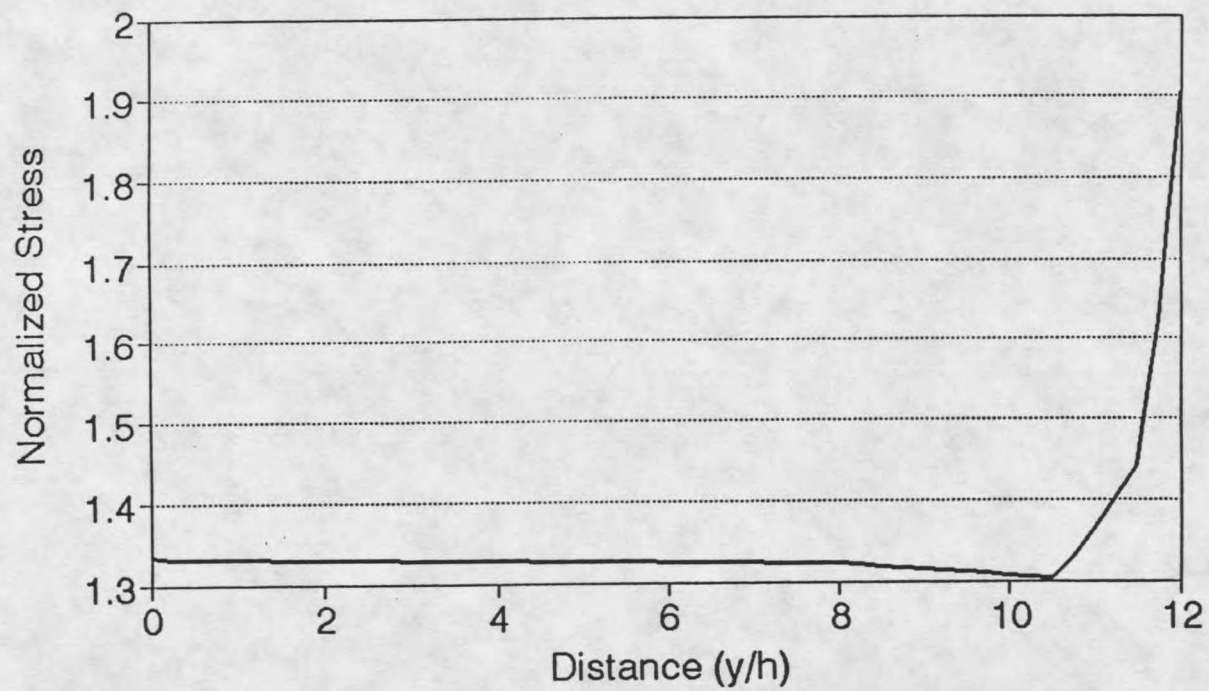
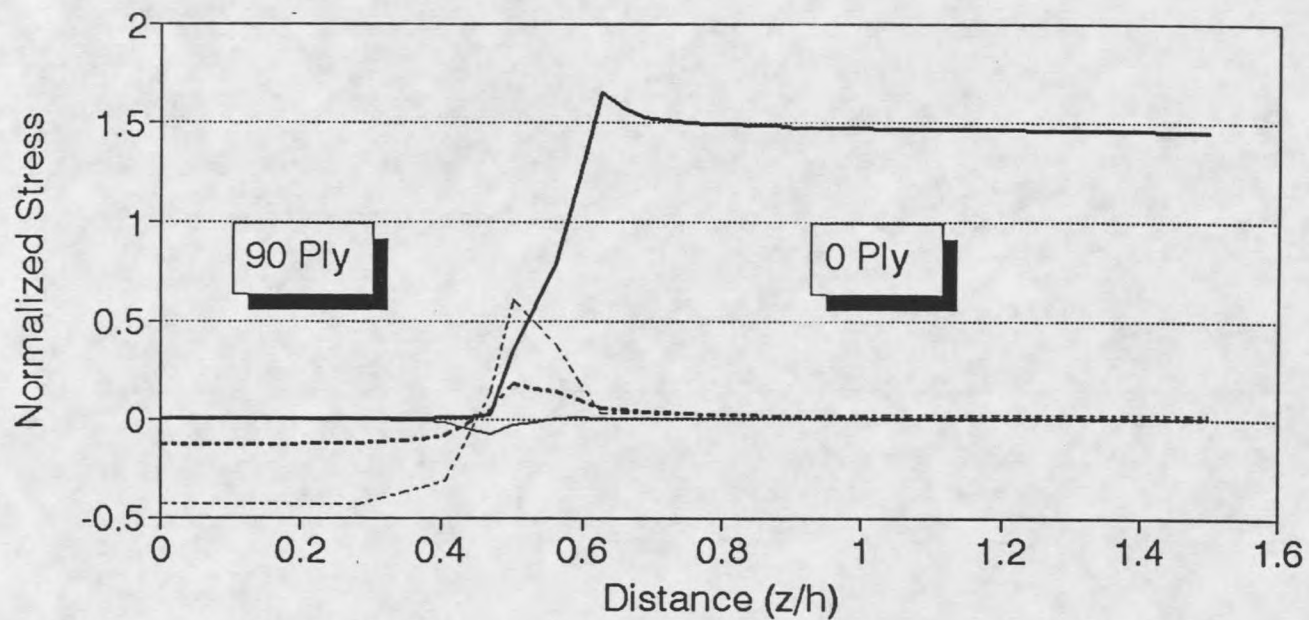


Figure 25. Stresses in the Y direction at the 0/90 Interface (glass/epoxy laminate).



(Epoxy layer between plies is not cracked)

Figure 26. Stress in the Y direction in the 0° Ply (glass/epoxy laminate).



(Epoxy layer between plies is not cracked)

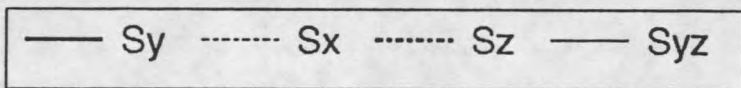
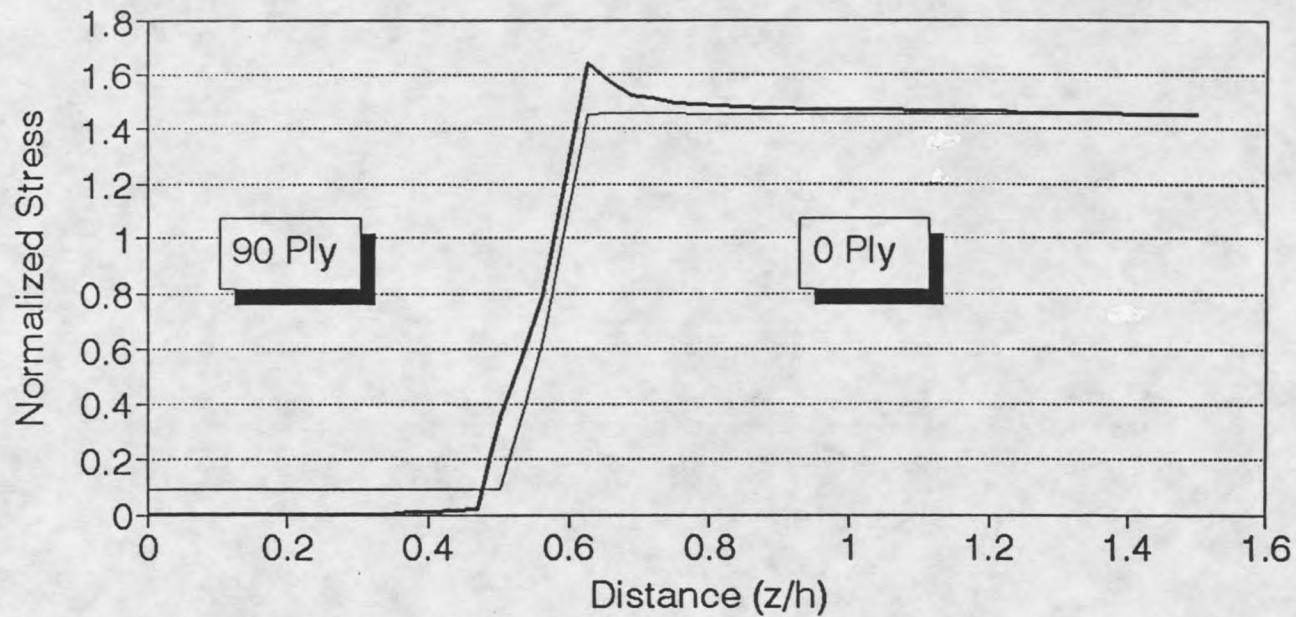


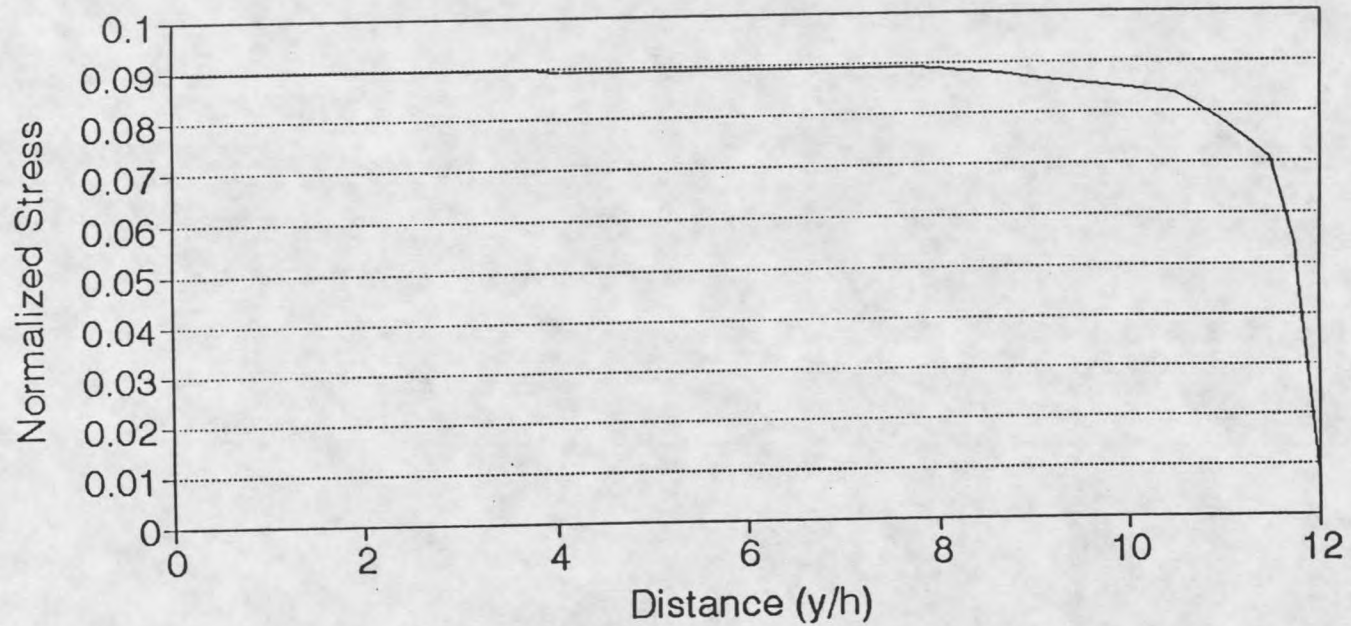
Figure 27. Through-thickness Stresses at the Crack (carbon/epoxy laminate).



(Epoxy layer between plies is not cracked)

— Sy Far-field — Sy at Crack

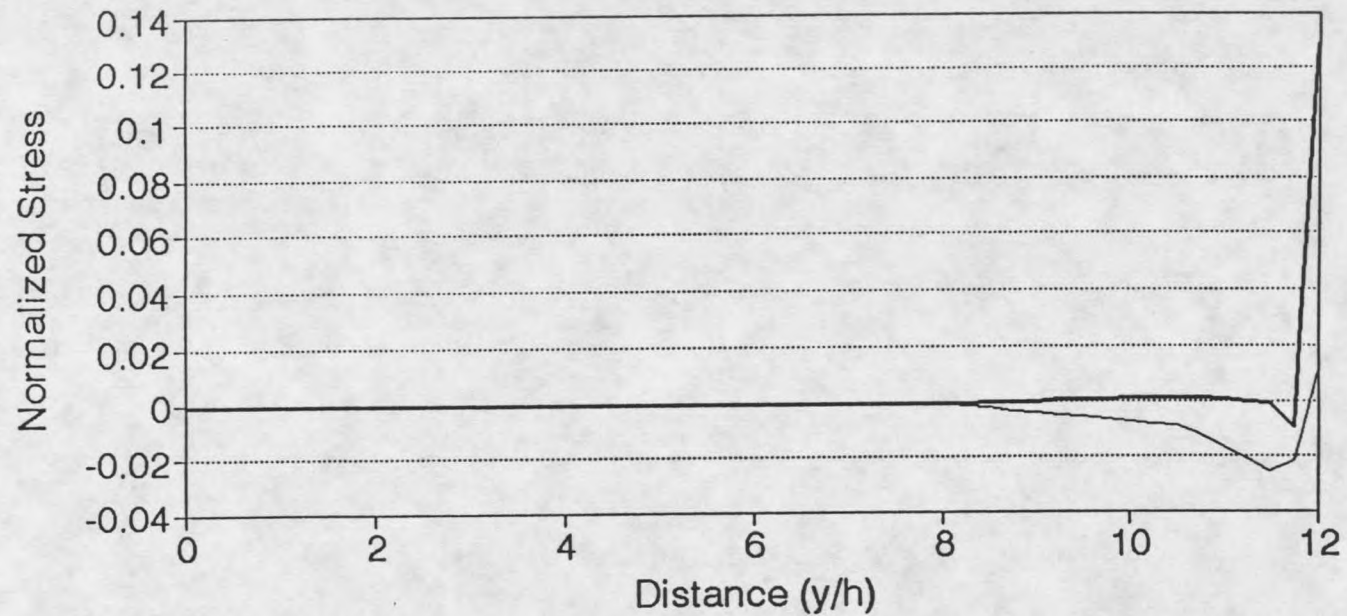
Figure 28. Through-thickness Stresses - Comparison (carbon/epoxy laminate).



(Epoxy layer between plies is not cracked)

— Sy

Figure 29. Stress in the Y direction in the 90° Ply (carbon/epoxy laminate).



(Epoxy layer between plies is not cracked)

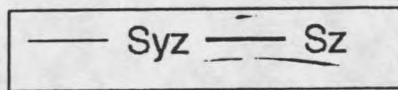
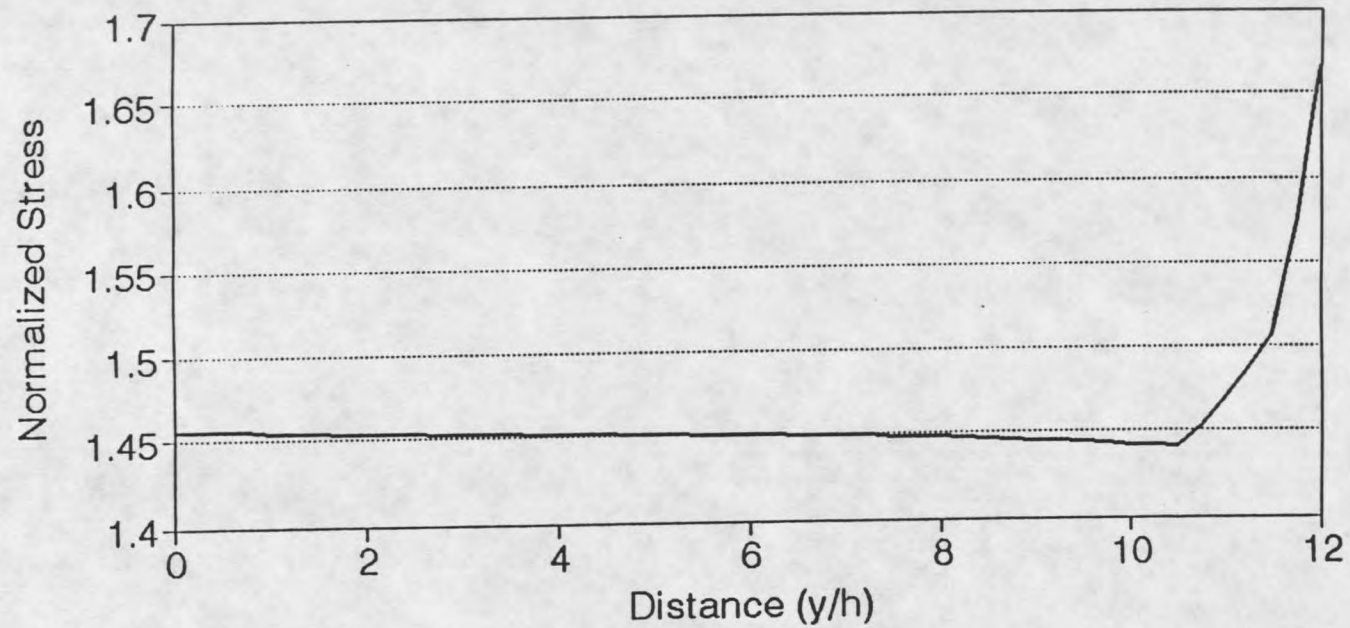


Figure 30. Stresses in the Y direction at the 0/90 Interface (carbon/epoxy laminate)



(Epoxy layer between plies is not cracked)

— Sy

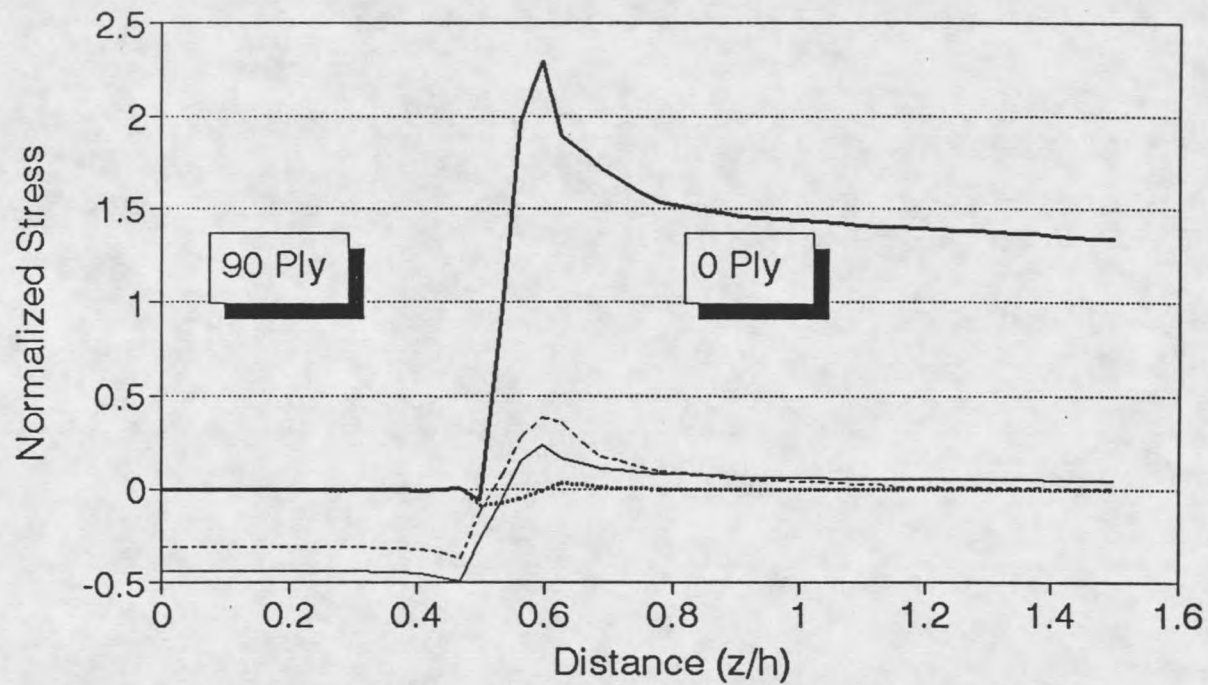
Figure 31. Stress in the Y direction in the 0° Ply (carbon/epoxy laminate).

epoxy layer is less than $h/10$ thick, but plays an important role in lowering the stresses around the crack near the ply interface.

The interlaminar shear and normal stresses, S_{yz} and S_z , are not very different from the case when there is no epoxy layer between plies. This is interesting because the epoxy layer only seems to lower the S_y stress concentration near the plies and not other stress values. The interlaminar stresses responsible for delamination seem unaltered by the presence of the epoxy layer. The normal stresses in the plies along the length of the laminate follow a similar trend as the models with no epoxy layer.

Now let us consider models where the epoxy layer is cracked, as is frequently observed in experiments. Certain interesting differences were observed for these models as compared to models without a cracked layer.

First, in the glass/epoxy laminate with a cracked layer, S_y increased from a maximum normalized stress value of about 1.8 to 2.3 (refer Figures 23 and 32), while the interlaminar stresses S_{yz} and S_z decreased (Figure 25 vs. 35). In fact, S_{yz} was practically absent in the model with a cracked layer. S_y increased for the glass/epoxy case because an epoxy layer that is not cracked will be carrying some load and this load will be transferred to the 0° ply in a laminate with a cracked layer. In the carbon/epoxy laminate with a cracked layer, a similar trend was observed as regards to the interlaminar stresses (Figure 30 vs. 40), but the normal stress S_y did not show any significant change. This again may be due to the fact that the 90° ply was not carrying much load, so the effect of its cracking



(Epoxy layer between plies is cracked)

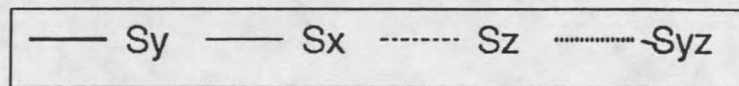
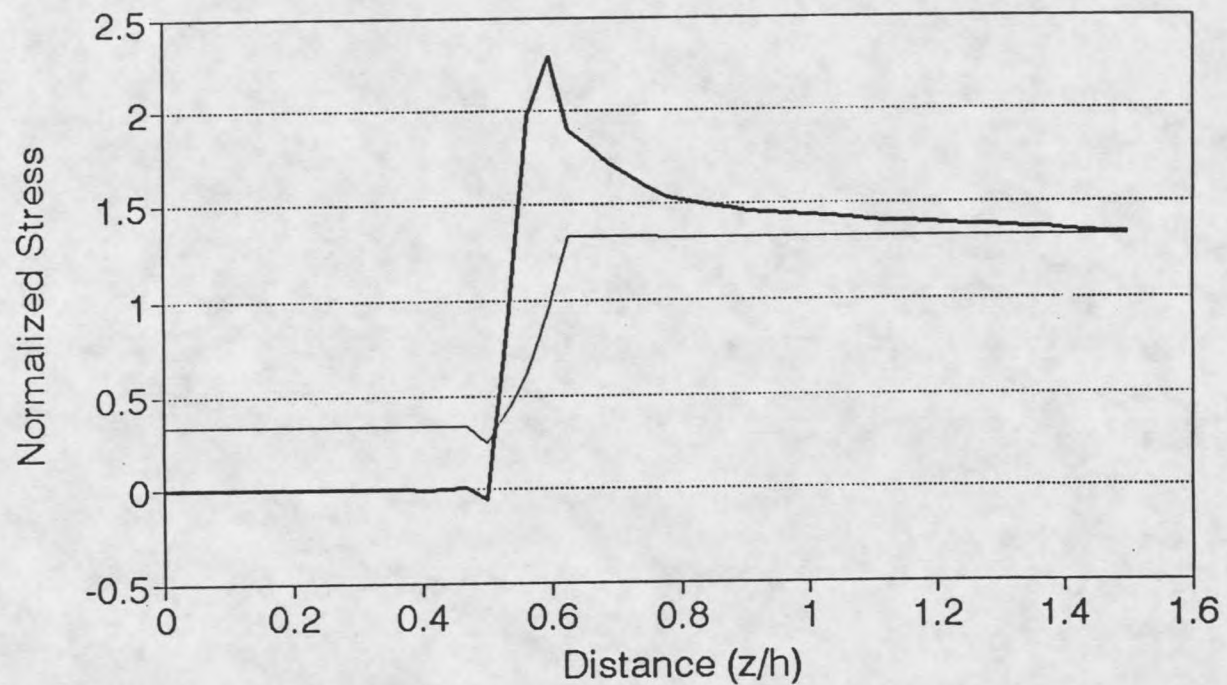


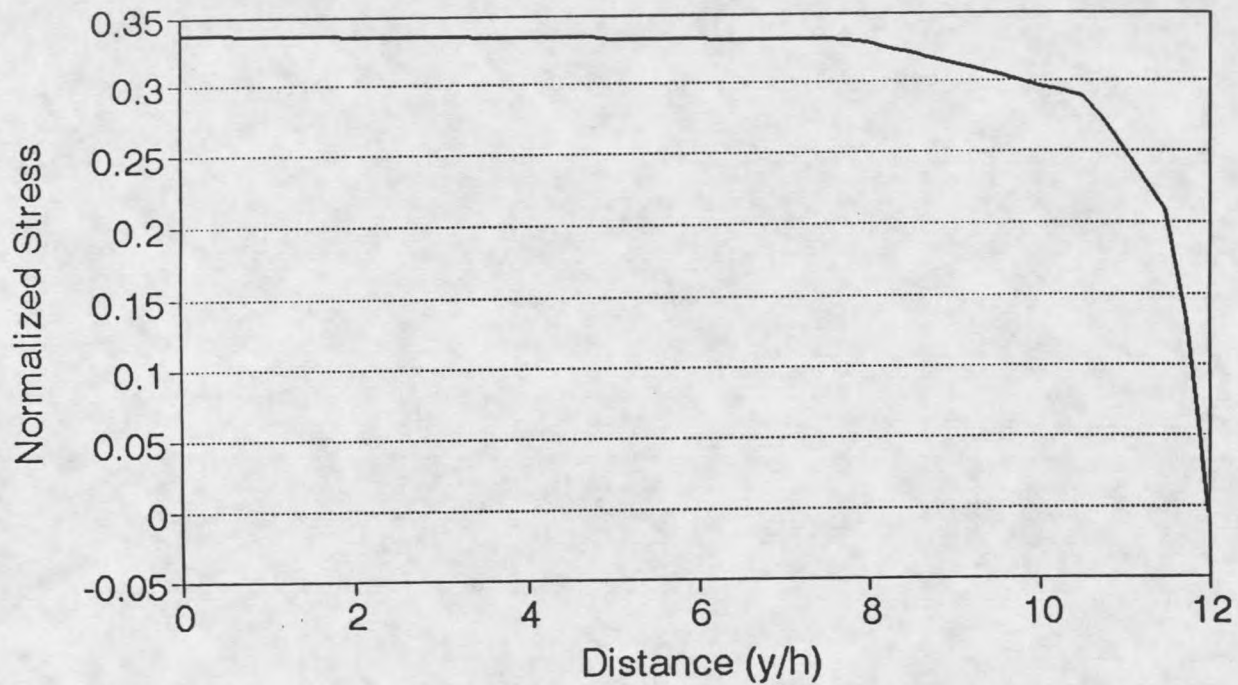
Figure 32. Through-thickness Stresses. [0/90/0] Glass/Epoxy Laminate.



(Epoxy layer between plies is cracked)

— Sy at Crack — Sy Far-field

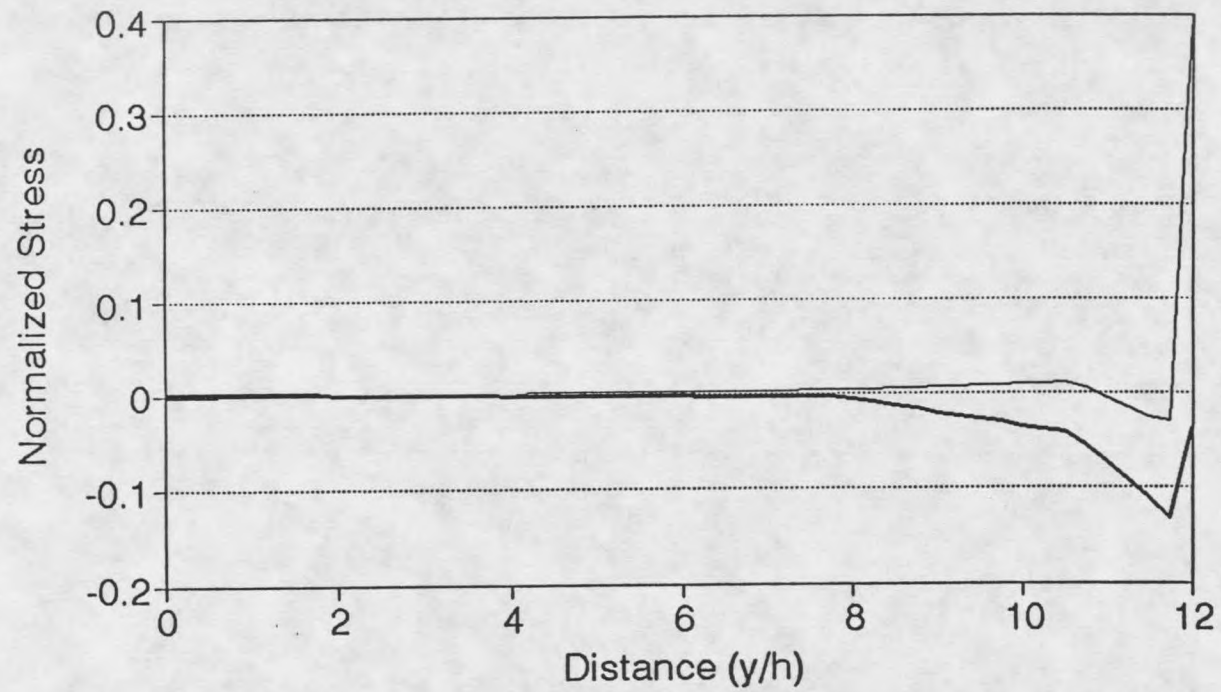
Figure 33. Through-thickness Stresses - Comparison (glass/epoxy laminate).



(Epoxy layer between plies is cracked)

— Sy

Figure 34. Stress in the Y direction in the 90° Ply (glass/epoxy laminate).



(Epoxy layer between plies is cracked)

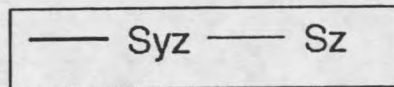
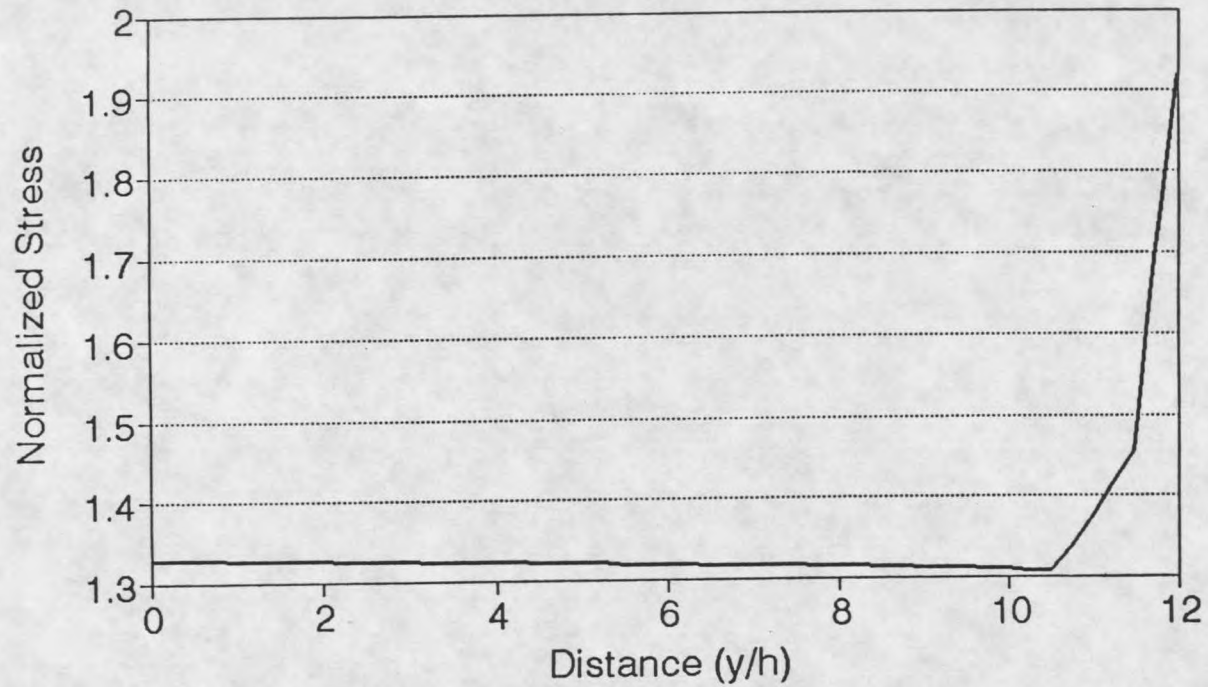


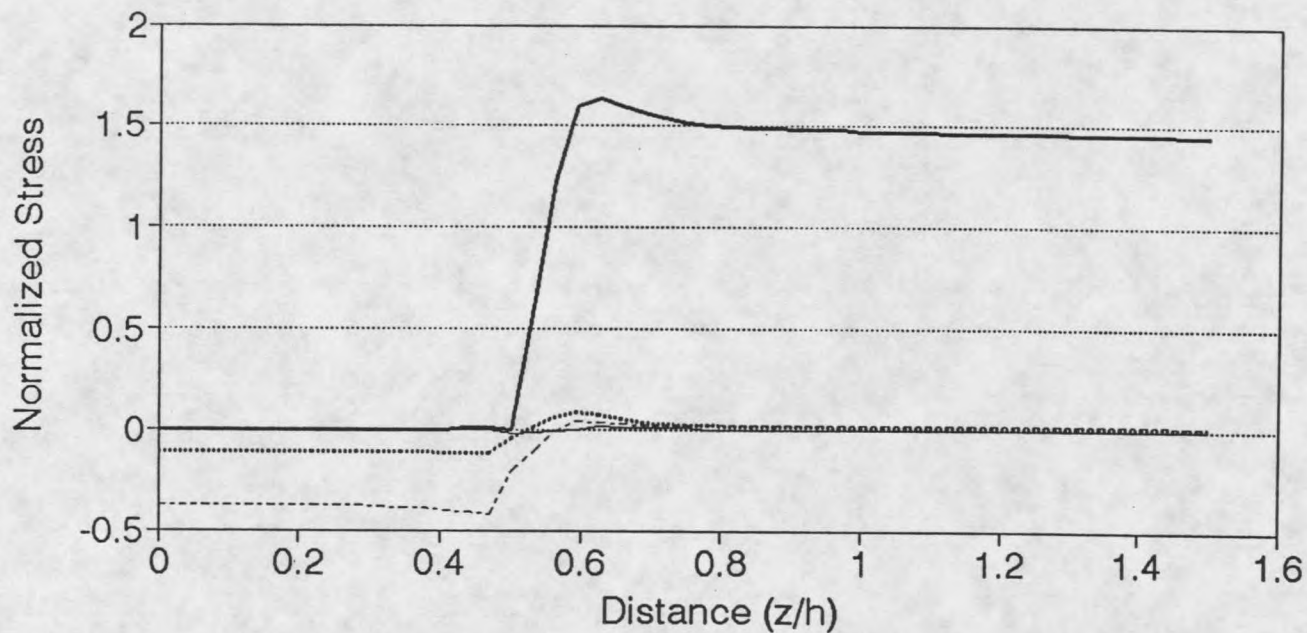
Figure 35. Stresses in the Y direction at the 0/90 Interface (glass/epoxy laminate).



(Epoxy layer between plies is cracked)

— Sy

Figure 36. Stress in the Y direction in the 0° Ply (glass/epoxy laminate).



(Epoxy layer between plies is cracked)

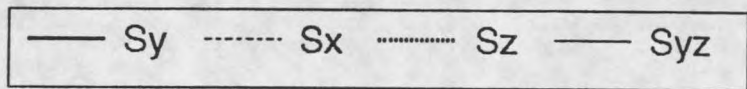
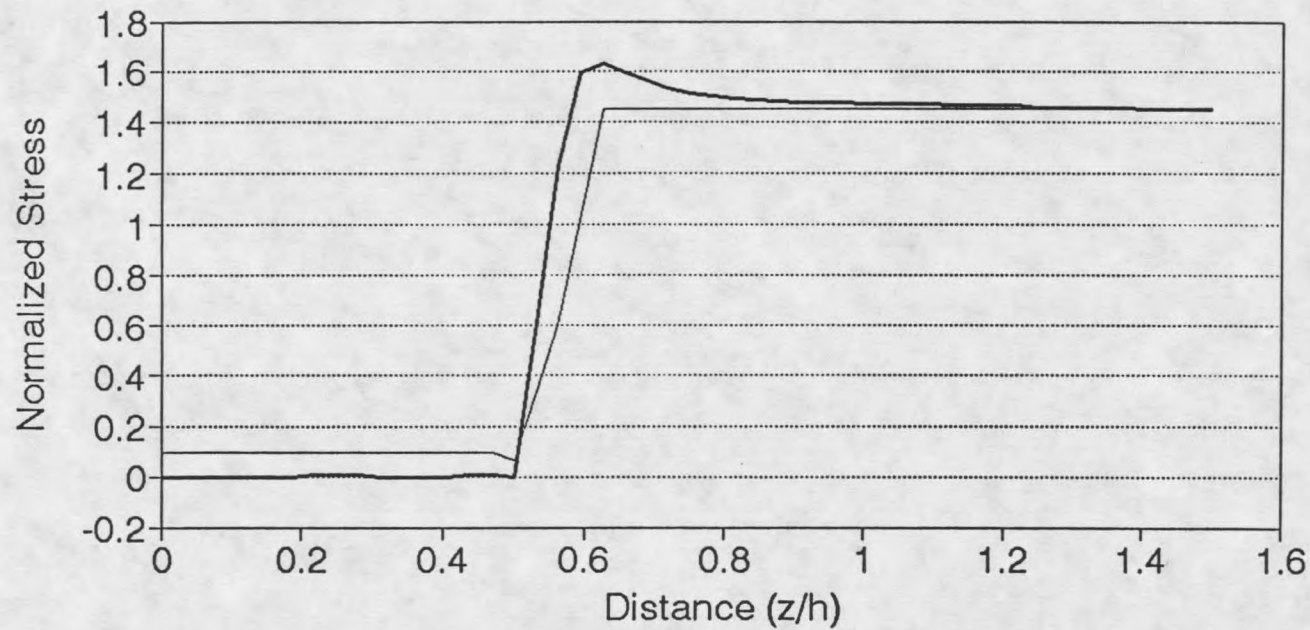


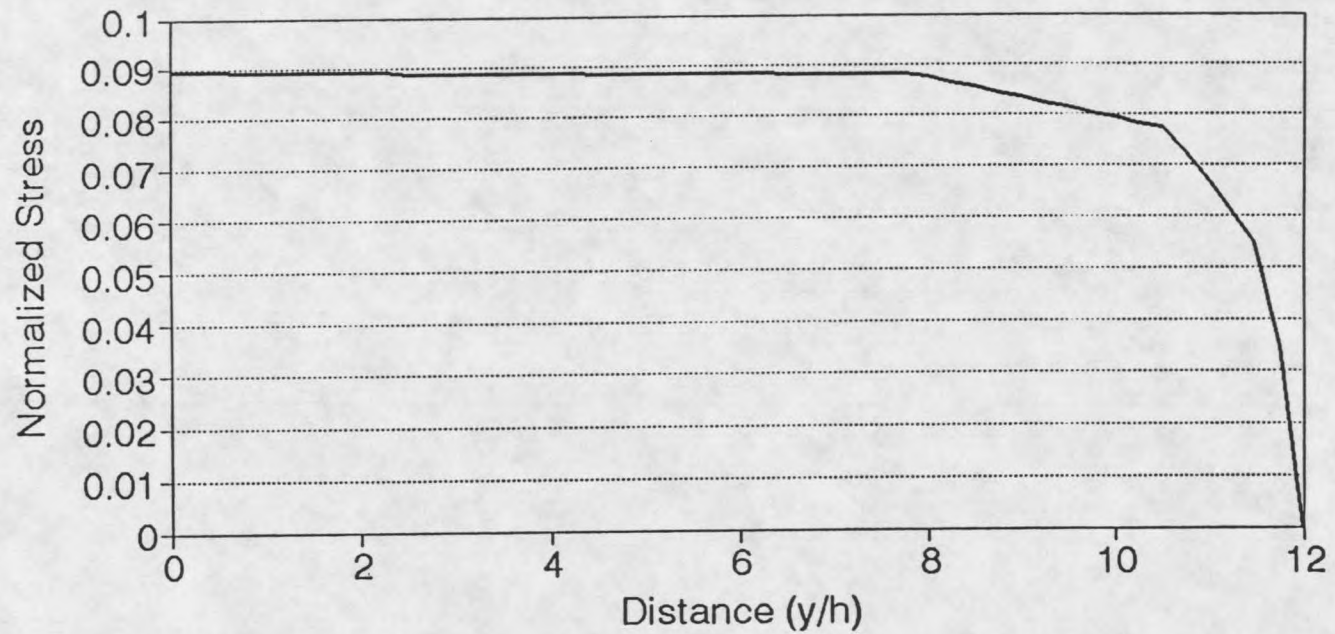
Figure 37. Through-thickness Stresses at the Crack (carbon/epoxy laminate).



(Epoxy layer between plies is cracked)

— Sy Far-field — Sy at Crack

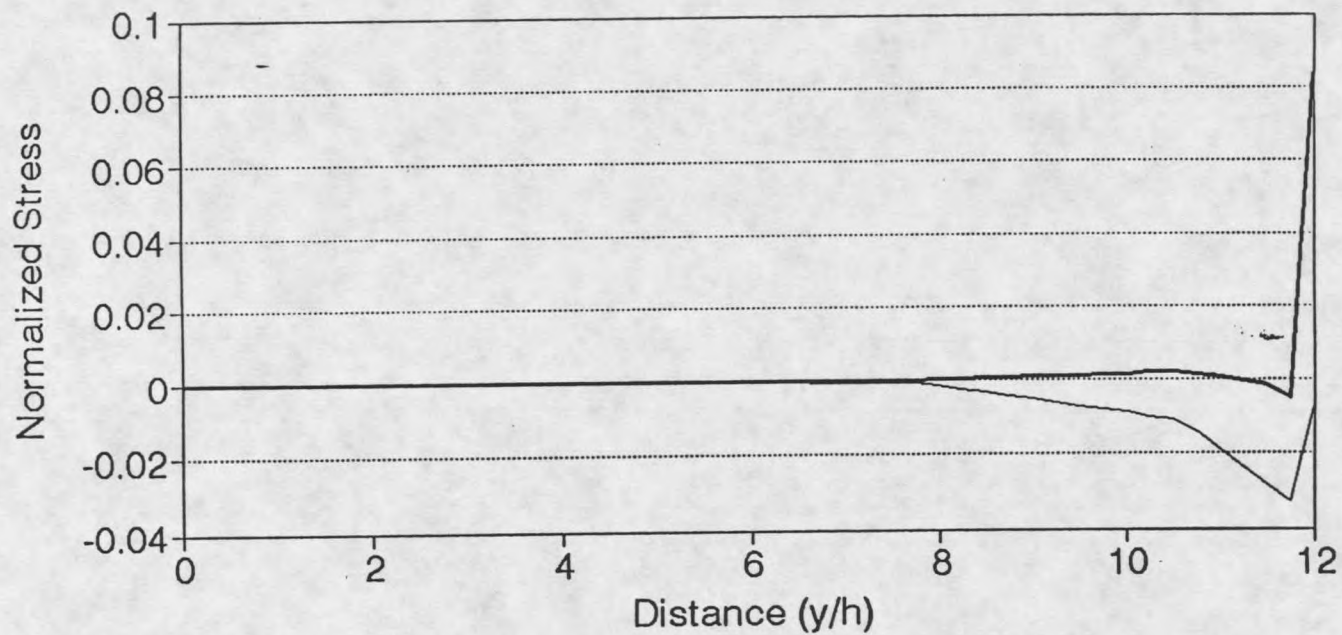
Figure 38. Through-thickness Stresses - Comparison (carbon/epoxy laminate).



(Epoxy layer between plies is cracked)

— Sy

Figure 39. Stress in the Y direction in the 90⁰ Ply (carbon/epoxy laminate).



(Epoxy layer between plies is cracked)

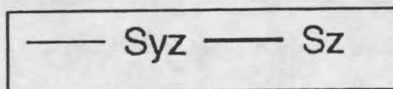
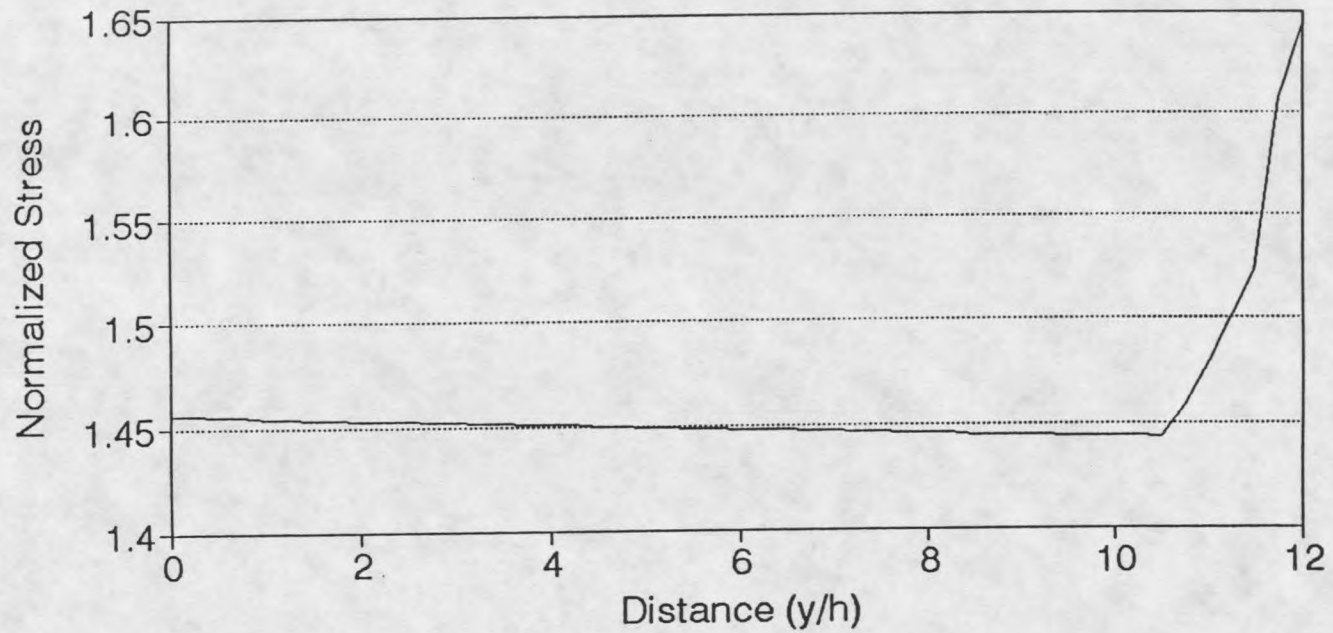


Figure 40. Stresses in the Y direction at the 0/90 Interface (carbon/epoxy laminate)



(Epoxy layer between plies is cracked)

— Sy

Figure 41. Stress in the Y direction in the 0° Ply (carbon/epoxy laminate).

on the S_y stress in the 0° ply is not significant. So, a cracked epoxy layer does help reduce the interlaminar peeling stresses responsible for delamination in a laminate. The reduction is more substantial for S_{yz} than S_z . In the carbon/epoxy laminate, much of the increase in S_y in the 0° ply was within a distance of $0.1h$, while in the glass/epoxy laminate, the corresponding distance was $0.2h$. The stresses in the 0° ply and 90° ply in laminates with a cracked epoxy layer followed trends similar to other models. The load was transferred to the 0° ply from the cracked 90° ply over almost the same distance in both the carbon/epoxy and glass/epoxy models.

Summary

The models with no epoxy layer between plies have the highest stress concentrations around the crack and higher stress gradients. The stress concentrations around the crack for carbon/epoxy models were lower than those for corresponding glass/epoxy models. Less load is transferred to the 0° plies for the carbon/epoxy models than the glass/epoxy models. Having an epoxy layer between plies reduces the 0° ply stress concentration considerably. The interlaminar stresses (S_{yz} in particular) around the cracks are lowered when the epoxy layer between plies is cracked instead of having a layer that is not cracked.

The results given here for the effects of the matrix layer between plies strongly support empirical findings in this area. In wind turbine blade materials, when the 0° ply strands are tightly stitched to the adjacent off-axis layer strands,

behavior in fatigue is poor. Matrix cracking in the off-axis material then produces failure of the 0^0 strands [26] (see Figure 42). The findings in this chapter indicate that eliminating the soft matrix between 0^0 and off-axis material causes a much greater stress concentration in the 0^0 material if the off-axis material is cracked.

CHAPTER 4

ANALYSIS OF [0/90/0] LAMINATES WITH A DISCRETE HIGH FIBER STRAND

Introduction

There is a class of materials called 'triax' that has strands of fiber oriented in three different directions, stitched together (like 0, +45 and -45). These materials are used in the manufacture of wind turbine blades. These fiber strands are regions of high fiber volume fraction, V_f . They carry higher load than any other region of the laminate by virtue of their higher elastic modulus in the direction of applied load. This chapter examines the stress fields around the high fiber region of [0/90/0] glass/epoxy laminates and compares them with the results obtained in Chapter 3. The models in this chapter simulate actual materials more closely than those in Chapter 3.

Model Analyzed

The models analyzed so far are assumed to have homogenous material properties. That is, the material properties can be thought of as being smoothly 'smeared' in each ply. This is not the case with real laminates, particularly for materials used in typical wind turbines. These laminates are very non-homogenous. Each ply has high modulus fiber strands stitched together, mixed with low modulus epoxy or other matrix materials. Figure 42 shows a photo-micrograph of cracked 0° strands in a typical wind turbine blade material [25]. The individual strands are

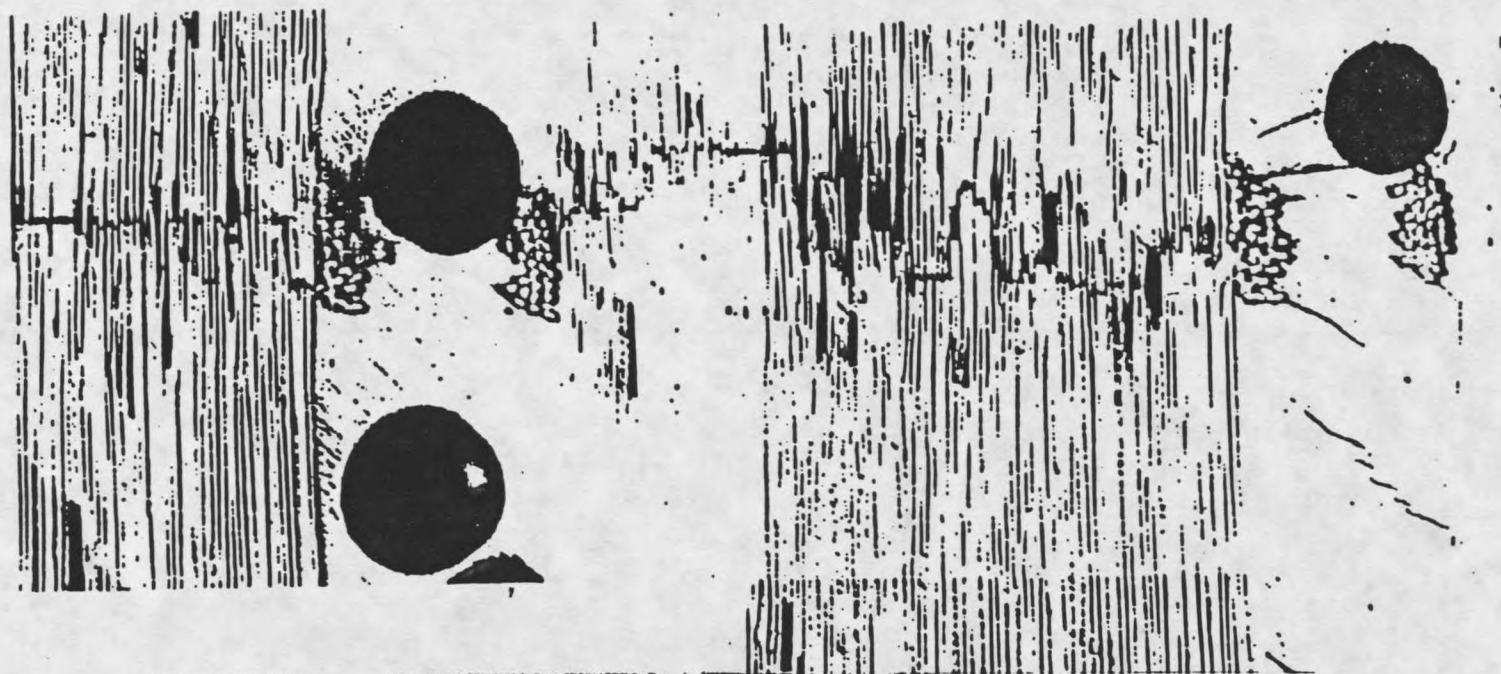


Figure 42. Cracking in the 0° ply of $[0/+45]$, Triax glass/polyester Wind Turbine blade material, showing high fiber content strands with matrix in between [25] .

evident, as are several pores and matrix cracks, and stitching material adjacent to the strands. Material properties vary greatly depending on the exact location in the ply. Even though the macro behavior of a laminate can be modelled to a reasonable degree of accuracy by assuming homogenous properties for each lamina, the nature of the stress distribution on a micro scale cannot be modelled precisely with such an assumption. However, modelling individual fibers will lead to an extremely high number of degrees of freedom and will stretch the computing resources for even a modest analysis. So, a compromise model must be defined. An effort was made to build a model with a region that is high in fiber content, adjacent to a low modulus region (epoxy matrix) in the 0^0 ply. The rest of the 0^0 ply has 'smeared' material properties. An attempt was made to study the nature of stresses around this high fiber region. This model does not delineate individual fibers, but has properties consistent with a strand high in fiber volume fraction, V_f . Thus, even though this 0^0 ply does not have homogenous material properties, its properties are 'smeared' in the sub regions. A matrix layer between plies is also included, as described earlier.

The elastic constants assumed for the high fiber content region are

$$E_L = 7.0 \times 10^6 \text{ psi}; \quad E_T = 1.5 \times 10^6 \text{ psi}; \quad G_{LT} = 0.75 \times 10^6 \text{ psi}; \quad \nu_{LT} = 0.25$$

representing a V_f of approximately 0.7. The remainder of the elastic constants are given in Chapter 3. The properties of the high and average fiber content region approximately represent the effect of grouping some of the fibers into a tight

strand, with pure matrix surrounding the strand, while maintaining the same overall fiber content of $V_f=0.5$ assumed in the remainder of the study.

The overall dimensions of this model are the same as the models which have already been analyzed. The difference is only in the 0° ply. This model has an epoxy layer between the 0° and 90° plies. The 90° ply still has homogenous material properties. The crack in the 90° ply extends through the epoxy layer between plies and also through the epoxy region near the high fiber region in the 0° ply. Consequently, the high fiber region is surrounded by the crack on all sides except on the free surface which is an outer face of the laminate. Of particular interest is the corner where the crack in the epoxy layer meets the crack in the epoxy region in the 0° ply. All the corner angles discussed in this chapter refer to this corner. Since two cracks meet here, this corner may be the point of high stress concentration. Different models are built to reduce this corner angle and to round this region as much as possible. The effect of such a reduction in the corner angle will be analyzed. Four models are built with progressively declining corner angles of 90° , 28° , 16° and 10° . The element type used does not permit further reduction in corner angle for this model. Stresses in the model with the least possible corner angle will be discussed in this chapter.

In actual composite laminates with fiber strands, the cross section of the fiber strands is elliptical, and a rounded cross section more accurately models the actual laminate. However, the effect of having a sharp-cornered rectangular high fiber region has to be examined to fully appreciate the nature of the stresses in that

region and their dependence on the shape of the high fiber region. Models with sharp corners will not be analyzed in any greater detail than this aspect, since actual strands are rounded. While it is easier to model strands with a rectangular shape, these results indicate that shape significantly affects the results.

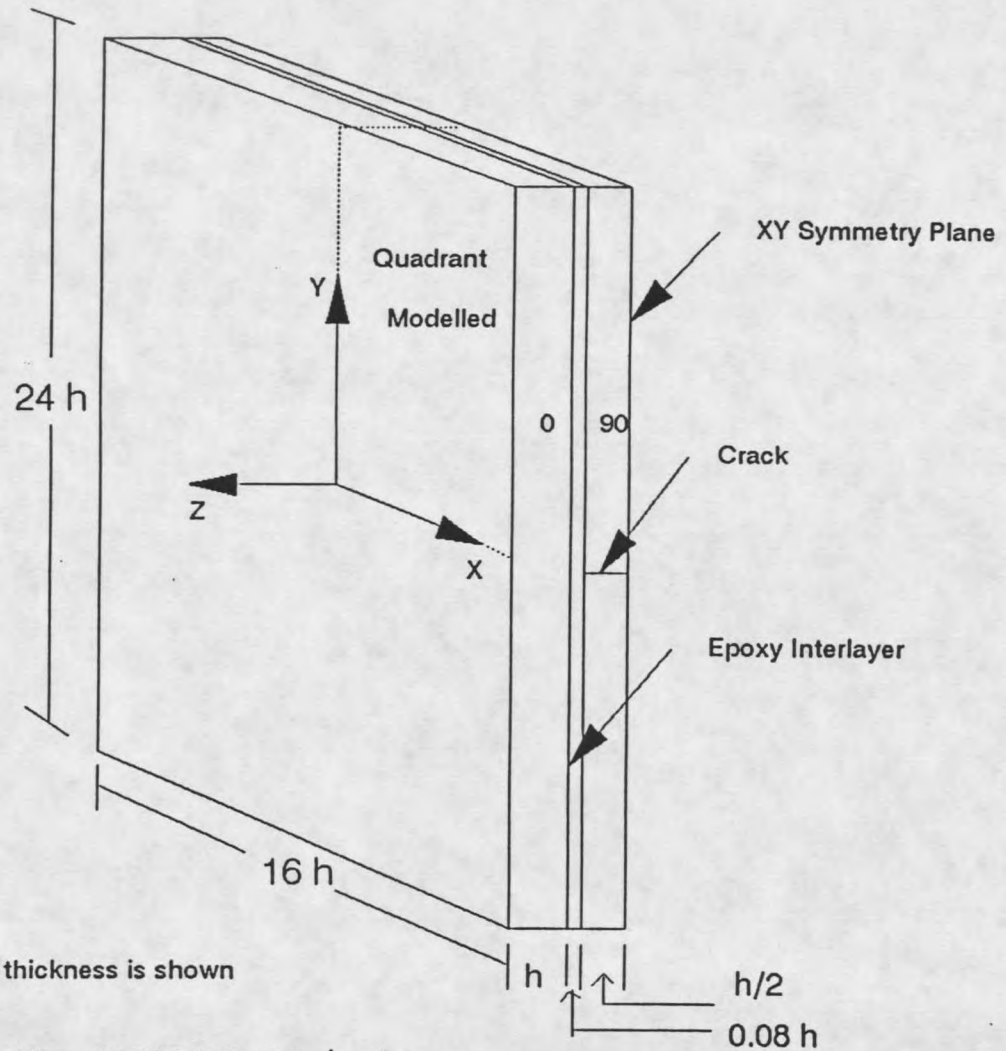
Figure 43 shows the general geometry of the model analyzed. Figures 44 and 45 show the cross section at the crack for models with rectangular and rounded high fiber regions. The crack is situated in the middle of the model which is $24 h$ long. Taking advantage of symmetry, only half the length of the model is analyzed. The following symmetry boundary conditions are imposed

$$U(0,y,z) = 0$$

$$V(x,0,z) = 0$$

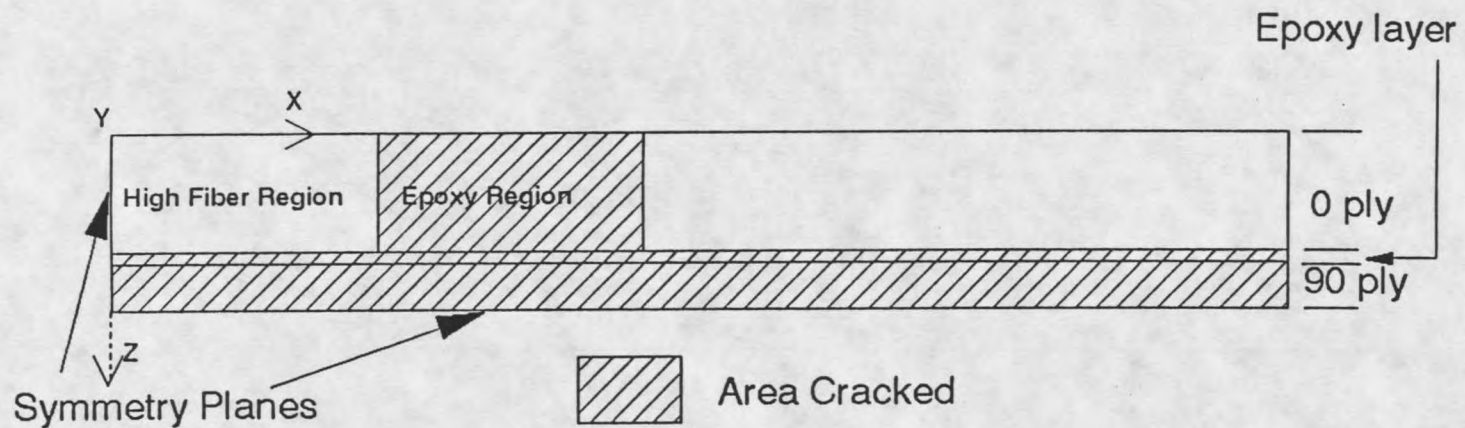
$$W(x,y,0) = 0$$

and the displacement boundary condition at $y = 12 h$ imposes an averaged stress (S_A) of 50,000 psi on the model. All stresses in the figures are normalized by this applied stress. A typical solution in this group contained approximately 20000 degrees of freedom. The smallest element dimensions used were $\approx h/125$. Figure 46 shows the meshing arrangement at a cross section $y = h/250$, which is at the crack. This problem was modelled on an IBM RS/6000 workstation and solved on a CRAY Y-MP.



Note : Only half the laminate thickness is shown
 Figure not to scale.

Figure 43. Model Geometry of the [0/90/0] Laminate.



Note : Only half the laminate thickness is shown

Figure is not to scale

Figure 44. Cross Section of the [0/90/0] Laminate at the Crack - Rectangular High Fiber Region.

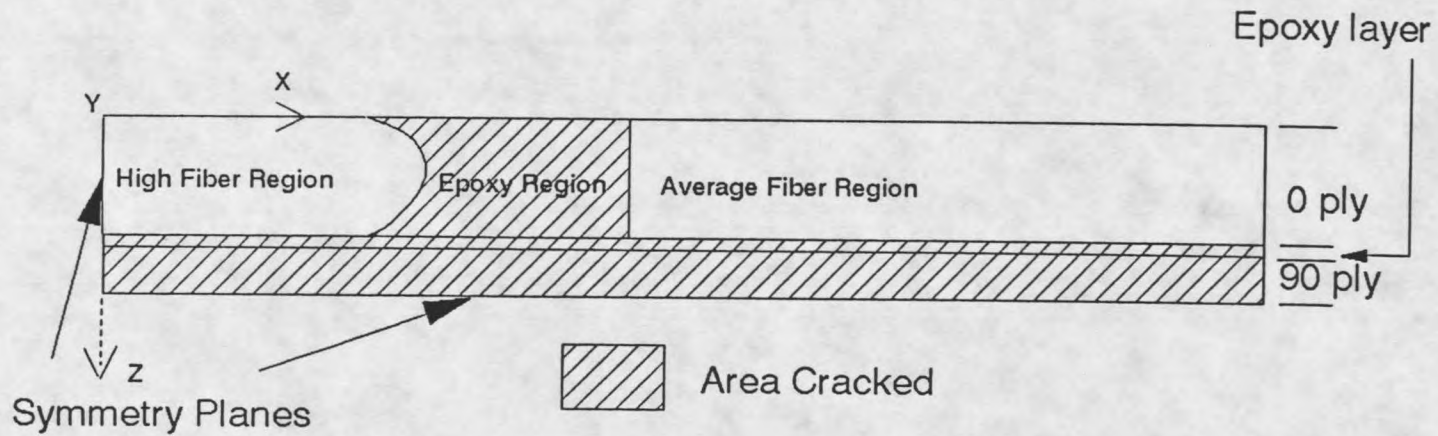
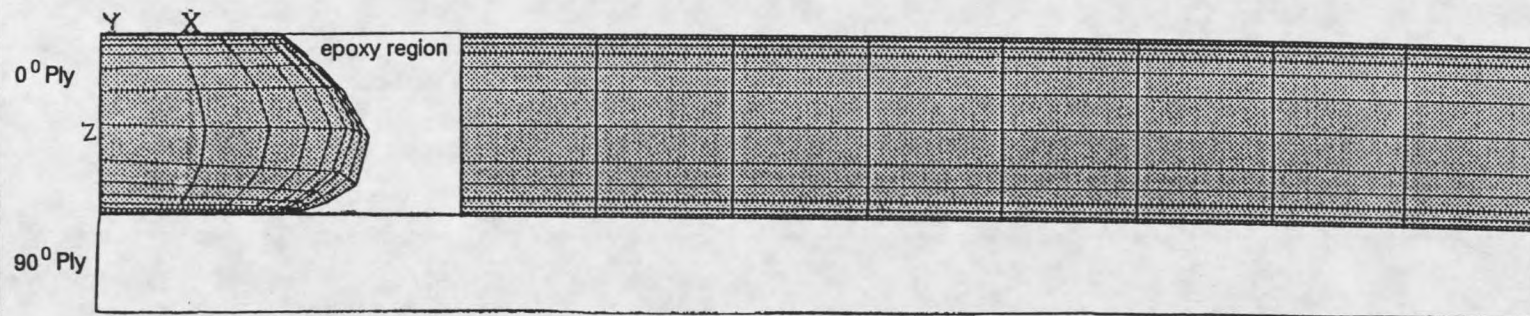


Figure 45. Cross Section of the [0/90/0] Laminate at the Crack - Rounded High Fiber Region.



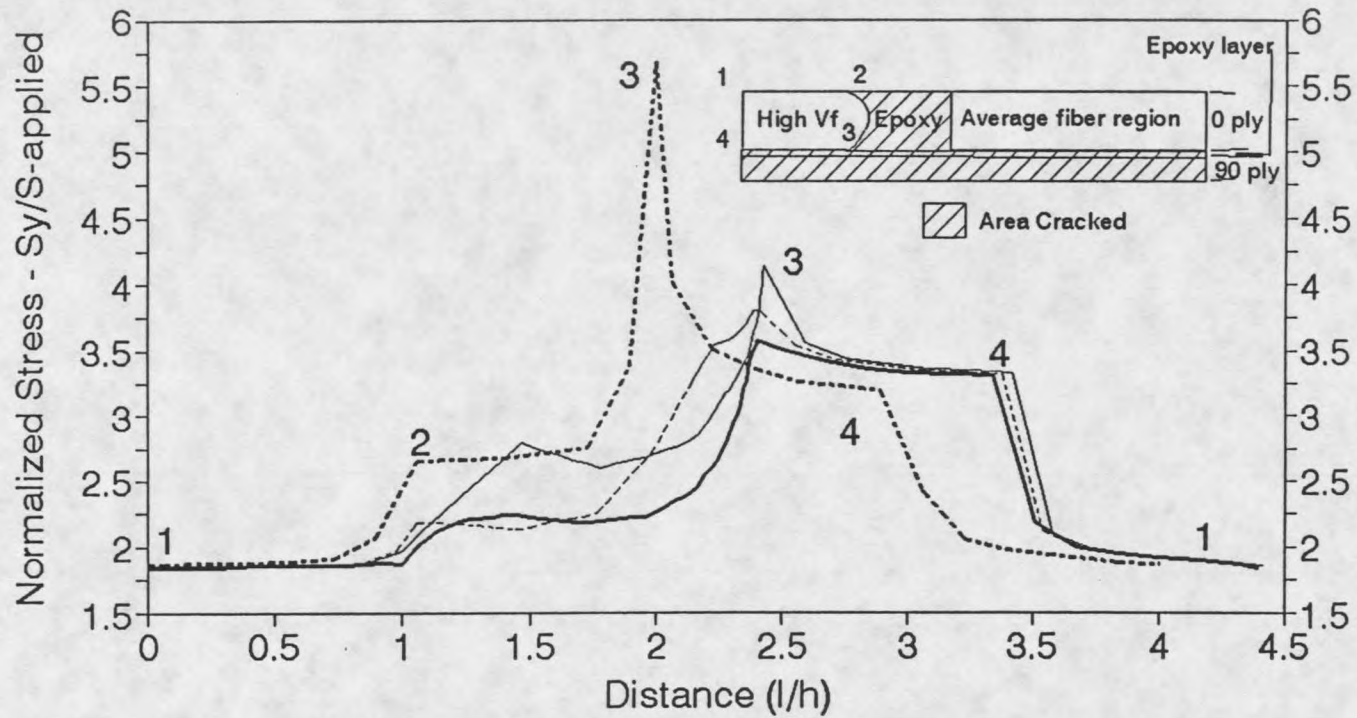
Note: The cross-section shown is at the crack.
Figure is to scale.

Figure 46. Finite Element Mesh at the Crack - Rounded High Fiber Region.

Results and Discussion

The stresses near the corner of the high fiber region for a model with a rectangular high fiber region were very high. The corner in the high fiber region at the intersection of two cracks in the epoxy layer and epoxy region was the site of maximum stress. The corresponding values for models with progressively declining corner angles yielded lower stress values. At the lowest possible corner angle of 10° for the element type selected, the stress spike at the corner essentially flattens out. It is expected that further reductions in this corner angle will not yield significantly lower stress values, as the stress values seem to converge to the value at the flat portion of the curve near the corner. Reducing the corner angle from 90° to 28° yielded a significantly lower stress value.

The inset in all the graphs in this chapter shows the cross section of the laminate at the crack except when stated otherwise. Figure 47 shows the effect of corner angle on the stress value. As can readily be seen, there is a significant reduction in corner stress values as the corner angle is reduced. Corners 2 and 3 are rounded in the high fiber region, and the effects of rounding on the stresses are more pronounced for corner 3 as compared to corner 2. This is so because corner 2 is on a free surface and corner 3 is at the junction of cracks in the epoxy layer and the epoxy region in the 0° ply, which is a point of high stress concentration. On sides 1-2, 3-4 and 4-1, stress values away from corners 2 and 3 are more or less the same. Side 3-4 carries a higher average stress than any other side. This is because the adjacent 90° ply is cracked and all the load is



Note : The distance 'l' is plotted around the high fiber region starting at point (1) on the inset diagram, and proceeding clockwise.

Corner angle at (3)

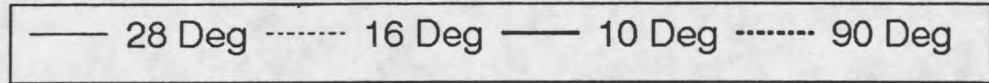


Figure 47. Stresses around the High Fiber Region - Effect of Corner Angle.

transferred to the 0^0 ply through the 0 /epoxy layer interface, and side 3-4 lies on this interface. In the Figure 47, l refers to the distance along the sides 1-2-3-4 from the starting point 1. For the model with rectangular high fiber region, the total length of the four sides is $4h$, while it is slightly more than that for the models with rounded high fiber region (this represents half of the symmetric strand width). This is also the reason why the plot for the model with corner angle 90^0 is shifted to the left. This is done to ensure that corners 1,2,3 and 4 are not disturbed and the stresses at the corners are at exactly the same points for all the models. The only side that changes with corner angle is side 2-3.

Now let us examine the stresses through the thickness of the laminate. Figure 48 shows the stresses passing through the high fiber region. Points 1, 2 and 3 are on the YZ symmetric plane. So, in the actual laminate, 1-2-3 divides the high fiber region in half. Load is transferred to the 0^0 ply from the cracked 90^0 ply at point 2, and S_y reaches a rather high normalized value of about 3.6 and slowly drops to far-field values away from 2. Compare this with a similar plot (Figure 49) through the average fiber region. Points 1, 2 and 3 here, pass through a line which divides the average fiber region in half. These two plots follow the same trend, but S_y values are substantially lower at point 2 in this case. The interlaminar stresses S_{yz} and S_z are about the same for both the cases. Since the properties used for the average fiber region are the same as those for glass/epoxy laminate used in Chapter 3, let us compare the through thickness stresses in the average fiber region with those for a glass/epoxy laminate with a cracked epoxy layer. In Figure

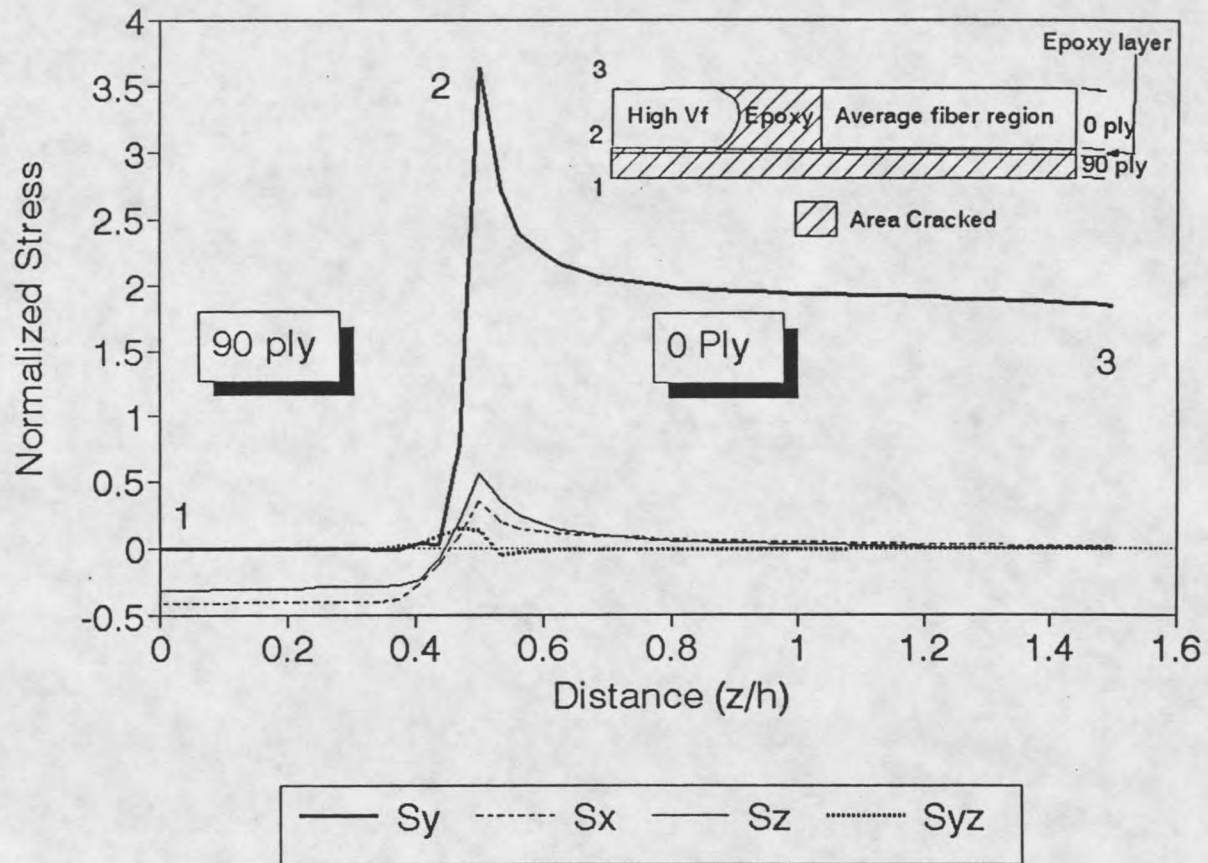


Figure 48. Through-thickness Stresses in the High Fiber Region.

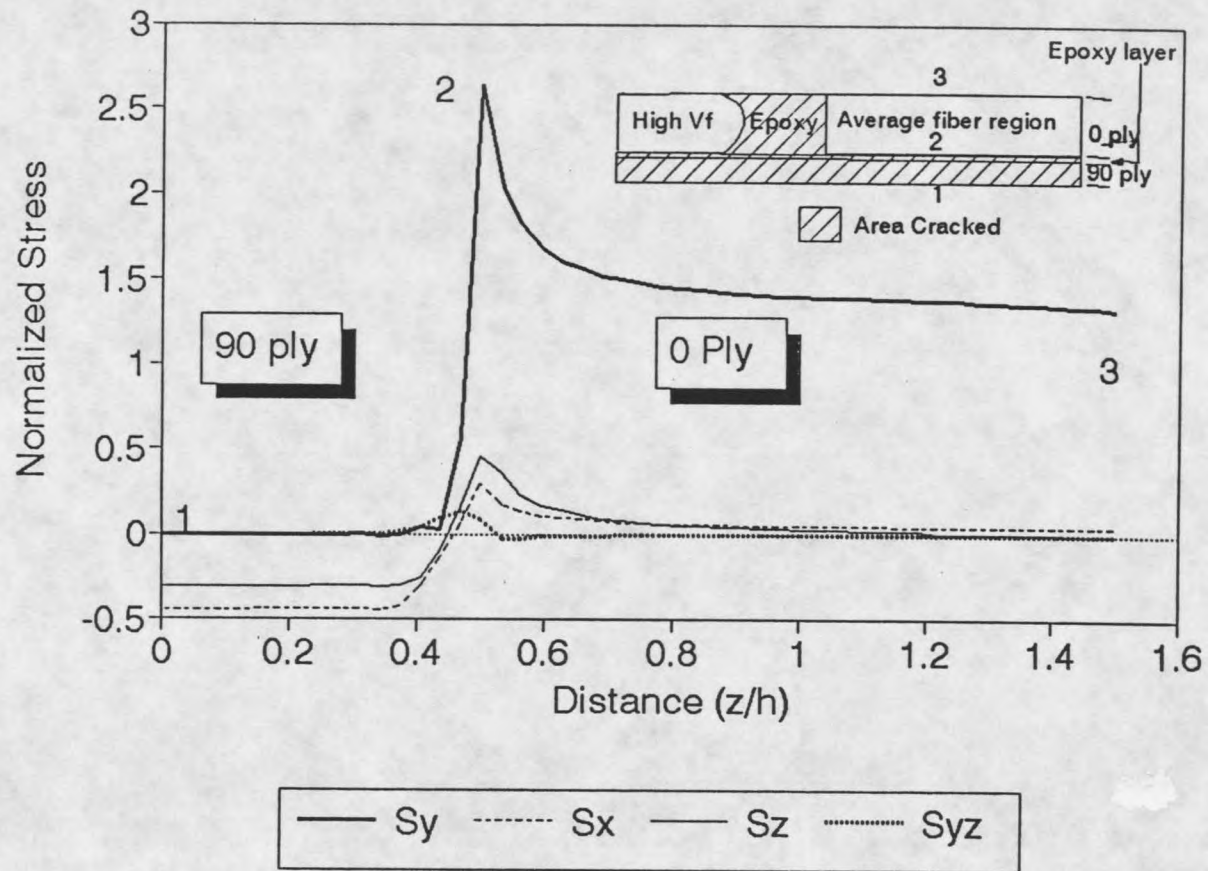


Figure 49. Through-thickness Stresses in the Average Fiber Region.

49, the maximum S_y stress is about 0.3 lower than the maximum in Figure 32 (2.3 vs. 2.6). Having a discrete high fiber region and a cracked epoxy region in the 0^0 ply does play a part in raising the S_y value in the 0^0 ply. In Figure 32, the laminate does not have any crack in the 0^0 ply and the properties are homogenous within the ply. These are two critical differences from our present model. The mesh for the two cases also differs in this region, with the smallest element dimension being $h/125$ in the high fiber region and $h/62$ in the average fiber region, as opposed to $h/25$ for the model in Chapter 3.

The interlaminar stresses are not different from the model with homogenous material properties. This is important because, having a discrete high fiber region does not make any difference in these stresses and thus will not have much effect on future delaminations based on interlaminar stresses. However, these stresses are probably high enough to cause delamination even at moderate stresses in both cases.

Figure 50 shows the stresses along the width of the laminate in the 0^0 ply. Points 1, 2, 3 and 4 are on a line which divides the 0^0 ply in half. Note the slight rise in S_y in the high fiber region near the cracked epoxy region. The same rise in S_y is much more gradual in the average fiber region. Also, there is a significant difference in S_y levels in the high and average fiber regions. This is due to the difference in their moduli, as the far-field strains in the y -direction are constant across the width. The interlaminar stresses S_{yz} and S_z are not significant because the plot is along a line away from the ply interface.

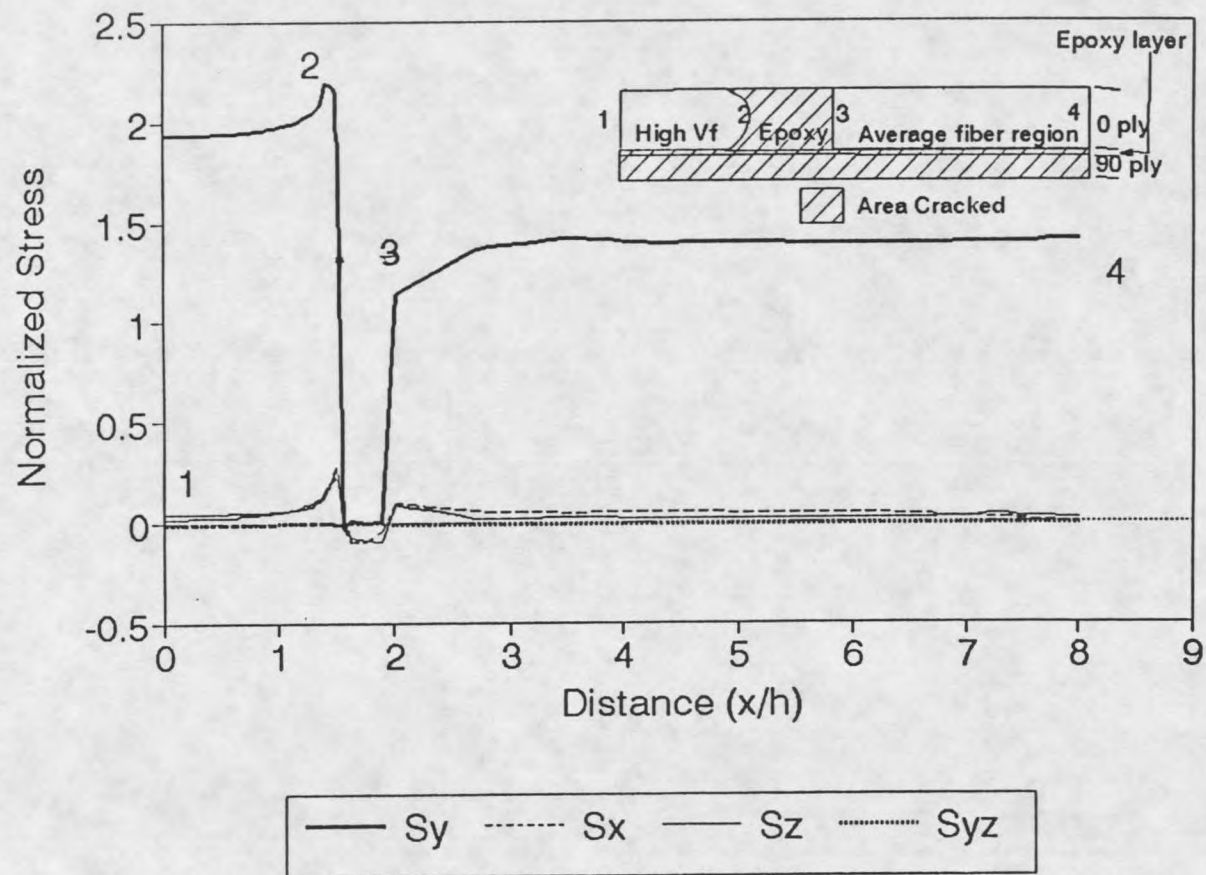
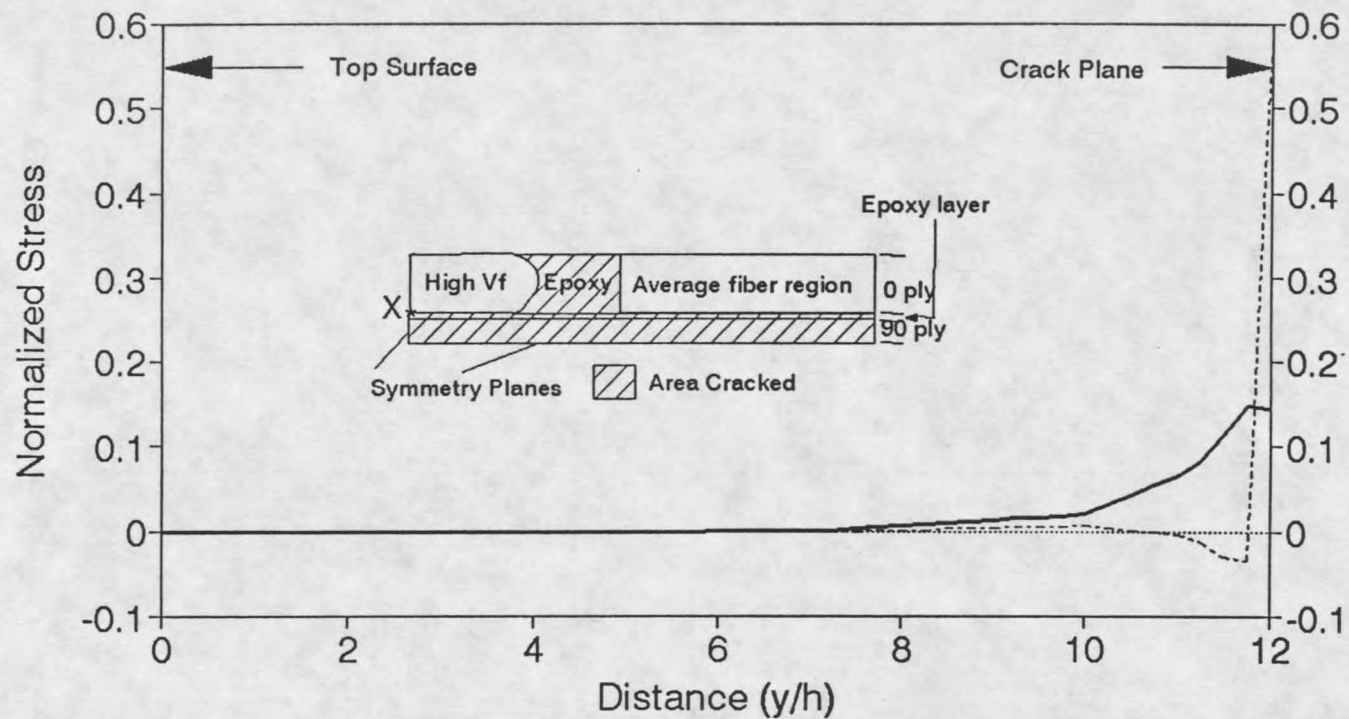


Figure 50. Stresses in the 0^0 ply parallel to the X axis at the 0^0 ply/epoxy layer interface.

Let us examine the interlaminar stresses along the length of the laminate at the 0/epoxy layer interface. Two physical points of interest are a) the high fiber region at the symmetric plane which divides the high fiber region in half, and b) the corner in the high fiber region which is the meeting point of cracks in the epoxy layer and epoxy region (corner 3, Figure 47). These points are denoted by X in the inset. Even though the inset shows the cross section at the crack, these plots along the length of the laminate traverse the entire length of the laminate parallel to the Y axis and pass through the point marked X. For further clarity, the graphs show the top surface and the crack plane to indicate that these plots are from the top surface where uniaxial extension is applied down to the plane of the crack.

Interlaminar stresses in Figures 51 and 52 follow a very similar trend, the only difference being the magnitude of the maximum stress values. S_z rises very sharply near the crack. In less than $1/3 h$, it climbs from a normalized stress value of near 0 up to 0.6. In contrast, S_{yz} rises much more gradually and it does not reach as high a value as does S_z . S_{yz} starts rising at a distance of $4 h$ from the crack, though the significant rise starts occurring at a distance of $2h$ from the crack. These plots show clearly the localized nature of the stresses at the interface. The interlaminar peeling stress S_z is about 60 % of the applied stress in this region, which is very high. The interlaminar strength is typically on the order of a few thousand psi, while the in-plane strength of a 0/90/0 laminate would be on the order of 100,000 psi. More importantly, the increase in S_z occurs within $1/3 h$ of the crack. Compare Figure 52 with Figure 35 which shows the interlaminar



X - Plot along the length of the laminate through this point

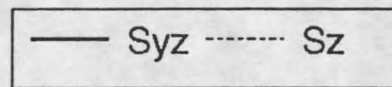
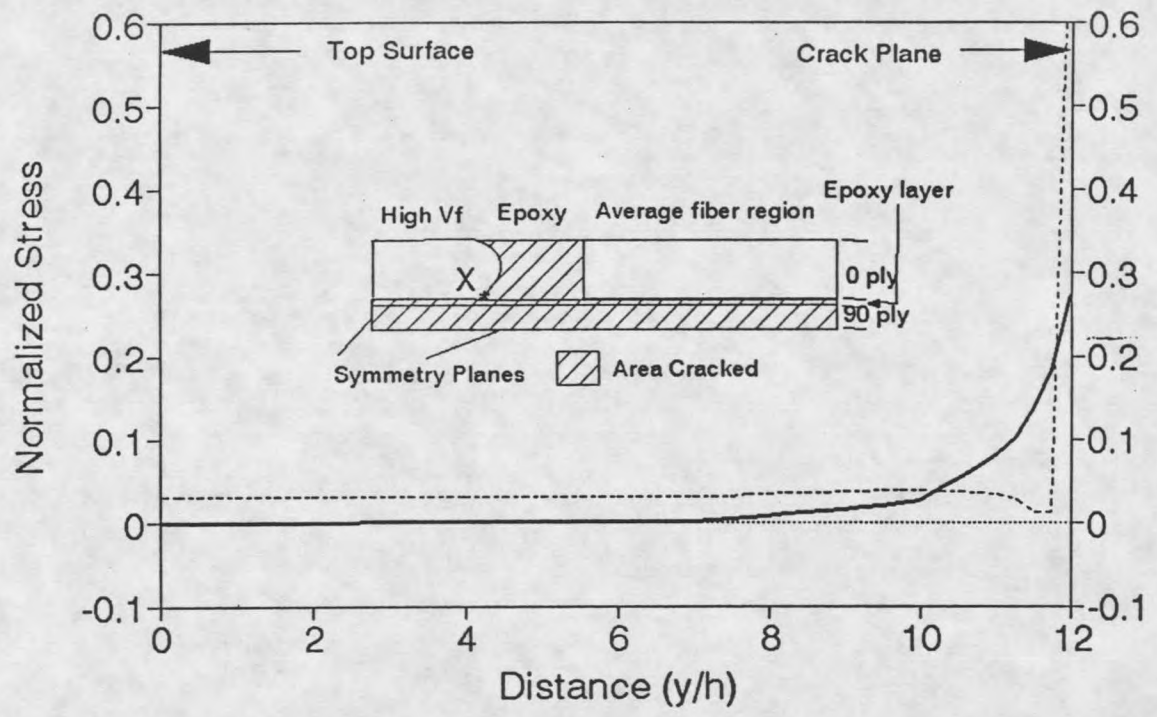


Figure 51. Stresses in the Y direction at the High Fiber/Epoxy Interface.



X - Plot along the length of the laminate through this point

— Syz - - - - Sz

Figure 52. Stresses in the Y direction at the High Fiber/Epoxy Interface.

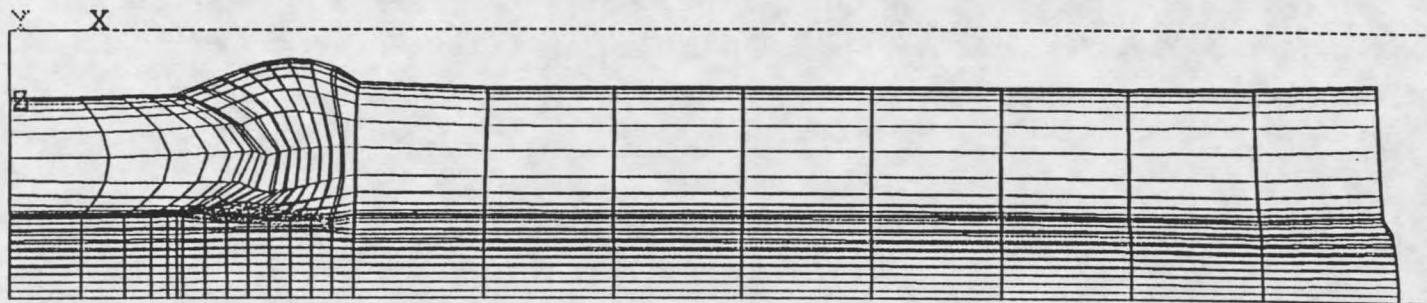


Figure 53. Deformation in the Laminate (deformation exaggerated).

stresses at the 0/epoxy layer interface. S_z stresses are similar. In the model with the discrete high fiber region, the S_z is slightly higher, while the S_{yz} looks quite different. In the model with homogenous material properties, there is a steady dip which rises near the crack plane. It still does not rise above 0. In the model with discrete high fiber region, however, there is a steady rise. This could be because of the nature of the crack in the two cases. In the earlier model, there is no crack in the zero ply, while a crack surrounds the high fiber region in the present model. Thus, the stress fields are different in this model.

Figure 53 shows the cross section at the crack after the load was applied. Notice the distortion of the epoxy region in the 0° ply. The dotted line indicates the original cross section before the application of load (deflections are greatly exaggerated).

Summary

The corner in the high fiber region where the cracks in the epoxy layer and in the epoxy region in the 0° ply meet, is a point of high stress concentration if the corner is sharp. Rounding of this corner has a profound effect in lowering the maximum stress values. There is a direct correlation between the corner angle and the stress S_y at the corner. The stress decreases as the corner angle decreases, and it tends towards a constant value as the corner angle approaches zero. This constant value is the value on the side adjacent to the 90° ply and matrix layer crack (3-4 in Figure 47). Thus, there is actually no more stress concentration at the

well-rounded corner than there is along the edge of the 0° ply adjacent to the 90° ply crack at the higher fiber content region.

The high fiber region is subjected to a higher S_y stress than the average fiber region. This moderate effect is due to the higher modulus of the high fiber content region. The interlaminar stresses are about the same for high and average fiber content regions. Hence, having a discrete high fiber region does not seem to affect the interlaminar stresses. In the longitudinal direction, the interlaminar stress S_z rises sharply as it approaches the crack, and it reaches 60 % of the applied stress near the interface within a distance of $1/3 h$ from the crack. This results in very high stress gradients near the crack at the ply interface, which could cause delamination. The S_{yz} stress reaches about 30 % of the applied stress near the corner of the high fiber region and this also might contribute to delamination. One interesting difference between this model and the model with homogenous ply properties is that the S_{yz} steadily rises as it approaches the crack in this model as opposed to having a negative value away from the crack and rising to near zero value near the crack in the homogenous ply model. In the present model, S_{yz} reaches maximum value at the crack. Having a discrete fiber region does not alter the S_z value greatly and hence the primary contribution to delamination is not altered to a great degree by having non homogenous ply properties. Since the opening mode crack resistance is typically much lower than for the shearing mode, especially with brittle matrices [26], S_z will probably dominate the delamination process under applied tensile stress.

CHAPTER 5

ANALYSIS OF $[0/\pm 45]_s$ LAMINATE WITH CRACKED ANGLE PLIES

Introduction

This chapter examines the stresses in a $[0/\pm 45]_s$ laminate with cracked $+45^\circ$ and -45° plies. As these materials are used in the manufacture of wind turbine blades, it is important to have a knowledge of the nature of stresses in these materials with characteristic damage in the off axis plies. Cracks in the off axis plies are often the sites where delamination starts. An examination of stresses around such cracks provides valuable insight into the nature of stress distribution in the area, helps determine the region(s) where delamination is likely to start, and establishes the degree of stress concentration in the 0° ply fibers resulting from the angle ply cracking.

Model Analyzed

The $[0/\pm 45]_s$ laminates are more typical of many applications than $0/90$ laminates, and this is the case with wind turbine blades. As in $0/90$ cases, cracks form parallel to the off-axis layers penetrating through each layer, but stopping at the boundary of adjacent layers. The model is shown in Figure 54. Three of the six plies in the actual laminate are included in the FE mesh, taking advantage of the symmetry. Because of the ply arrangement, the only plane of symmetry that exists is the XY plane as shown. This leads to a model with higher degrees of freedom

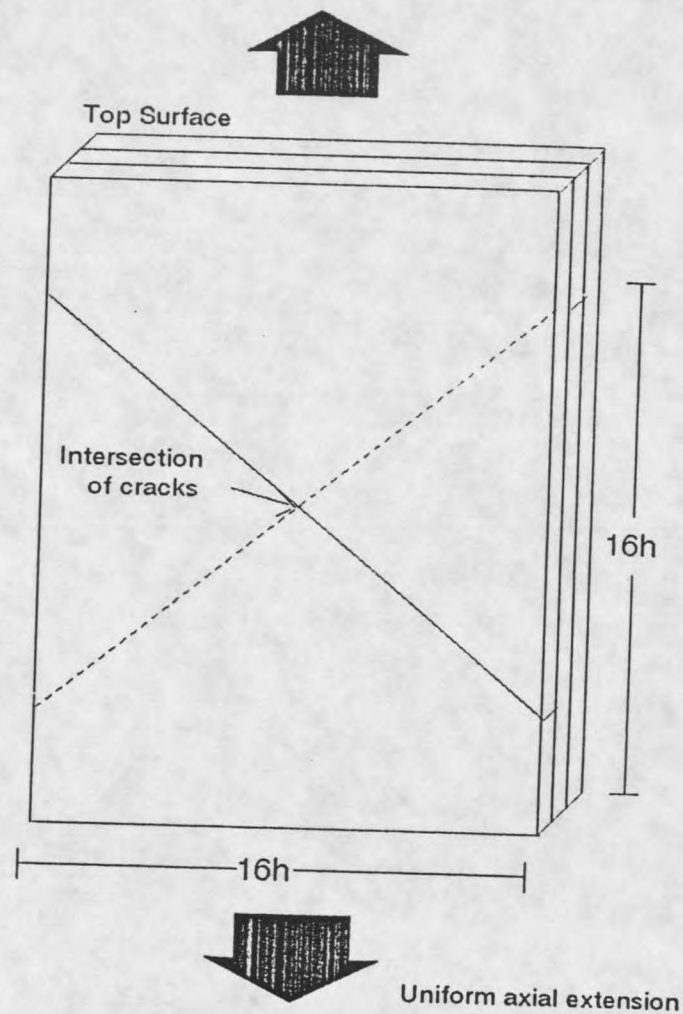


Figure 54. $[0/\pm 45]$, Laminate Model Geometry

than the 0/90 cases which had a more symmetric stress field.

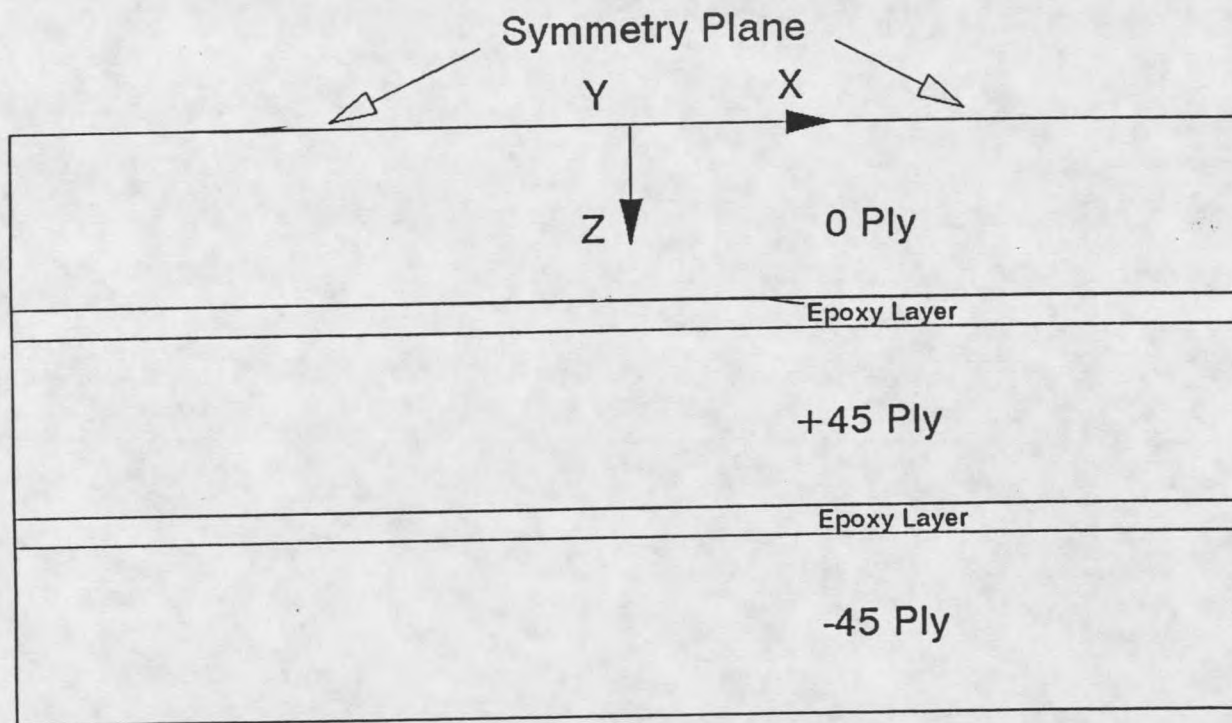
The +45 and -45 plies are cracked as indicated. There are epoxy layers between the +45, -45 and 0 plies as shown in the cross section in Figure 55. The cracks in the angle plies extend through the thickness of the plies and through the adjacent epoxy layer. The 0° ply is not cracked. The cracks are modelled as a gap $1/125 h$ deep measured perpendicular to the plane of the crack. The laminate is subjected to uniaxial extension at the ends. This displacement condition, calculated from lamination theory, is chosen to effect an average stress of 50,000 psi on the laminate cross section. All the stresses are normalized by this value, as usual. All dimensions of the laminate are relative to the ply thickness, h .

The geometry of the model presented some meshing difficulty. The element type used does not allow automatic meshing of triangular prism volumes. Consequently, the corners were meshed by triangular prism elements which are a special form of the brick elements used so far. Refer to the Appendix B for more details on this element type and shape functions. The material properties used for the glass/epoxy laminate and epoxy layer in Chapter 3 were also used for this model. Each ply has homogenous material properties.

The following symmetry condition was imposed on the XY plane

$$W(x,y,0) = 0.$$

The displacement boundary condition imposed at $y = \pm 8h$ was chosen to impose an average stress of 50,000 psi.



Not to Scale

Figure 55. Cross Section of the [0/±45], Laminate.

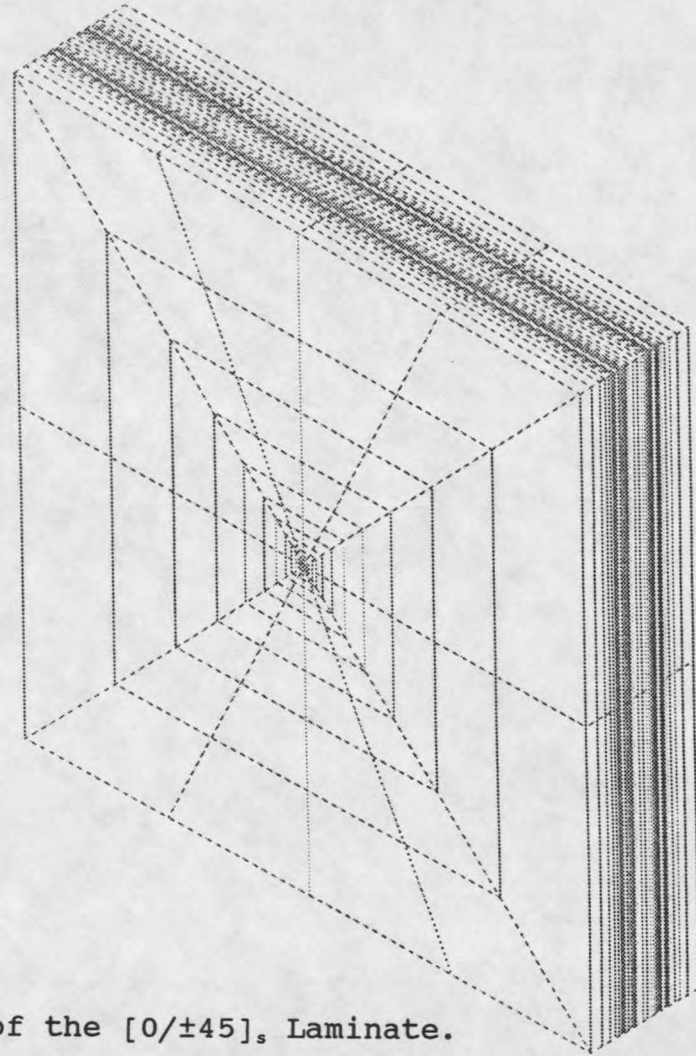


Figure 56. Finite Element Mesh of the $[0/\pm 45]_s$ Laminate.

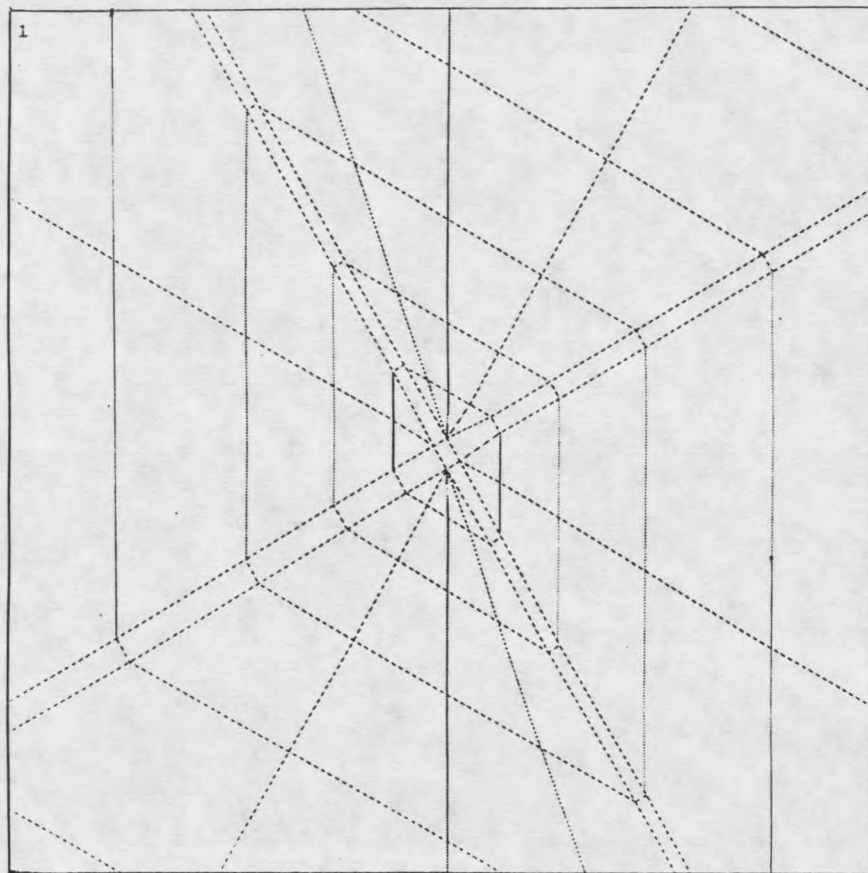


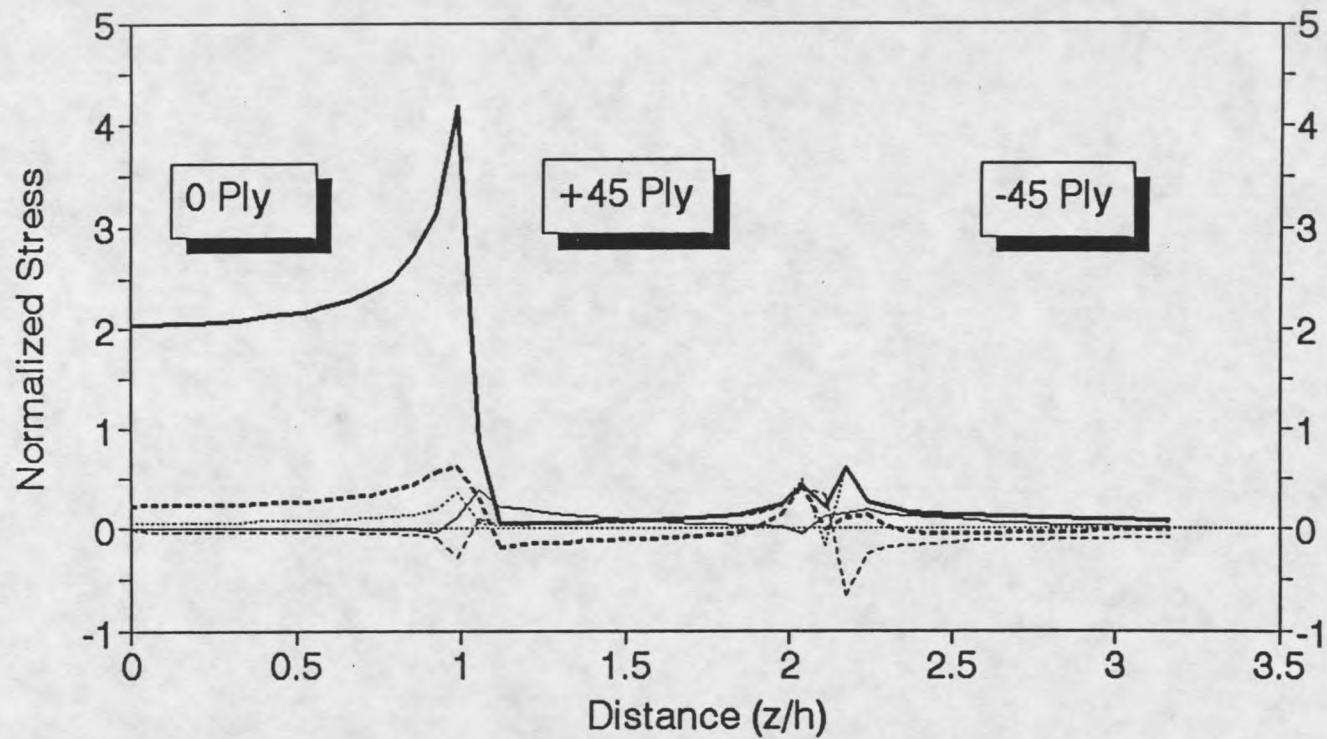
Figure 57. Finite Element Mesh of the [0/±45], Laminate (Close-up View).

The finite element mesh of the model is shown in Figure 56. The model has 11040 nodes and 9053 8-noded anisotropic brick elements. With three translational degrees of freedom for each node, we have 33120 degrees of freedom. The large wavefront of the model in the ANSYS solver is lowered by using a wavefront minimizing routine available in the software. The initial wavefront of 10650 was lowered to 795. This problem was modelled on an IBM RS/6000 workstation and solved on a CRAY Y-MP 4 machine.

Results and Discussion

Consider the stress through the thickness of the laminate at the intersection of the cracks in the +45 and -45 plies. Figure 58 shows the stresses $1/30 h$ above the intersection of the +45 and -45 ply cracks. This position is chosen to avoid inaccuracies associated with the last element near the intersection. S_y rises as it approaches the epoxy layer between the 0 and +45 plies. Most of the stress increase occurs within $0.5 h$ of the interface, but the most significant rise occurs within $0.25 h$ of the ply interface. The rise is smooth and it reaches a normalized stress value of about 4.3, which is quite high. Then, it falls sharply to zero in the +45 and -45 plies. There is a slight rise of S_y near the +45/-45 interface. Note that it is only at the precise intersection of the + and -45 cracks that both off-axis plies are cracked in the same position.

Examining the interlaminar stresses, we find, S_z rising near the 0/epoxy layer interface. S_z changes sign to compression in the epoxy layer and the +45°



(Epoxy layers between plies are cracked)

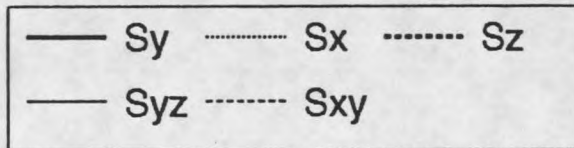


Figure 58. Through-thickness Stresses at the Intersection of +45 and -45 Cracks.

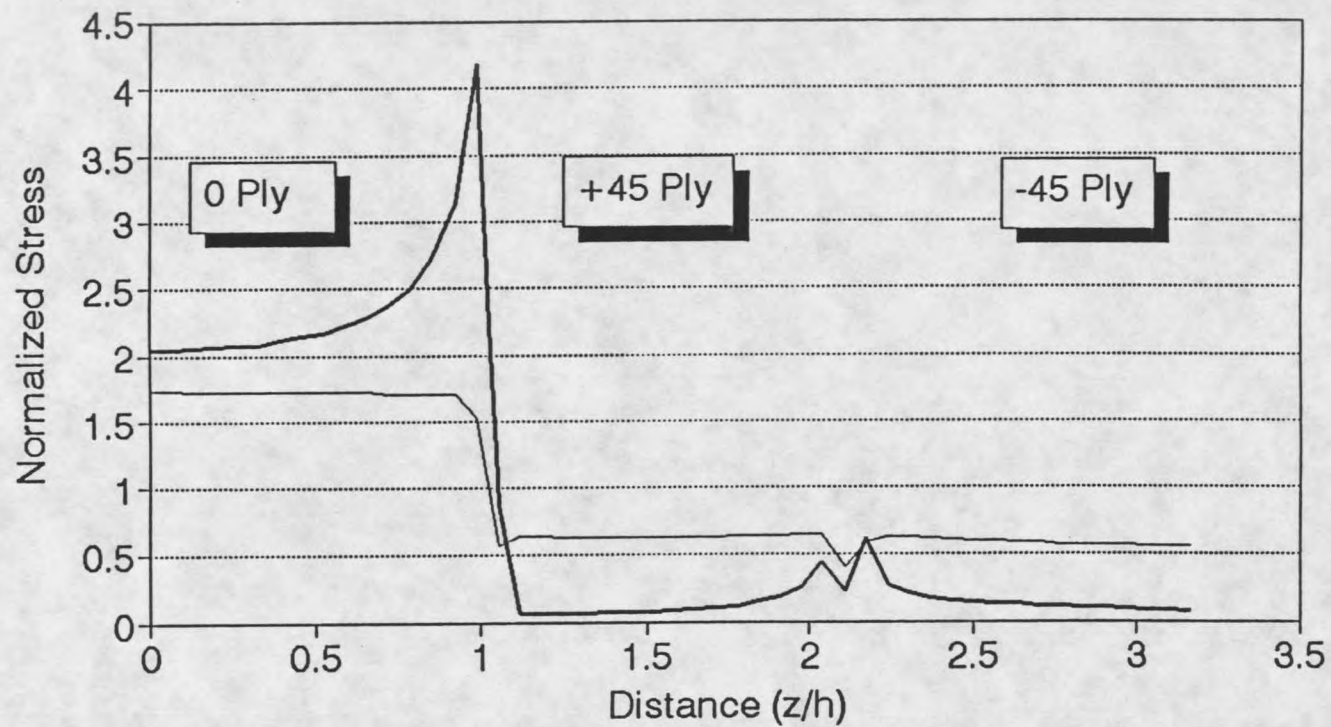
ply. The absolute value is not as high as it was in the 0^0 ply. S_z rises once again as it reaches the -45^0 ply but it is still low compared to the value between the 0 and $+45$ plies. S_z decreases to 0 as it reaches the stress free outer surface. S_{yz} is practically absent at points removed from the ply interfaces. At the 0/epoxy layer interface near $+45^0$ ply, it rises to noticeable values. It falls in the $+45^0$ ply to rise again near the $+45$ /epoxy layer interface near the -45^0 ply. It goes to zero like all other stresses as it reaches the stress free outer surface. The shear stress S_{xy} is high near the $+45/-45$ ply interface. It also changes sign from $+45$ to -45 ply. There is also some shear stress near the 0/ $+45$ ply interface.

Figure 59 compares the stress at the crack intersection to the far-field stress. S_y reaches peak value near the 0/ $+45$ interface. It does not go down to the far-field value even away from this interface. This is because both the $+45$ and -45 plies are cracked and all the load is transferred to the 0^0 ply here. The maximum value of S_y here is 4.3 in the 0^0 ply, compared with 2.3 for the analogous 0/90 case (Figure 33). This is because the two off-axis plies at $\pm 45^0$ carry much more far-field stress than in the 0/90 case (there are two 0^0 plies in the laminate in each case). The maximum S_y is 2.5 times the far-field 0^0 ply stress here, but only 1.7 times the far-field 0^0 ply stress in the 0/90 case. Deleting off-axis plies entirely would produce a 0^0 ply stress 1.8 times higher than the intact far-field value for a $[0/\pm 45]_s$ laminate, compared with 1.15 times higher for the $[0/90/0]$ laminate. Thus, the stress concentrations associated with the off-axis ply cracks are

considerably more severe than if the off-axis plies were simply deleted (as is often done in 2-dimensional approximations).

Figures 60 and 61 show the stresses along the ply crack/epoxy layer interface from the top surface to the intersection of cracks in the middle. Refer to the schematic drawing Figure 54. All the stresses go towards zero at the intersection except S_{xy} which reaches maximum value at the intersection of the cracks. S_y falls rather gradually compared to S_{yz} , which drops to zero within a distance of h . S_z changes from a low compression at the top to tension as it approaches the intersection of the cracks, then back to compression as it gets within $0.5 h$ from the intersection and then towards zero at the intersection.

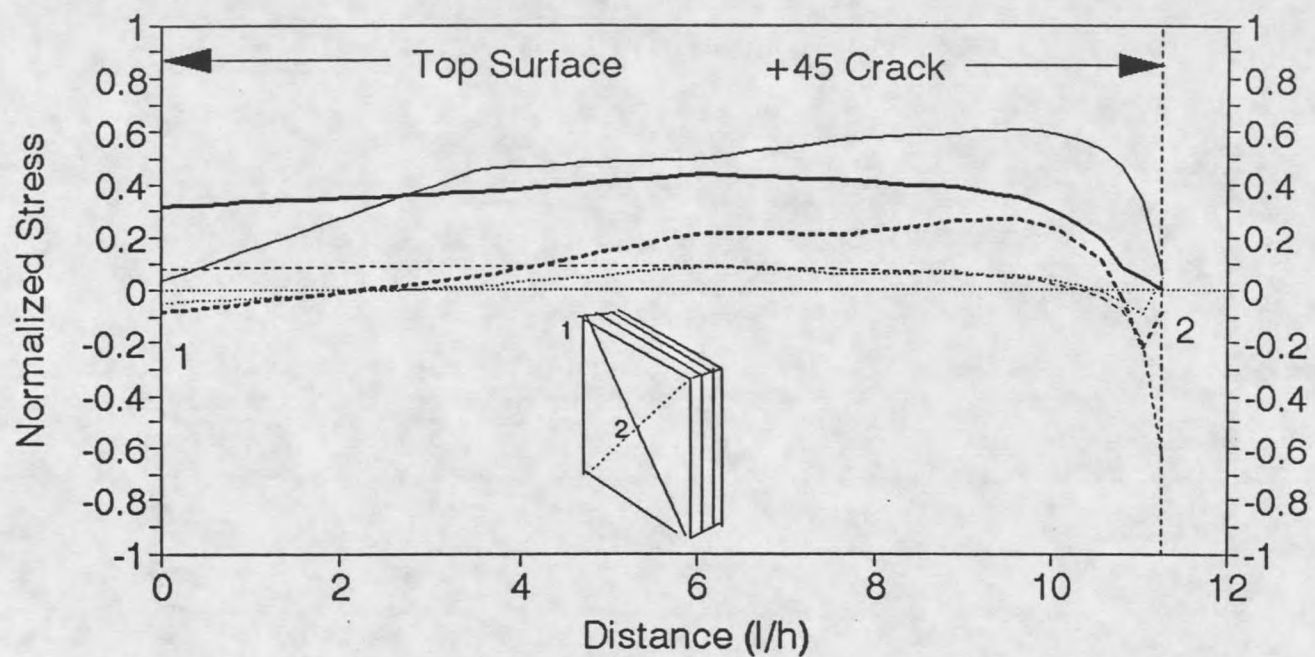
Figures 62 and 63 are plots through the thickness of the laminate at a point $1/30 h$ away from the intersection of the $+45^\circ$ and -45° ply cracks. Figure 62 is at a cross section passing through the $+45^\circ$ crack only. The -45° ply is intact at this cross section. Similarly Figure 63 is at a cross section which goes through the -45° ply crack only, the $+45^\circ$ ply is intact at this cross section. Both the plots are at points very close to the intersection of the cracks. Looking at Figure 62, there is little difference in S_y values on this graph compared to those plotted at the crack intersection. However, S_z shows a significant difference. From a normalized value of around 0.6 at the crack intersection, it is up to 1.4 in this plot. A cracked $+45^\circ$ ply seems to increase the interlaminar normal stress S_z by a significant amount. Another difference from the plot at the crack is the stress S_{yz} . At the crack intersection, S_{yz} is higher at the $0/+45$ interface than the $+45/-45$ interface. But



(Epoxy layers between plies are cracked)

— Sy - Far-field — Sy - Crack

Figure 59. Through-thickness Stresses at the Intersection of +45 and -45 Cracks (Comparison).



(Epoxy layers between plies are cracked)

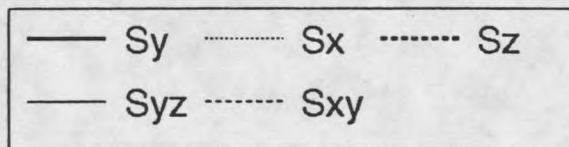


Figure 60. Along the -45 Crack/Epoxy Layer Interface from point (1) to point (2).

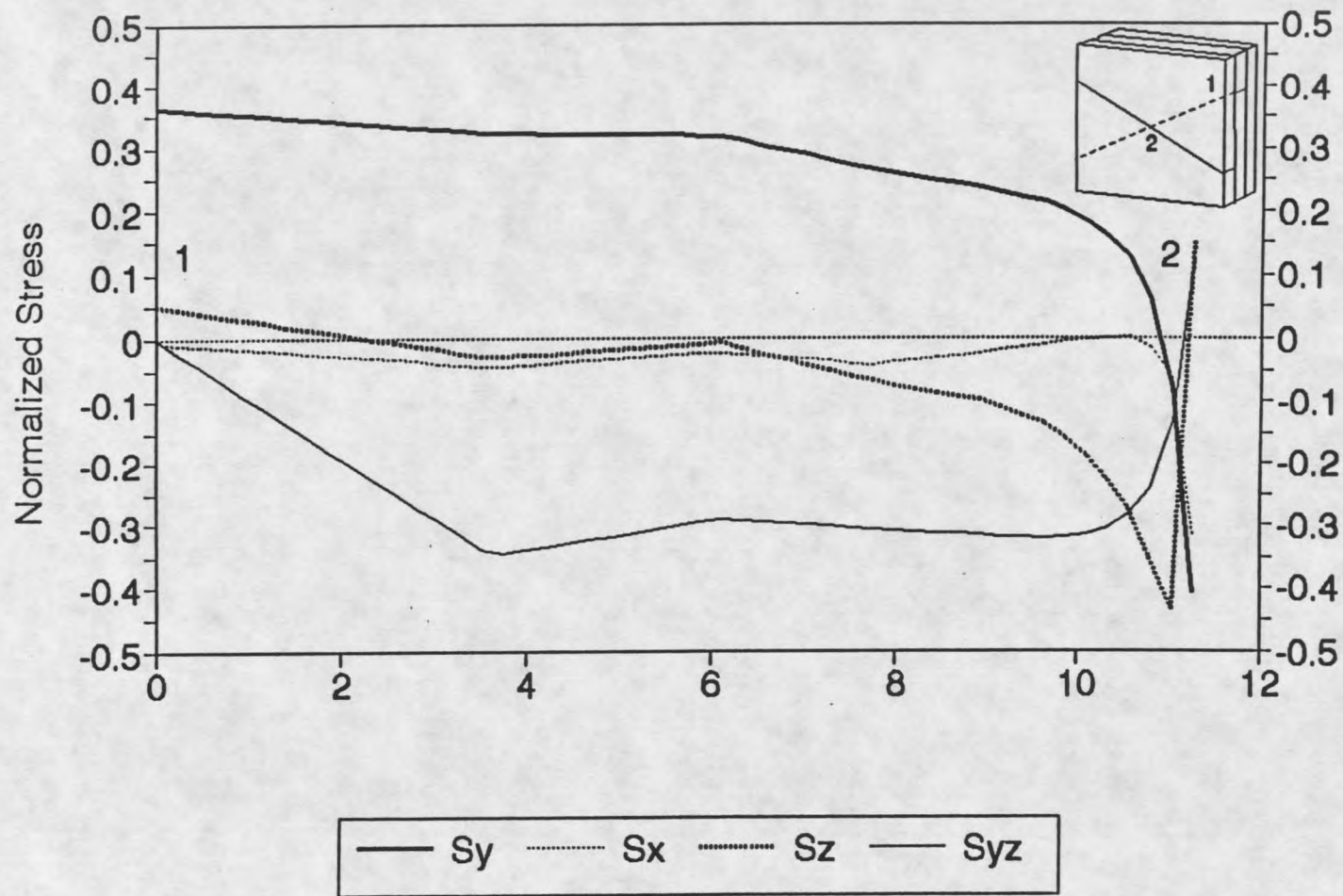
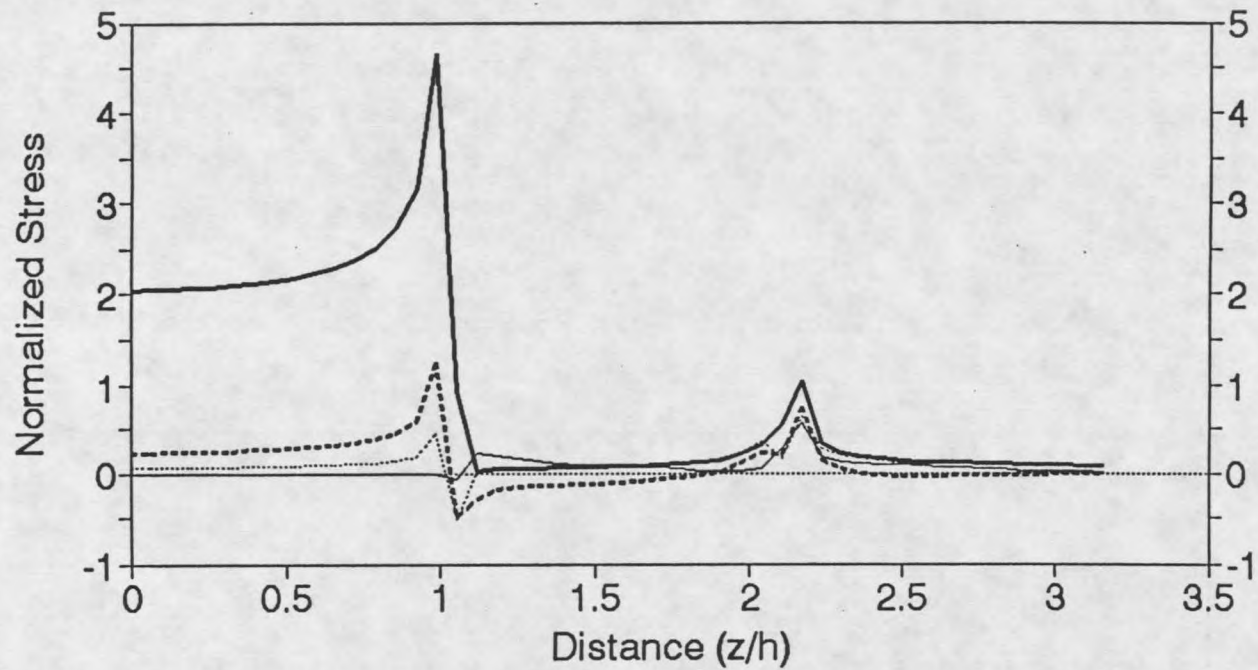


Figure 61. Along the +45 Crack/Epoxy Layer Interface from point (1) to point (2).



(Plot through a point $1/30$ h away from intersection of cracks)

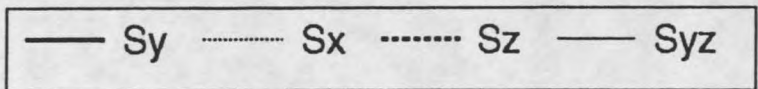
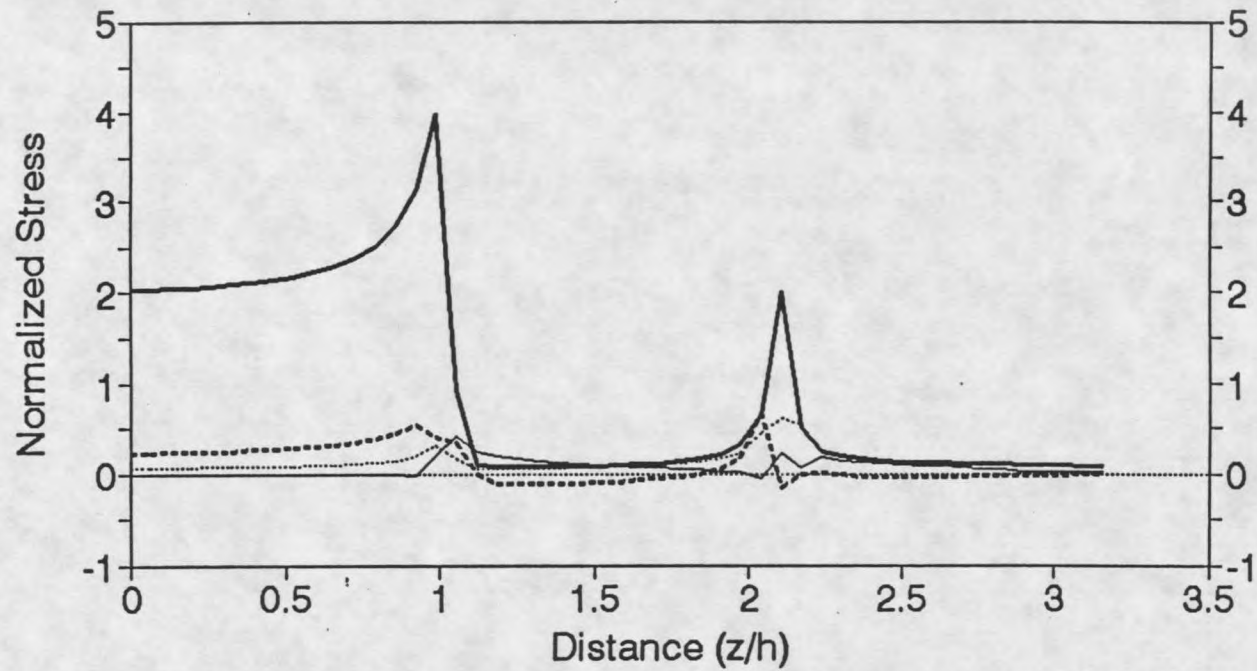


Figure 62. Through-thickness Stresses near the Crack Intersection, passing through +45 Crack only.



(Plot through a point 1/30 h away from intersection of cracks)

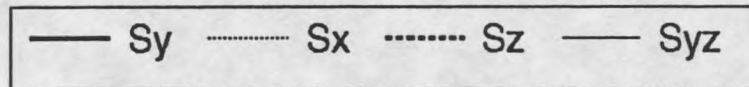
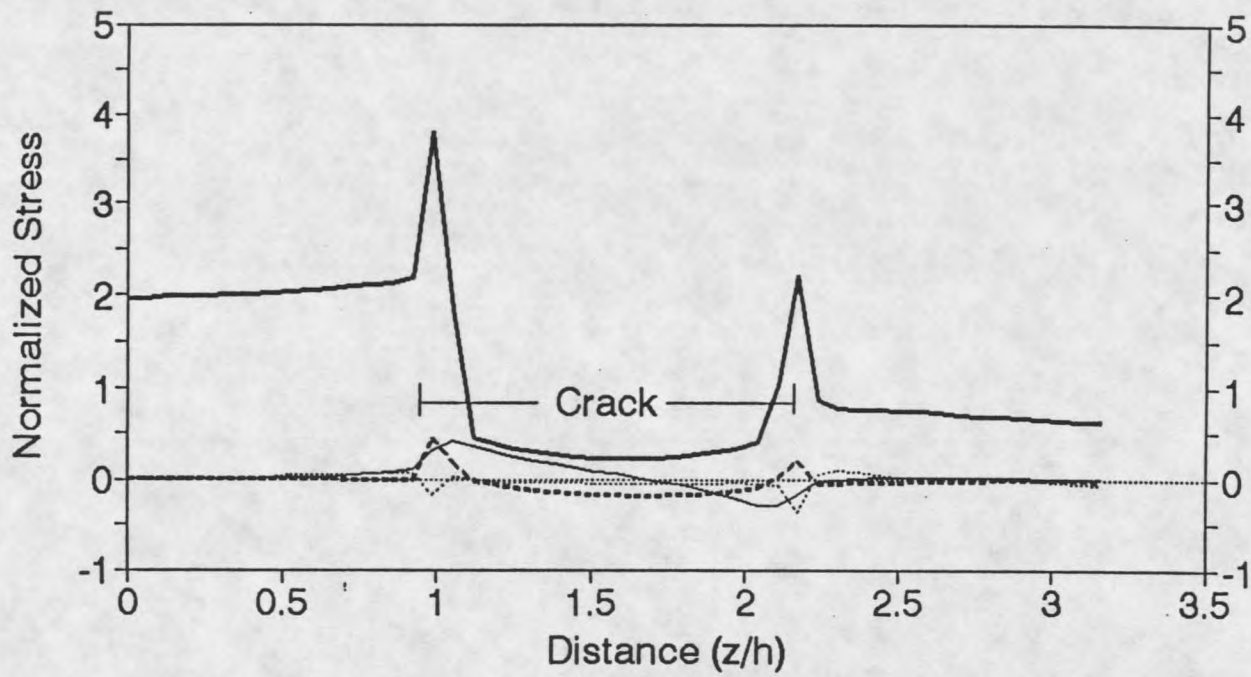


Figure 63. Through-thickness Stresses near the Crack Intersection, passing through -45 Crack only.

in Figure 62, it is reversed, with S_{yz} being higher at the +45/-45 interface. In this figure, only the +45° ply is cracked, while at the crack intersection, both +45 and -45 plies are cracked. This may play a part in altering the nature of the interlaminar stresses. Figure 63 shows a similar plot through the -45 crack. The peak S_y is lower compared to the previous plot, but its value near the +45/-45 interface is higher than in the previous case. Also, S_z is higher near the +45/-45 interface in this case as opposed to the higher value near the 0/+45 interface in the previous plot. S_{yz} in this case is higher near the 0/+45 interface. The interlaminar stresses are in general lower in this case as compared to Figure 62.

Figures 64 and 65 are similar to the previous set of two figures. The difference is that these plots are further away from the intersection of cracks. They are 3.5 h away from the intersection, again passing through one of the two cracks, at a distance 3.5h along the crack from the intersection. S_y shows a noticeable difference. It is close to zero in the cracked plies and the load is transferred to other plies. Also in these plots the 0° ply carries less load as compared to the load carried by it nearer the crack intersection. In these plots, the angle ply not cracked carries some load, but near the crack intersection, even the undamaged angle ply does not seem to be carrying much load at all. Figure 64, which includes the +45° ply crack only, shows more or less equal S_z values near the 0/+45 ply interface and +45/-45 interface. S_{yz} changes sign between the undamaged plies. Figure 65 shows some differences compared to Figure 64. S_y is lower at the crack/undamaged ply interface. The interlaminar peeling stresses S_{yz} and S_z are



(Plot through a point 3.5 h away from intersection of cracks)

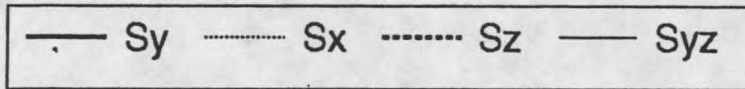
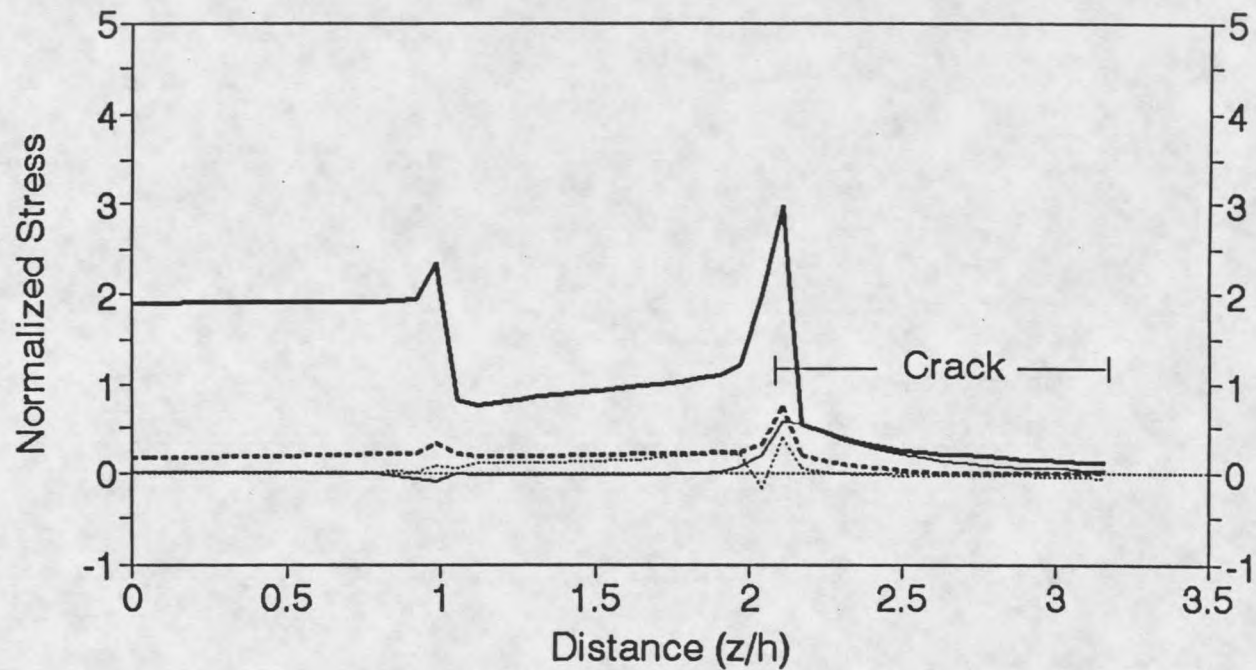


Figure 64. Through-thickness Stresses, passing through +45 Crack only.



(Plot through a point 3.5 h away from intersection of cracks)

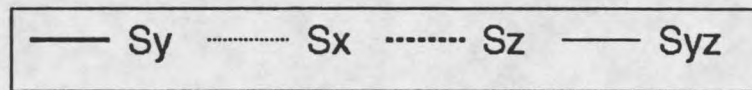


Figure 65. Through-thickness Stresses, passing through -45 Crack only.

low all through the laminate and they both rise as they approach the crack. Much of the rise occurs within a distance of $0.1 h$ from the crack. They both rise to about 50 % of the applied stress, which is quite significant. This is slightly more than the peak interlaminar stress values of Figure 64. The S_z is slightly more than S_{yz} and it is in tension. For sufficiently high applied stress, this stress can peel off the plies. Also the stress gradients are high. Much of the rise occurs within a range of $0.1h$ from the cracks.

Summary

The plots are all non dimensionalized, but useful conclusions can be drawn from them by assuming the moderately high applied stress, of say 50,000 psi. The interlaminar stresses at the intersection of cracks in the +45 and -45 plies are high enough to cause damage in the laminate. These stresses are higher near the $0/+45$ interface than near the +45/-45 interface. So, damage is likely to occur first near the former interface. The 0^0 ply carries significant load near the intersection of cracks. Nearly four times the applied load is carried by the 0^0 ply here. This is likely to cause failure of the 0^0 ply, as is observed when ± 45 plies crack in fatigue [14]. At points away from the crack intersection, the interlaminar stresses continue to be significant. The interlaminar stresses at the undamaged ply / cracked ply interface are high enough to precipitate damage for sufficiently high applied stress. The interlaminar stresses also are highly concentrated near the cracks. Delaminations are likely to occur for sufficiently high applied stress. The plots in

this chapter give the nature of the stress fields and they can be used to predict where the damage is likely to start.

CHAPTER 6ANALYSIS OF A $[0/\pm 45]_s$ LAMINATE WITH A DISCRETE FIBER STRANDIntroduction

In this chapter, we analyze a $[0/\pm 45]_s$ laminate with a discrete fiber strand in the 0° ply and matrix cracks in the off-axis plies. This model more closely represents the triax materials used in the manufacture of wind turbine blades. Cracks in the off axis plies are observed in the high cycle fatigue testing of these materials. As the intersections of the matrix cracks are often (not always) the sites where delamination starts, a knowledge of the stress fields around such cracks will provide some useful insight into the factors that contribute to delamination. The 0° ply stress concentration resulting from $\pm 45^\circ$ ply cracking relates directly to observed laminate fatigue failures.

Model Analyzed

The model is a $16 h \times 24 h$ $[0/\pm 45]_s$ laminate with a ply thickness of h , as shown in Figure 66. There are $0.08 h$ thick epoxy interlayers between plies. The 0° ply has non-homogenous material properties. It has a fiber strand modelled as a region of high fiber volume fraction with elastic constants the same as those of the high fiber content region described in Chapter 4. This region of high fiber content is surrounded by an epoxy region similar to that described in Chapter 4. Refer to Figure 66 which is a schematic drawing of the model and Figure 67 which

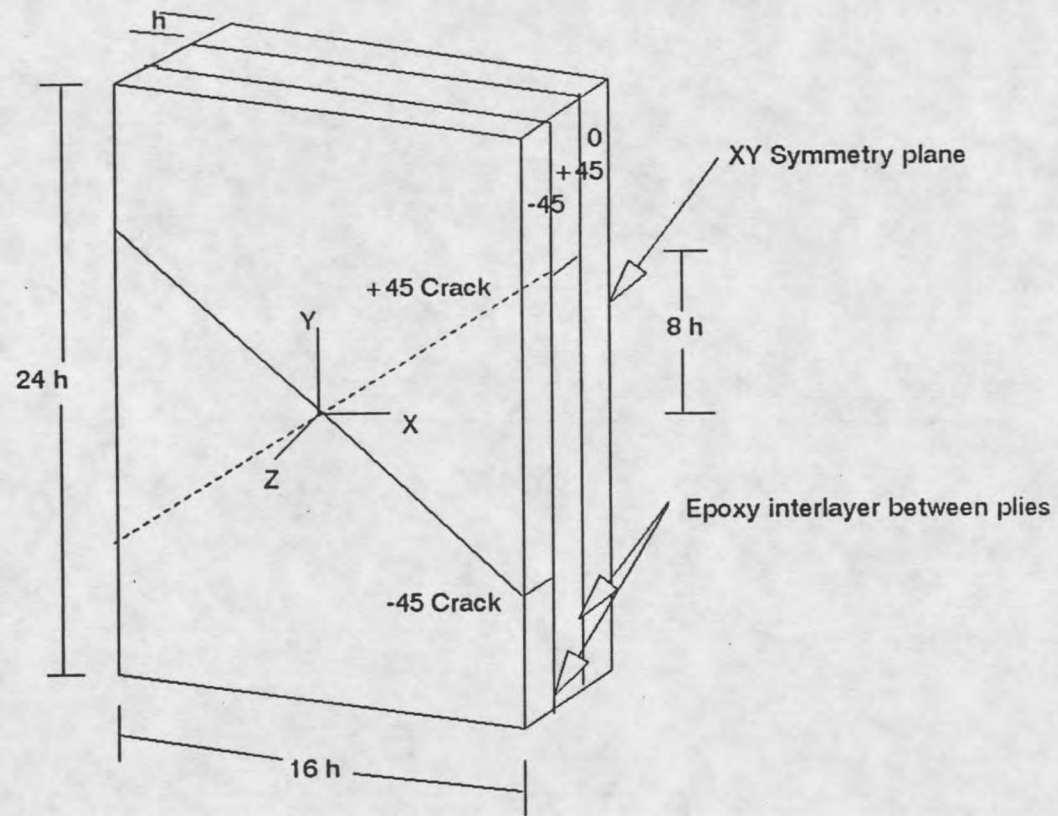


Figure 66. [0/±45], Laminate with Discrete High Fiber Strand - Model Geometry

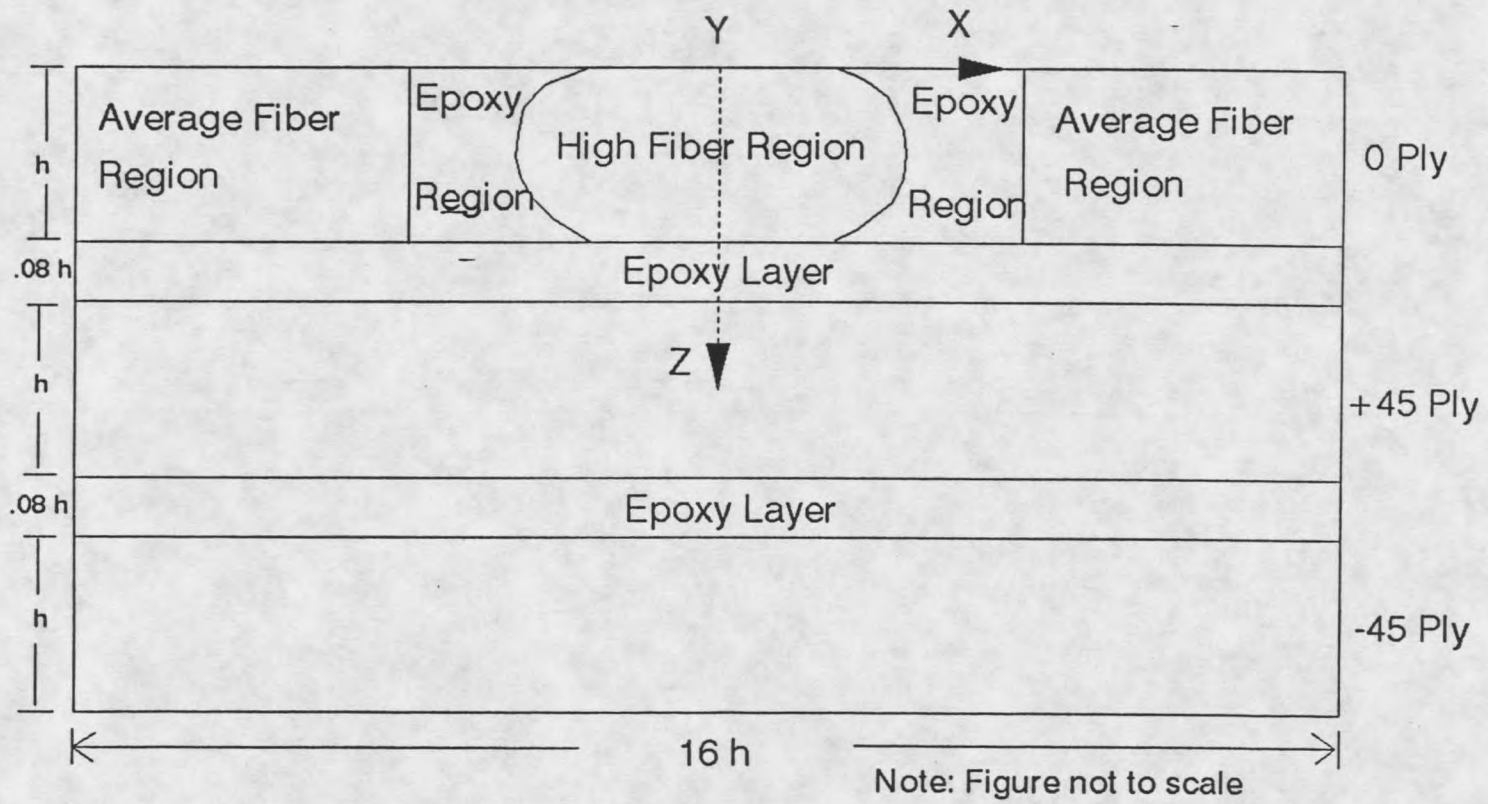


Figure 67. $[0/\pm 45]_s$ Laminate with Discrete High Fiber Strand - Cross Section

shows the cross section of the model. The cross section shows only three of the six plies in the actual laminate as this is a symmetrical laminate.

The material properties for the epoxy region and the average fiber content region are the same as used for the model in Chapter 4. There is a crack in each of the angle plies. These cracks run parallel to the fibers in the angle plies. The cracks span the whole ply thickness and extend into the matrix layer(s) next to the ply. In the case of the +45 crack (matrix cracks in the +45 and -45 plies are referred to as +45 and -45 cracks), the crack extends across the ply thickness and into the epoxy layers between the 0^0 and +45 0 plies and the +45 0 and -45 0 plies. In the case of the -45 crack, the crack extends across the thickness of the ply and into the epoxy layer between the +45 0 and -45 0 plies. The crack in the +45 0 ply also extends into the epoxy region between the high fiber region and the average fiber region in the 0^0 ply. The crack in this epoxy region lies on the plane of the +45 0 ply crack. Thus, the high fiber region is surrounded on all sides by the crack except the side 1-2 on the inset in Figure 72. This side is on the symmetric plane. The term epoxy region refers to the region in the 0^0 ply, while the term epoxy layer is used to describe the interlayer between plies. The displacement boundary condition applied at $y = \pm 12h$ are chosen to effect an average applied stress (S_A) of 50,000 psi. All the stresses are normalized by S_A . The cracks are modelled as a gap 0.008 h deep measured perpendicular to the plane of the crack. The smallest element size used is 0.016 h. This problem was modelled on an IBM RS/6000 and solved on a CRAY Y-MP.

Results and Discussion

We will first examine the through thickness stresses at the intersection of the +45 and -45 cracks as shown in Figure 68. The S_y in the 0° rises sharply near the $0/+45$ ply interface. There is an epoxy layer between these plies as described earlier. The normal stress S_y is nearly 8 times the applied stress value. S_y is almost absent in the off-axis plies as expected. The interlaminar stress S_z is quite significant, about $1.5 S_A$ in tension. This value is high enough to cause delamination for even a moderate value of applied stress (S_A). The interlaminar stress S_{yz} is not very significant. S_{xy} is high near the $0/+45$ ply interface and goes to near zero in the +45 and -45 plies (note that these plies would have significant in-plane shear stress throughout the region at 45° to the X-Y direction). Comparing Figure 68 with Figure 58, we find that the S_y peak value for the laminate with uniform ply properties is considerably lower than the value obtained in the present model (4.3 vs. 7.8). This may be due to the fact that the present model has a high fiber content region with higher elastic properties, and thus carries higher load. Also in this model, the epoxy region adjacent to the high fiber region is cracked, while there are no cracks in the 0° ply of the model in Chapter 5. These factors may be contributing to higher load transfer to the high fiber region in this model and thus higher S_y gradient in the 0° strand. An interesting difference is in the interlaminar stresses. Both S_{yz} and S_z are significant in Figure 58, and S_{yz} is slightly higher than S_z . However, in Figure 68, S_{yz} is quite insignificant, while S_z dominates.

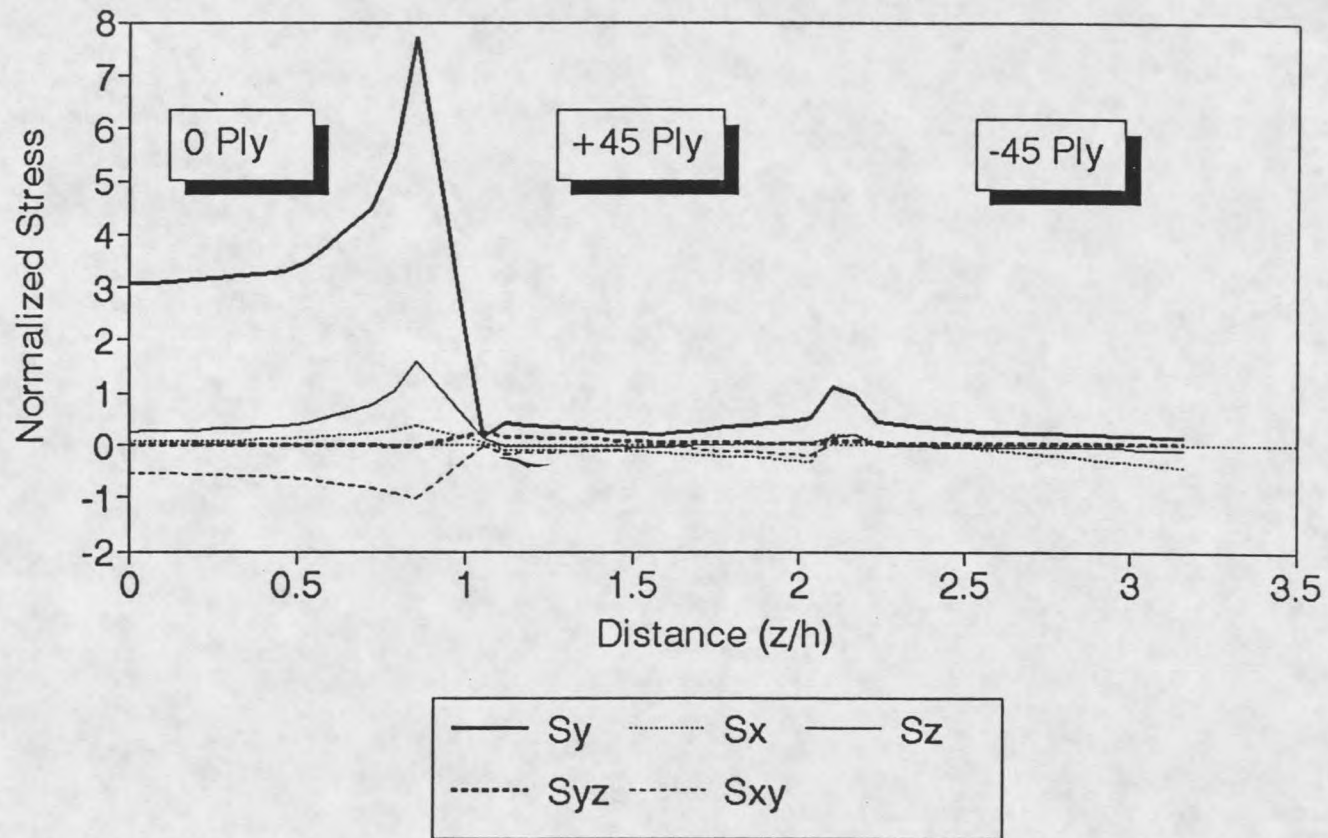


Figure 68. Through-thickness Stresses at the Intersection of +45 and -45 Cracks.

Figure 69 compares the far-field stress S_y (in the average fiber region) with the S_y at the intersection of cracks in the +45 and -45 plies. The S_y at the crack intersection does not go to far-field values away from ply interface, partly because the far-field value in the high fiber region would be higher than that shown. The effect of the cracks in the off-axis plies is felt all through the 0^0 ply near the crack intersection, as the ply must carry all of the load shed by the cracked ± 45 plies at this point. The maximum S_y here is about 4.6 times the far-field 0^0 ply stress, much higher than for the uniform ply case in Chapter 5 (again partly because the far-field value is taken in the average fiber region). Relative to the approximation of deleting the ± 45 plies entirely, and ignoring high modulus in the high fiber region, the maximum S_y of 7.8 is much higher than the value of 1.8 obtained by the ply discount method. This is partly due to the higher modulus of the high fiber region which gives higher stress at the same strain, and partly to the higher stress concentration in this geometry.

Stresses along the cracks (Figures 70 and 71) are different from the values obtained for the model without the discrete fiber strand (Figures 60 and 61). S_y goes to zero near the intersection of the +45 and the -45 cracks in Figures 60 and 61, while in the present model, S_y stays constant until it reaches the intersection of cracks (point 2) and gradually rises to a steady value and dips down near point 3 (for stresses along the -45 crack). The interlaminar stresses are not prominent because these stresses are plotted away from ply interfaces where the interlaminar stress gradients are high. S_y along the +45⁰ ply crack goes to near zero values

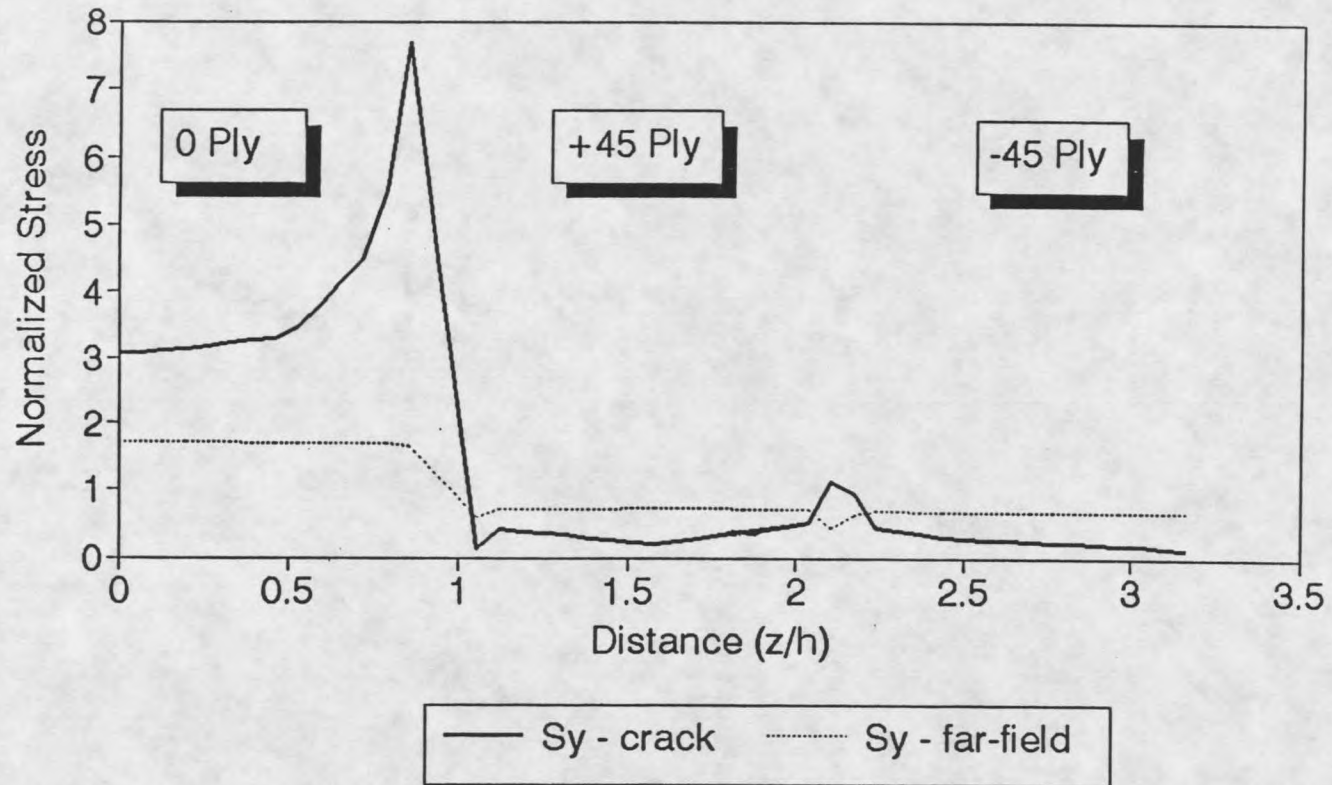
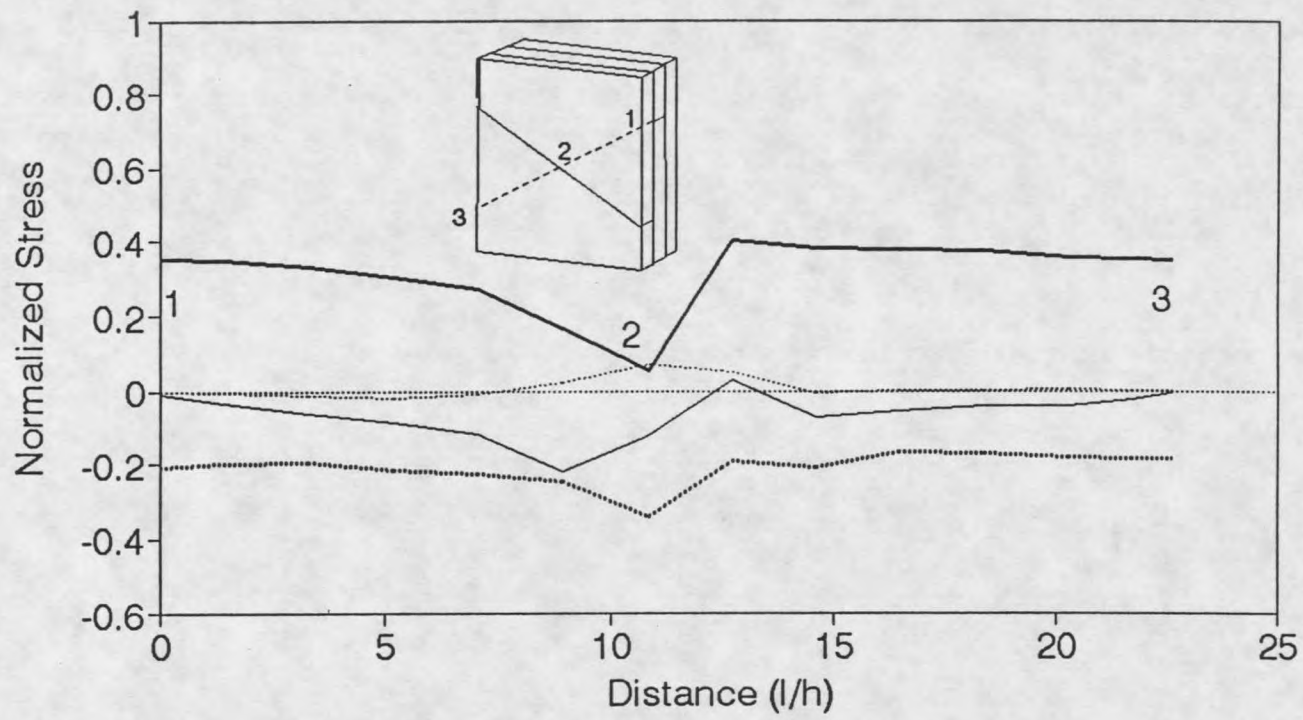


Figure 69. Through-thickness Stresses at the Intersection of +45 and -45 Cracks (Comparison).



— Sy Sx - - - - Sz - - - - Syz

Figure 70. Along the +45 Crack/Epoxy Layer Interface. (along 1-2-3).

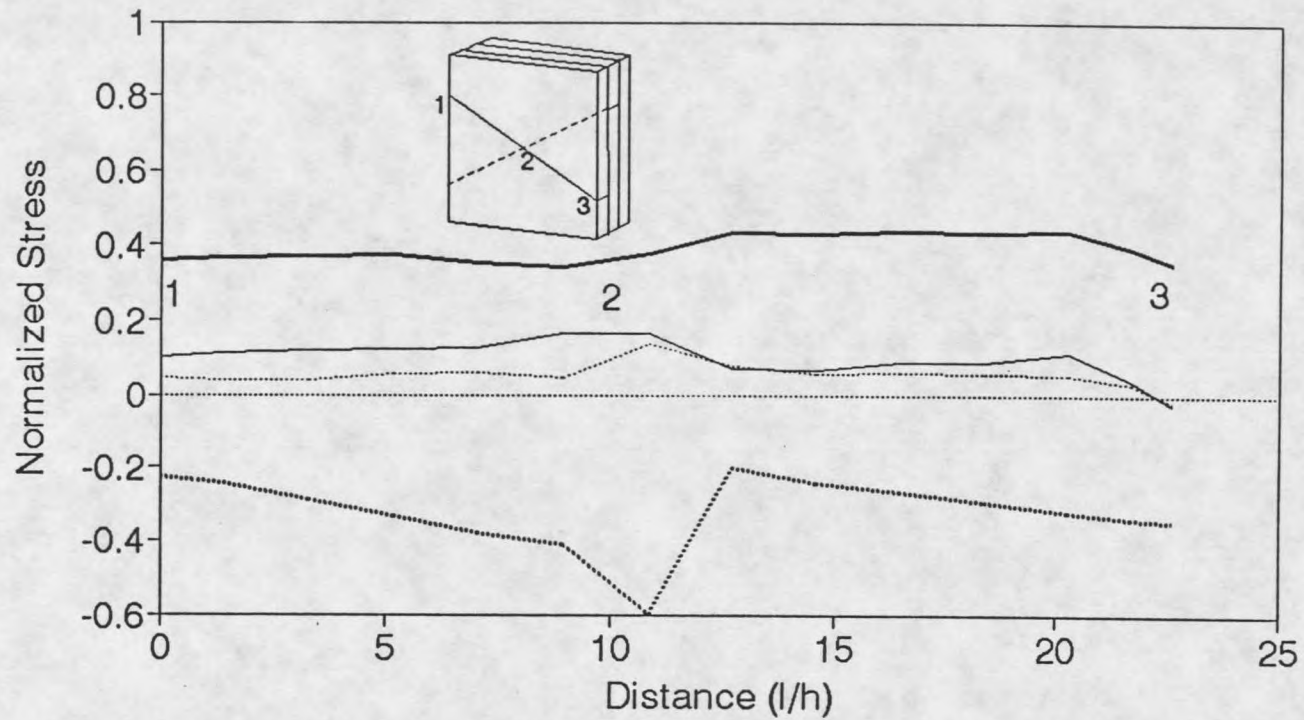
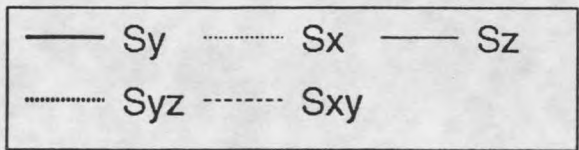
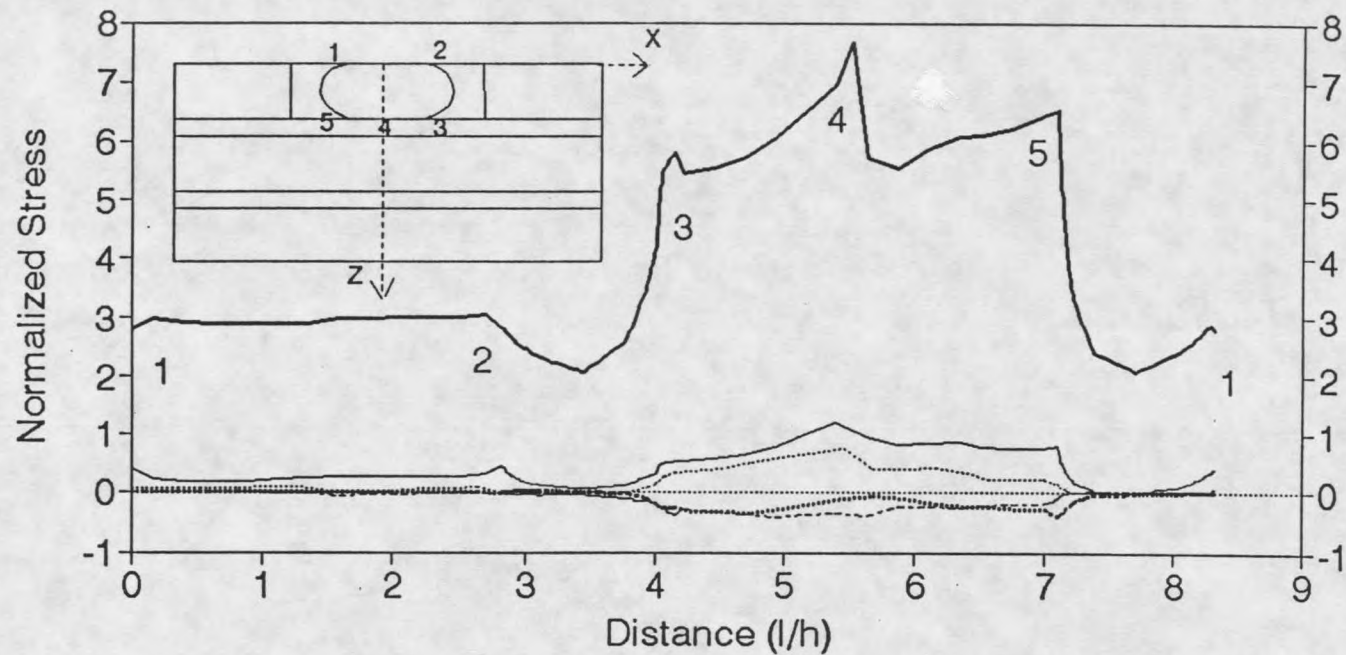


Figure 71. Along -45 Crack/Epoxy Layer Interface. (along 1-2-3).

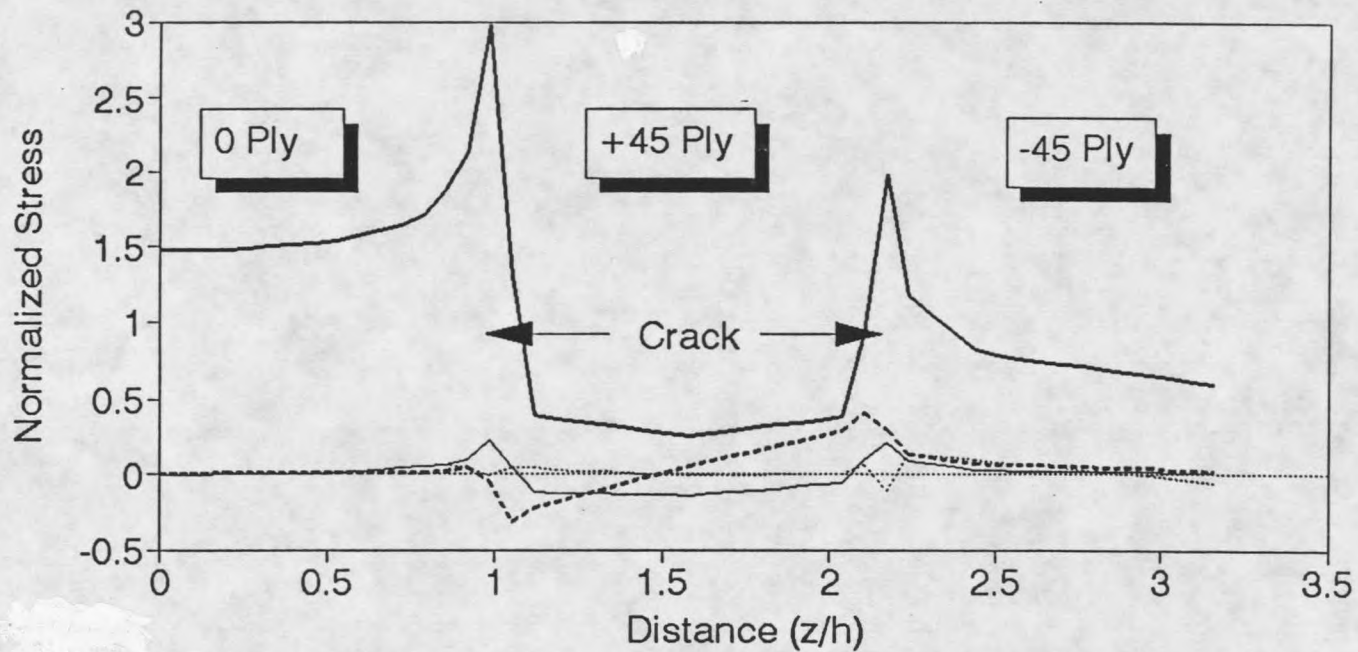
at the intersection of the +45 and the -45 cracks and rises again to a steady value along 2-3.

Examining the stresses around the high fiber region (Figure 72), we find that the S_y reaches peak value at point 4, which is at the intersection of the cracks. The inset shows the cross section at the plane of the +45° ply crack. The +45° ply, the epoxy interlayer on either side of it, and the epoxy regions adjacent to the high fiber region are cracked in this inset. The stresses are plotted along 1-2-3-5-1. The distance 'l' is measured starting from point 1 and proceeding clockwise. Along the side 1-2, which is on the symmetric plane, S_y is constant. On side 2-3, which is the rounded side, the stress drops steadily and then rises to a normalized value of about 6 at point 3. S_y continues to rise to the significant value of almost 8 at point 4. This is a point in the 0° ply which is closest to the point of intersection of the cracks in the +45 and -45 plies. Thus, the effect of all the cracks surrounding the high fiber region is felt most at this point. The value of 8 times the applied stress is very high and is likely to cause fiber failure for moderate values of S_A . In practical cases, however, delamination is expected to occur near the intersection of the matrix cracks long before S_y can reach this high value in the 0° ply. The high S_z value at this point reinforces this expectation. S_{yz} values are not significant except along 3-4 and 3-5. S_{yz} reaches about 40 % of S_A on these sides, while going to almost zero everywhere else. S_x reaches high levels at point 4 along with S_z . The shear stress S_{xy} reaches its peak value at point 4.



Note: The distance 'l' is plotted around the high fiber region starting at point (1) on the inset diagram and proceeding clockwise

Figure 72. Stresses Around the High Fiber Region at the +45 Crack Plane.



(Through a point 2.8 h from the intersection of cracks)

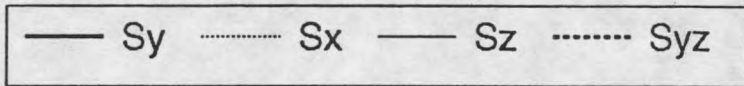
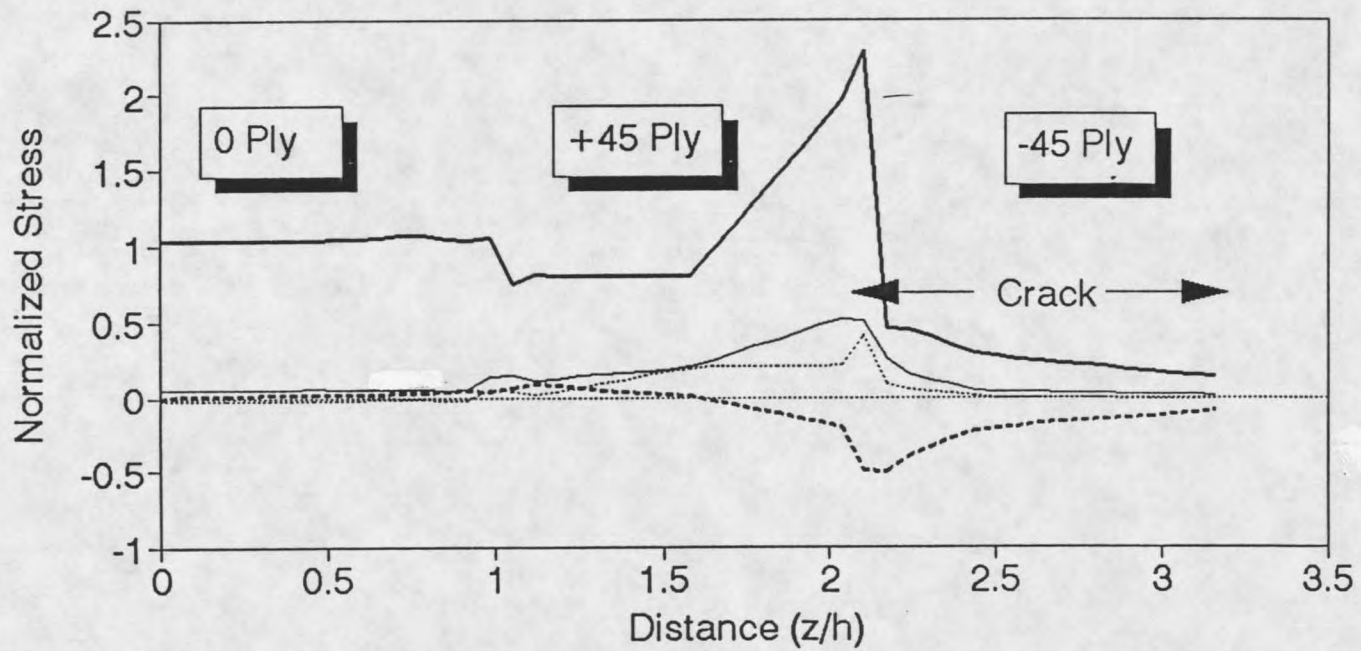


Figure 73. Through-thickness Stresses, passing through +45 Crack only.



(Through a point 2.8 h from the intersection of cracks)

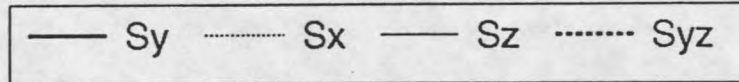


Figure 74. Through-thickness Stresses, passing through -45 Crack only.

Figures 73 and 74 show the stresses plotted through the thickness of the laminate. These stresses are plotted at points $2.8 h$ away from the intersection of the cracks, measured from the intersection along the $+45$ or the -45 crack. For example, for the plot that includes the $+45^0$ ply crack only, the stresses are plotted through the thickness of the laminate (parallel to the z axis), through a point that is located $2.8 h$ from the intersection of the cracks, measured along the $+45$ crack. Thus, the through thickness stresses, depending on the point chosen, will include only the $+45$ crack or the -45 crack. Figure 73 shows the stresses at a section which includes $+45$ crack only. As expected, S_y reaches low values through the $+45^0$ ply. S_y is high near the $0/+45$ ply interface. This value of 3 is much lower than the value obtained for stresses plotted through the thickness at the intersection of the $+45$ and the -45 ply cracks. Compare this with a similar plot from Chapter 5 (Figure 64). The stresses follow a similar trend, but the S_y values are lower in the present model. Figure 74 shows the stresses through a section that includes the -45^0 ply crack only. Comparing this with Figure 65, we find that the stresses follow a similar trend, however the values are lower in the present model. Another difference is in the sign of S_{yz} at the $+45/-45$ interface. In the present model, S_{yz} is negative as opposed to a positive value in the model with homogenous material properties (Figure 74 vs. Figure 65).

Summary

The normal stress S_y plotted at the intersection of the +45 and -45 cracks reaches very high values (8 times S_A) at the 0/+45 interface. S_z is also high at this point. The high value of S_z at point 4 in Figure 72, suggests the likelihood of delamination at this point, while the S_y value would produce fiber failure at low applied S_A . The stresses through the thickness of the laminate including only one of the angle ply cracks, follow a similar trend to the model with homogenous material properties (Chapter 5). The difference is in the sign of S_{yz} , and the stress values are lower in the present model. Stresses along the -45 crack are different from the model in Chapter 5. S_y is constant till the intersection of the cracks in the present model, while it drops to zero in the model in Chapter 5. The presence of a high fiber strand seems to influence these changes, but the F.E. mesh also differs. The important difference is in the S_y and S_z values at the intersection of the cracks. The values obtained in this model are significantly different from the ones obtained from Chapter 5. The higher interlaminar stress points to a strong possibility of delamination. Since the stresses are higher in this model, delamination is expected to occur earlier. Having a discrete high fiber region increases the possibility of a delamination for the $[0/\pm 45]_s$ laminate. This is an important conclusion because, as opposed to the $[0/90/0]$ case, having a discrete fiber region does changes the interlaminar stresses significantly. The most significant contribution to delamination comes from S_z .

CHAPTER 7

CONCLUSIONS AND RECOMMENDATIONS

Conclusions

The purpose of this study was to examine the nature of stress fields around matrix cracks in off-axis plies. Stresses around matrix cracks in $[0/90/0]$ and $[0/\pm 45]_s$ laminates with different geometries have been explored. The presence of an epoxy interlayer between plies plays a significant role in reducing the stress concentration at the interfaces. As there is a thin matrix interlayer in actual laminates, and as this interlayer tends to crack adjacent to a crack in the off-axis ply, models with a cracked epoxy interlayer more closely represent an actual laminate. While modelling a laminate with a discrete high fiber strand, stresses were high when this region was represented by a rectangular prism. Substantial lowering of stresses was observed when this high fiber region was rounded. This rounding more closely represents the fiber strands in an actual laminate. The stresses in the high fiber region were higher than the stresses in the average fiber region. For the $[0/90/0]$ laminate, having a discrete high fiber region does not alter the interlaminar stresses by a significant amount. Hence, for the $[0/90/0]$ case, it is expected that delamination will occur at about the same stress level for laminates with homogenous ply properties and laminates with a discrete fiber strand.

Cracking of the 90° ply in the $[0/90/0]$ laminate does produce a significant concentration of the stress S_y in the 0° ply fibers relative to the uncracked laminate.

The stress concentration is much higher for glass/epoxy than for carbon/epoxy due to the higher proportion of the load originally carried by the 90° plies with the glass/epoxy. The S_y stress concentration and stress gradient in the 0° ply in glass/epoxy is significant, so that approximate analyses which assume a uniform S_y across the 0° ply as the 90° ply cracks significantly underestimate the stress on the 0° fibers adjacent to the crack. While a matrix interlayer reduces this stress concentration, it is still too high to be ignored. For the $[0/\pm 45]_s$ laminate, cracking of the ± 45 plies produces an even higher stress concentration in the 0° material at the crack intersection. The ± 45 plies carry a higher fraction of the load than do 90° plies to begin with, due to their orientation and higher modulus in the load direction. When they crack, they shed more load to the 0° plies. There is also a higher fraction (67%) of off-axis plies in the $[0/\pm 45]_s$ laminates than in the $[0/90/0]$ laminate. Modelling a discrete fiber region in the $[0/\pm 45]_s$ case further increases the S_y in the high fiber content strand to almost eight times the applied stress. This is consistent with the experimentally observed failure of the 0° material in wind turbine blade materials when the ± 45 layers crack in fatigue.

The interlaminar stresses near the intersection of the cracks in the $+45$ and -45 plies are high enough to cause delamination in the $[0/\pm 45]_s$ laminates. These stresses reach their peak at the $0/+45$ interface and hence, delamination is likely to start there. Also, these interlaminar stresses are highly concentrated near the cracks and may contribute to damage development. In the $[0/\pm 45]_s$ laminate with a discrete high fiber region, the S_y and S_z stresses are very high and indicate a

strong possibility of an early delamination near the intersection of the +45 and -45 cracks. Having a discrete high fiber region significantly raises the stresses near the intersection of the cracks. The peak S_z value in the model with a discrete fiber strand is almost twice as high as the corresponding value in the model with uniform ply properties. Having a discrete fiber strand increases the peak interlaminar stress values. This is different from the conclusion drawn about the [0/90/0] laminates, where the discrete fiber strand does not alter the interlaminar stresses significantly. Since S_z is high and the opening mode crack resistance is typically much lower than for the shearing mode, especially with brittle matrices [26], S_z is expected to dominate the delamination process in all the models analyzed.

Recommendations

The present work has been devoted only to matrix cracks in off-axis plies. The high interlaminar stresses around the matrix cracks suggest a strong possibility of delamination. It is recommended that models with delamination cracks be explored. The presence of such delamination is expected to lower the stress concentrations seen around cracks in the present study. Delamination will also more closely represent the damages that occur in an actual laminate subjected to fatigue cycles. As delamination is a common type of damage to occur in laminates under fatigue loading, such modelling will provide insight into the failure mechanisms of actual wind turbine blades.

One important conclusion from the present study is that having a matrix interlayer between plies substantially lowers the stress concentration at ply interfaces. As this correlates with experimental observations, it is recommended that a matrix interlayer be maintained between plies and that the stitching together of fiber strands of different orientations (like 0, +45, -45) be avoided. The presence of a matrix layer is expected to improve the performance of the laminate, especially in glass/epoxy laminates. The effect of the thickness of the matrix interlayer has not been explored in detail here, and should be investigated in future models which also include delaminations.

The interlaminar stress distribution around free edges in undamaged laminates have been shown by [24] to vary with the ratio of ply thickness (h) to laminate width (b). The present study has examined laminates with the ratio $b/h = 16$. It is recommended that laminates with different ratios of b/h and cracks in off-axis plies be examined and compared with the present study.

In the $[0/\pm 45]_s$ laminate with a discrete fiber region, the crack modelled in the epoxy region in the 0° ply is in the plane of the +45 crack. Experimental observation suggests that cracks form perpendicular to the direction of applied force in all plies in the matrix rich regions. Further study is recommended with this type of crack in the matrix region. It is expected that such a crack will alter the nature of the stress fields significantly at ply interfaces.

REFERENCES

REFERENCES

1. Peters, P.W.M., "Constrained 90° Ply Cracking in 0/90/0 and $\pm 45/90/\mp 45$ CFRP Laminates", Composite Materials : Fatigue and Fracture, ASTM STP 907, H.T. Hahn, Ed., American Society for Testing and Materials, Philadelphia, 1986, pp. 84-99.
2. Ramesh, T., "Damage Mechanics of Composite Materials Based on Thermodynamics with Internal Variables, Durability of Polymer Based Composite Systems for Structural Applications, Edited by A.H. Cardon and G.H. Verchery, Elsevier Applied Science Publication.
3. Jamison, R. D., Schulte, K. Reifsnider, K. L. and Stinchcomb, W. W., "Characterization and Analysis of Damage Mechanisms in Tension-Tension Fatigue of Graphite/Epoxy Laminates". In Effect of Defects in Composite Materials, ASTM STP 836, ASTM, Philadelphia, 1984, pp. 21-25.
4. K.W. Garrett, J.E. Bailey., "Multiple Transverse Fracture in 90° Cross Ply Laminates of a Glass Fiber Reinforced Polyester", J. of Material Science 12 (1977) pp. 157-168.
5. L.J. Broutman and F.J. McGarry, 17th Reinforced Plastics Conference (Society of Plastics Industry, New York, 1962) Section 1E.
6. L.J. Broutman and H. Krock, "Modern Composite Materials", (Addison - Wesley, New York, 1967) Chapter 13.
7. M.J. Owen and R. Dukes, J. of Strain Analysis (1967) 272.
8. F.J. McGarry "Fundamental Aspects of Fiber Reinforced Composites", edited by R.T. Schwartz (Wiley, Kingston, 1968) pp. 63-87.
9. T.R. Smith and M.J. Owen, 23rd Reinforced Plastics Conference (Society of Plastics Industry, New York, 1968).
10. A.D.S. Diggwa and R.H. Norman, RAPRA Research Report 194, (July 1971).
11. E. pink and J.D. Campbell, J. of Material Science 9 (1974) 658.
12. H.T. Hahn and S.W. Tsai, J. of Composite Materials 8 (1974) 288.

REFERENCES-Continued

13. "Assessment of Research Needs for Wind Turbine Rotor Technology", Report of the committee on Assessment of Research Needs for Wind Turbine Rotor Materials Technology, National Research Council, National Academy Press, Washington D.C (1991).
14. J.F. Mandell, R.M. Reed, D.D. Samborsky, and Qiong (Rena) Pan, "Fatigue Performance of Wind Turbine Blade Composite Materials", SED-Vol. 14, Wind Energy, Ed. S. Hock, ASME, 1993.
15. "Life Prediction Methodologies for Composite Materials", Report of the Committee on Life Prediction Methodologies for Composite Materials, National Materials Advisory Board, NRC, National Academy Press, Washington D.C (1991).
16. K.L. Reifsneider, Ed., Fatigue of Composite Materials, Vol. 4, Composite Materials Series, Ed. R.B. Pipes, Elsevier Publishing Co., London (1991).
17. J.F Mandell, "Fatigue Behavior of Fiber Resin Composites", Developments in Reinforced Plastics -2, G. Pritchard, Ed., Applied Science Publishers, London, p. 67 (1982).
18. P.K. Mallick, "Fiber-Reinforced Composites - Materials, Manufacturing and Design, Marcel Dekker, Inc. New York.
19. N.J. Pagano and J.C. Halpin, "Influence of End Constraints in the Testing of Anisotropic Bodies", J. of Composite Materials, Vol. 2 (1968), p. 18.
20. R.B. Pipes, "Effects of Interlaminar Shear Stress upon Laminate Membrane Performance", Airforce Materials Laboratory / Industry Sponsored IRAD Status Report on Composite Materials, Bethpage, N.Y., April 1970.
21. A.H. Puppo and H.A. Evensen, "Interlaminar Shear in Laminated Components under Generalized Plane Stress", J. of Composite Materials, Vol. 4, (1970), p. 360

REFERENCES-Continued

22. R.B. Pipes and N.J. Pagano, "Interlaminar Stresses in Composite Laminates under Uniform Axial Extension". J. of Composite Materials, Vol. 4, 1970, p.538.
23. A.S.D. Wang and Frank W. Crossman, "Some New Results on Edge Effects in Symmetric Composite Laminates", J. of Composite Materials, Vol. 11 (1977), p.292.
24. J.T.S. Wang and J.N. Dickson, "Interlaminar Stress in Symmetric Composite Laminates", J. of Composite Materials, Vol. 22 (1978), p. 390.
25. Qiong (Rena) Pan, Graduate Student, Department of Chemical Engineering, Montana State University, Bozeman, Montana. Personal Communication.
26. Alan J. Russel and Ken N. Street, "Moisture and Temperature Effects on the Mixed Mode Delamination Fracture of Unidirectional Graphite/Epoxy", ASTM STP 876, pp. 349-370.
27. ANSYS Engineering Analysis System (Version 4.4a) - User and Theoretical Manuals, Swanson Analysis Systems, Inc., Houston, Pennsylvania.
28. N. J. Pagano and J.M. Whitney, "Geometric Design of Composite Cylindrical Characterization Specimens", J. of Composite Materials, Vol. 4, (1970), p. 360.

APPENDICES

APPENDIX ASTATIC ANALYSIS USING ANSYS 4.4 a [27]Assumptions and Restrictions

Inertial and damping effects are ignored, except for static acceleration fields.

Description of Analysis

The overall equilibrium equations for static analysis are :

$$[K]\{u\} = \{F\} \quad (1)$$

or

$$[K]\{u\} = \{F^a\} + \{F^r\} \quad (2)$$

where,

$$[K] = \text{total stiffness matrix} \quad \sum_{m=1}^N [K_e]$$

$\{u\}$ = nodal displacement vector

N = number of elements

$[K_e]$ = element stiffness matrix

$\{F^r\}$ = reaction load vector

$\{F^a\}$, the total applied load vector, is defined by :

$$\{F^a\} = \{F^{nd}\} + \{F^{ac}\} + \sum_{m=1}^N (\{F_e^{th}\} + \{F_e^{pr}\} + \{F_e^{pl}\} + \{F_e^{cr}\} + \{F_e^{sw}\} + \{F_e^{rt}\}) \quad (3)$$

where :

$\{F^{nd}\}$ = applied nodal load vector

$\{F^{ac}\} = [M]\{a_T\}$ = acceleration load vector

$[M]$ = total mass matrix $\sum_{m=1}^N [M_e]$

$[M_e]$ = element mass matrix

$\{a_T\}$ = total acceleration vector

$\{F_e^{th}\}$ = element thermal load vector

$\{F_e^{pr}\}$ = element pressure load vector

$\{F_e^{pl}\}$ = element plastic strain load vector

$\{F_e^{cr}\}$ = element creep strain load vector

$\{F_e^{sw}\}$ = element swelling strain load vector

$\{F_e^{rt}\}$ = element large displacement load vector

APPENDIX B

Three Dimensional Anisotropic Solid Element - STIF 64Table 2. STIF64 Element Description

MATRIX / VECTORS	SHAPE FUNCTIONS	INTEGRATION POINTS
Stiffness matrix	$u = \frac{1}{8}(u_i(1-s)(1-t)(1-r)$ $+ u_j(1+s)(1-t)(1-r)$ $+ u_k(1+s)(1+t)(1-r)$ $+ u_l(1-s)(1+t)(1-r)$ $+ u_m(1-s)(1-t)(1+r)$ $+ u_n(1+s)(1-t)(1+r)$ $+ u_o(1+s)(1+t)(1+r)$ $+ u_p(1-s)(1+t)(1+r))$ $v = \frac{1}{8}(v_i(1-s) \dots$ $w = \frac{1}{8}(w_i(1-s) \dots$ <p>(similar to u)</p>	<p>3 x 3 x 3</p> <p>or</p> <p>2 x 2 x 2</p>
Mass Matrix	Same as stiffness matrix without extra shape functions	Same as stiffness matrix

Table 2. Continued

MATRIX / VECTORS	SHAPE FUNCTIONS	INTEGRATION POINTS
Stress Stiffness Matrix	Same as stiffness matrix without extra shape functions	Same as stiffness matrix
Thermal Load Vector	Same as stiffness matrix	Same as stiffness matrix
Pressure Load Vector	No shape functions are used. Rather for triangular faces, one third of the pressure times the area if applied to each node. In case of four noded faces, the face is first subdivided into the four triangles which are formed by connecting the opposite nodes and then using half the pressure.	None

Element Temperature Distribution	Varying trilinearly across the element
Nodal Temperature Distribution	Same as element temperature distribution
Pressure Distribution	Uniform on each side

Stress-Strain Matrix

The stresses and strains are related by :

$$\{\sigma\} = [D](\{\epsilon\} - \{\epsilon^{th}\})$$

or

$$\{\epsilon\} = \{\epsilon^{th}\} + [D]^{-1}\{\sigma\}$$

while $\{\epsilon^{th}\}$ is restricted to orthotropic input, $[D]$ may be input as a full anisotropic matrix because 21

independent values are used in its makeup. Symmetry of the $[D]$ matrix is ensured, but the user must provide values so that the matrix is positive definite. If it is not, the program terminates. A matrix is positive definite if the determinants of all the submatrices of the series including the full 6×6 matrix $[D]$ are positive. Thus the two necessary (but not sufficient) condition for a matrix to be positive definite is,

$$D_{i,i} > 0$$

$$D_{i,j} < \sqrt{D_{i,i} D_{j,j}}$$

The matrix may be input and used as $\{\sigma\} = [D_K](\{\epsilon\} - \{\epsilon^{th}\})$

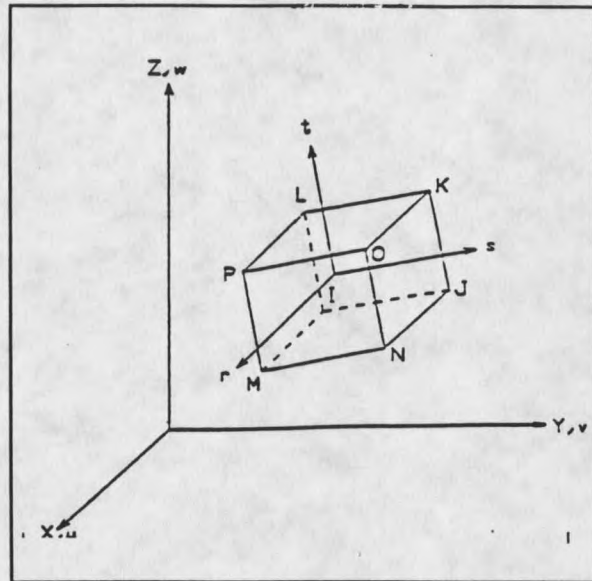


Figure 75. STIF 64 3-D Solid Element.

APPENDIX CWavefront Solver in ANSYS

The number of equations which are active after any element has been processed during the solution procedure is called the wavefront at that point [27]. The ANSYS program uses the wavefront or frontal solution procedure. The method used places a wavefront restriction on the problem definition, which depends on the amount of core storage available for a given problem. Wavefront limits tend to be restrictive only for the analysis of arbitrary three-dimensional solids.

In the wavefront procedure, the ordering of the elements is crucial to minimize the size of the wavefront. Alternatively, for a banded solver, the band width is minimized by paying close attention to the ordering of the nodes. In both cases, this minimization is important for reasons of efficiency and problem size.

The computer time required for the solution procedure is proportional to the square of the mean wavefront size. Therefore, it is advantageous to be able to estimate and minimize the wavefront size. The wavefront size is determined by the sequence in which the elements are arranged. The nodal point numbers of all elements are scanned to determine which element is the last to use each nodal point. As the total system of equations is assembled from element matrices, the equations for a nodal point which occurs for the last time are algebraically solved in terms of the remaining unknowns and eliminated from the assembled matrix by Gauss elimination.

The equations for a nodal point which occurs for the first time are added to the assembled matrix as the solution progresses. Thus, the assembled matrix expands and contracts as nodal points make their first and last appearance in the element specifications. The varying size of the active matrix is the instantaneous wavefront size.

When several elements are connected to the same node point, the degrees of freedom associated with these elements remain active in core until the wavefront "passes" all elements connected to the node. Degrees of freedom related by constraint equations or coupled nodes remain active until the wavefront "passes" all elements connected to the related degrees of freedom.

To reduce the maximum wavefront size, the elements must be arranged so that the element for which each nodal point is mentioned first is as close as possible in sequence to the element for which it is mentioned last. In geometric terms, the elements should be arranged so that the wavefront sweeps through the model continuously from one end to the other in the direction which has the largest number of nodal points.

MONTANA STATE UNIVERSITY LIBRARIES



3 1762 10066706 0